AN EXPERIMENTAL AND NUMERICAL APPROACH TO SHALLOW FOCUS EARTHQUAKE MECHANISM

A THESIS SUBMITTED TO
THE GRADUATE SCHOOL OF NATURAL AND APPLIED SCIENCES
OF
THE MIDDLE EAST TECHNICAL UNIVERSITY

BY

DURSUN SARI

IN PARTIAL FULFILLMENT OF THE REQUIREMENTS FOR THE DEGREE

OF

DOCTOR OF PHILOSOPHY

IN

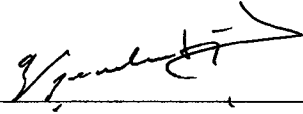MINING ENGINEERING

OCTOBER 1996

Approval of the Graduate School of Natural and Applied Sciences.
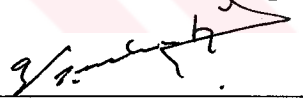
Prof.Dr. Tayfur Öztürk

Director

I certify that this thesis satisfies all the requirements as a thesis for the degree of Doctor of Philosophy.

Prof.Dr. A. Günhan Paşamehmetoğlu

Head of Department

This is to certify that we have read this thesis and that in our opinion it is fully adequate, in scope and quality, as a thesis for the degree of Doctor of Philosophy.

Prof.Dr. A. Günhan Paşamehmetoğlu

Supervisor
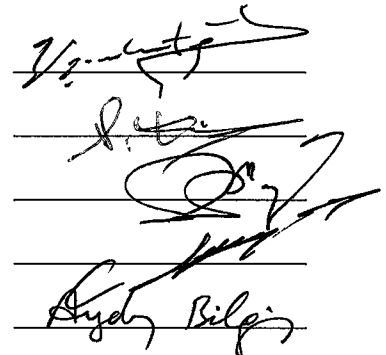
Examining Committee Members

Prof. Dr. A. Günhan Paşamehmetoğlu

Prof. Dr. Seyfi Kulaksız

Prof. Dr. Abdürrahim Özgenoğlu

Assoc. Prof. Dr. Gürel Şenyur

Assoc. Prof. Dr. Aydın Bilgin

ABSTRACT

AN EXPERIMENTAL AND NUMERICAL APPROACH
TO SHALLOW FOCUS EARTHQUAKE MECHANISM

Sarı, Dursun

Ph.D., Department of Mining Engineering

Supervisor: Prof. Dr. A. Günhan Paşamehmetoğlu

October 1996, 165 pages

The shallow focus earthquakes rupture causes the stress and strain release (destructive shocks) by a sudden shearing of seismogenic faults. This kind of earthquake occurrence closely relates to the friction phenomena developed in the upper parts of the Earth's lithosphere which can be characterised by predominantly brittle behaviour. Within this view, the laboratory frictional sliding experiments are considered to be a model of possible fault creep or stick-slip motions in the Earth crust. Due to this, there has been great deal of experimental research on the explanation of earthquake mechanism in the laboratory; and most of these works have been concentrated on frictional sliding model which are based on the history of sliding rate.

In this research, the shallow focus earthquake mechanism is investigated by experimental and numerical approaches. The vertical strike-slip seismogenic fault model is simulated considering the lateral variations of regional field stress. In order to carry out experiments on the simulated model in laboratory, a computer controlled direct-shear test apparatus is developed and manufactured in the Mining Engineering Department of Middle East Technical University

(METU). The experimental studies aim to model the sudden field stress change from the nominal stresses, in the normal and shear stress direction, effects on the seismicity of active faults. The effect of period, amplitude and cyclic loading of stress change in stepwise and functional mode are studied in detail and the results are tabulated and are mathematically modelled. These experimental studies are also supported by the results of the numerical distinct element method. At the end, an approach is established between the regional stress field variation and the shallow focus earthquake mechanism.

Key Words: Shallow Focus Earthquake, Earthquake Fault Models, Frictional

Sliding, Numerical Approach

ÖZ

SIĞ ODAKLI DEPREM MEKANİZMASINA
DENEYSEL VE NÜMERİK YAKLAŞIM

Sarı, Dursun

Doktora, Maden Mühendisliği Bölümü

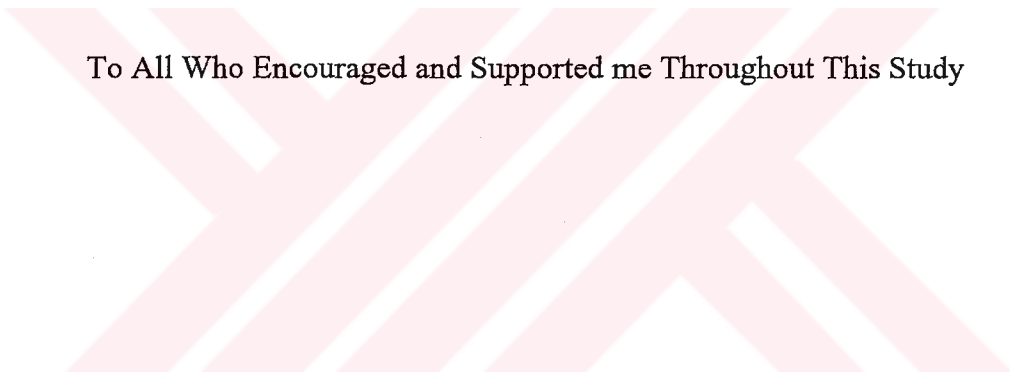Tez Yöneticisi: Prof. Dr. A. Günhan Paşamehmetoğlu

Ekim 1996, 165 sayfa

Deprem faylarının ani kaymasıyla meydana gelen sığ odaklı deprem parçalanmaları sonucunda yerkürede ani gerilim ve boşalmalar olur. Bu tür depremler yerkürenin üst kısımlarındaki kırılgan yapılı ortamda oluştuğundan, sürtünme olgusuyla çok yakından ilişkilidir. Bu açıdan bakılırsa, sürtünmeli kayma deneyleri yer kabuğundaki fayların sünme ve "stick-slip" haraketlerinin modellenmesinde kullanılabileceği düşünülür. Bundan dolayı deprem mekanizmasının açıklanmasına yönelik birçok deneysel çalışmalara ilgi duyulmuştur. Bu deneysel çalışmaların çoğu sistemin kayma hızındaki değişimin gözlemini içeren sürtünmeli kayma modellerinde yoğunlaşmıştır.

Bu çalışmada sığ odaklı deprem mekanizması deneysel ve nümerik yaklaşımlarla araştırıldı. Doğrultu kaymalı deprem oluşturan fay modelinin arazi yanal gerilim değişmeleriyle etkileşmesi simule edilerek çalışmalar yapıldı. Bu modellerin deneysel olarak çalışabilmesi için Orta Doğu Teknik Üniversitesi Maden Mühendisliği Bölümünde yeni bir bilgisayar kontrollü direkt-makaslama deney aleti gelştirilip yapıldı. Deneysel çalışmaların gayesi fay yüzeyine etkiyen arazi gerilmelerindeki ani değişikliklerin, gerek dikey gerekse yatay yöndeki fay yüzeyine etkisi modellenerek çalışılmasıdır. Gerilim değişikliğinin periyodu, artış

mıktarı ve periyodik etkimesi basamak ve fonksiyonel tarzlarda modellenen gerilim değişiklikleriyle araştırıldı. Bu çalışmaların sonuçları tablolar halinde sunulup matematiksel modellemeler elde edildi. Bu deneysel çalışmalar ayrıca nümerik ayrık metotlarla da desteklendi. En sonunda sığ odaklı deprem mekanizması ile ani arazi gerilimlerindeki değişikler arasındaki ilişkileri içeren bir yaklaşım geliştirildi.

Anahtar Kelimeler: Sığ Odaklı Deprem, Deprem Fay Modeli, Sürtünmeli Kayma, Nümerik Yaklaşım

To All Who Encouraged and Supported me Throughout This Study

ACKNOWLEDGEMENTS

TABLE OF CONTENTS

LIST OF TABLES

LIST OF FIGURES

CHAPTER 1

INTRODUCTION

Earthquakes can be briefly defined as sudden chaotic motions of the Earth crust; earthquake rupture causes the stress and strain to release by a sudden shearing of faults. According to their mechanical cause, the most common earthquakes are of tectonic type. They often cause destructive shocks as they have shallow focus (hypocenter less than 70 km from the Earth surface). From this point of view, investigation of the mechanism of tectonic earthquakes is of considerable importance in seismology.

One of the major approaches to the problem of clarifying the earthquake mechanism has been the examination of the frictional behaviour of faults since Bridgman in 1936 (Dieterich, 1972). Bridgman (1936) has suggested that the stick-slip sliding on sliding interfaces can be an explanation for earthquake faults. It is also known that unstable frictional sliding and earthquakes result from the interaction between the frictional properties of a sliding surface and an elastic loading system; and this can be characterised either as a fault in the Earth coupled to the Earth crust or a small specimen in an elastic testing system.

Sliding behaviour of fault model in a laboratory under test and earthquake mechanisms are similar phenomenon in that both are sudden instabilities which result in a sudden movement and in partial shear stress drop on pre-existing seismogenic faults or fault model in the laboratory. This phenomenon has been studied by various investigators particularly with different stress levels, rock types, surface and hydrothermal conditions. In other words, the vertical (depth) variations of frictional behaviour and fault zone rheology identifying the stability transitions at different depths have been investigated in detail; but not much attention is given to (Hobbs and Brady, 1985; Linker and Dieterich, 1992; Boatwright and Cocco,

1

1996) strength variation along the fault strike controlling the heterogeneity and segmentation of large earthquakes.

In this study, it is aimed to understand the mechanism of the shallow focus earthquakes by experimental and numerical approaches. The emphasis is given to simulate the fault under lateral (along the strike of the fault) variations of stress boundary conditions. This includes the abrupt variation of normal and/or shear stress which corresponds to changes of regional normal or shear stress due to nearby activities in the Earth crust (earthquake, volcanic eruption, etc.).

In order to study this phenomenon thoroughly, first of all, a computer controlled direct-shear apparatus is developed and manufactured at the Mining Engineering Department of Middle East Technical University (METU) so that the simulated earthquake fault model behaviour under the prescribed stress and strain boundary conditions could be precisely studied and well data-acquisition can be achieved continuously and be evaluated via. the developed software.

Then, the effects of sudden field stress change associated with earthquakes or artificial disturbance are simulated by the experimental fault model. These models consist of mainly two types; the first model includes stepwise and functional form of the normal stress change for the simulation of the influence of regional field stress change, in normal direction of the fault surface only, on shallow focus earthquake mechanism. The other model is simulated the effect of the sudden changes of regional field stress in simultaneous normal and shear stress in functional form. Besides this, the velocity-stepping tests are also carried out in order to establish a basis, compilation of rate- and state- dependent parameters for analysing the variational stress change experimental model results. At the same time, the experimental fault models are supported by the numerical simulation with the distinct element method.

At the final section of the study, the results are compiled and modelled for understanding the shallow focus earthquake mechanism. The relation between the sudden stress field change and earthquake mechanism considering the shear stress drop and variation of frictional strength parameters with the mathematical models are provided.

2

The causes and mechanism of earthquakes are summarised in Chapter 2. In the third Chapter, literature associated with frictional sliding of earthquake faults is reviewed . In this chapter, rather than giving the full description of the whole studies, the main topics related to the earthquake faults and their mechanisms are discussed. In Chapter 4, detailed information about the computer controlled direct-shear test apparatus is given . The results and interpretations of the experimental and numerical studies are presented in Chapter 5 and Chapter 6, respectively. Finally, the conclusion and the recommendations for further research are given in Chapter 7.

CHAPTER 2

CAUSES AND MECHANISM OF EARTHQUAKES

2.1. Introduction

The causes and mechanism of earthquakes are analysed by a seismology which is a branch of geophysics. From an engineering point of view, seismology has to provide data necessary for the prediction of seismic phenomena. Geologists investigate the movement and deformation and source of parameters of earthquakes: energy release, moment, stress drop, particle motion, rupture velocity, and source size. However, the meaning of these parameters in terms of the physics of the seismic source is quite uncertain (Scholz et al., 1972). Beside this, the purpose of seismologists is to investigate the past and present nature of the Earth's crust in order to predict future mechanism of the crust. Their main concern is to establish the possibility of sudden failure of the crustal rock mass and the sudden slip of pre-existing faults. Study of faults behaviour under unstable loading conditions is also essential for understanding earthquake mechanism and learning how to predict its occurrence.

On the other hand, in recent years rock mechanics is providing an important scientific foundation for other branches of the Earth sciences related to rock engineering. In seismology, experimental research on frictional slip in brittle rock materials could be a powerful tool in highlighting the mechanism of earthquakes.

This chapter is not meant to be a complete overview of seismology. The aim is to identify the principal data which allow the definition of the seismic action and a rather a presentation of those aspects considered to be important for earthquake engineering. Thus, a brief description of the inner structure of the Earth is included initially, followed by some aspects of plate tectonics. Then, the main characteristics and mechanism of the Earth seismic zones are presented. The discussions on earthquake prediction are finally given.

4

2.2. The inner structure of the earth

The Earth consists of three concentric layers having different physical properties. These are crust, mantle and core (Fig. 2.1).

The core, which has a radius R=3470 km and consists of an inner core (R=1370 km) and an outer core (1370 km < R < 3470 km). The core is composed of molten iron, probably mixed with small quantities of other elements such as nickel and sulphur or silicon.

The mantle, which is a 2900 km thick layer, consists of upper mantle, reaching a depth of 400 km, made up olivine and pyroxene and transition zone, 237 km thick, constituted of olivine and the lower mantle made of a more homogeneous most of magnesium and iron oxides and of quartz.
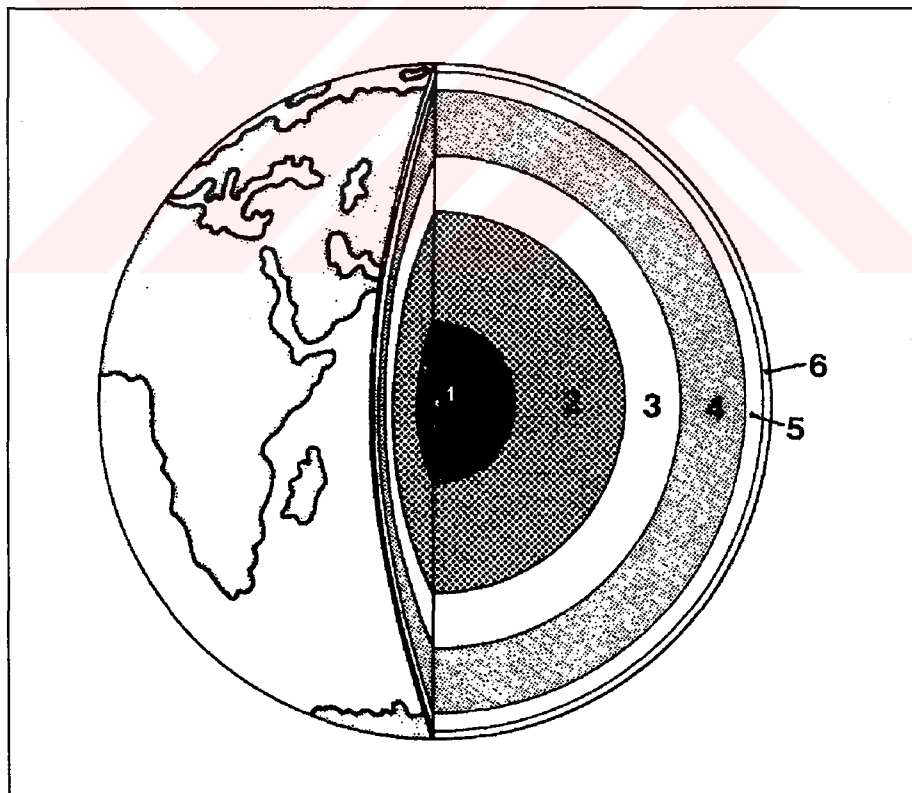
Figure 2.1 Earth's structure
(1) inner core; (2) outer core; (3) lower mantle; (4) upper mantle;
(5) transition; (6) crust.

5

The crust or the lithosphere, which is the outer part of the Earth, having a high rigidity and anisotropy. It has a thickness of about 60 km. The crust consists of ocean basins especially of basaltic rock and granitic rock. The crust of the varies in thickness from 20 to 70 km under the continents and between 5 km and 10 km under the oceans (Jaeger and Cook, 1976). The surface separating the crust from this layer is referred to as the Mohorovicic discontinuity, after its discoverer and is commonly named the Moho. The Earth crust together with the Moho are illustrated in Fig. 2.2. The depth of the Moho may vary between 8 km under the ocean bottom and 3.5 km under mountains (Barbat and Canet, 1989).

The variation of some physical characteristics of the Earth according to depth is shown in Fig. 2.3. The characteristics analysed in this figure are density, pressure and temperature. The mantle core discontinuity may be noticed in the density diagram.
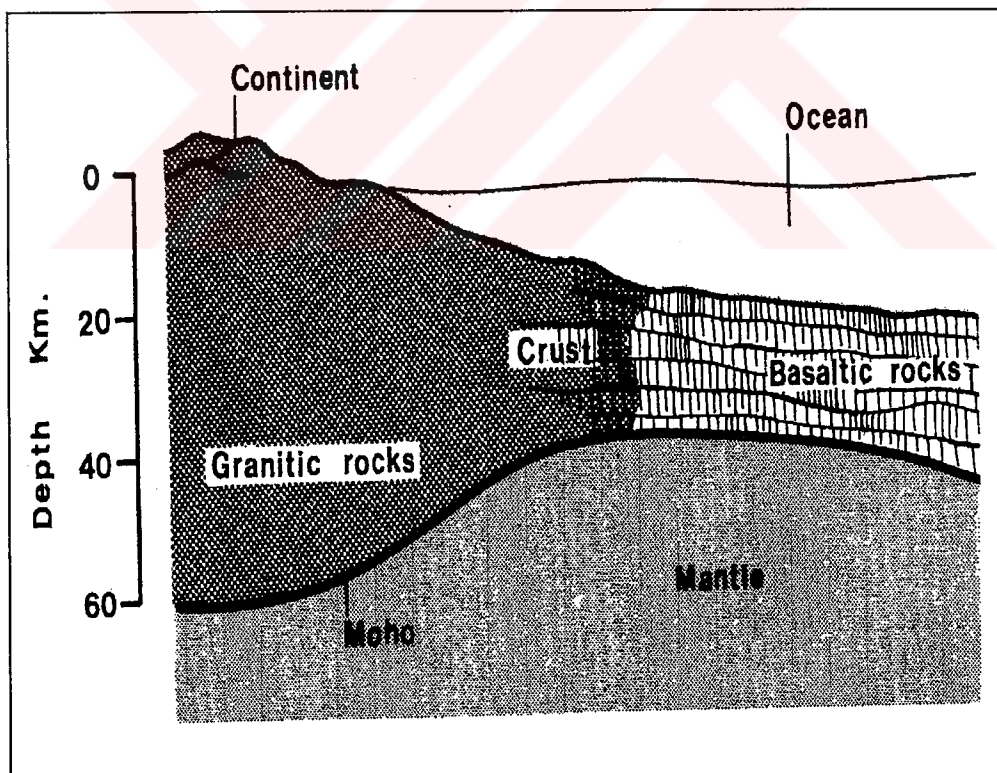
Figure 2.2 Crust and Moho (After McAlester, 1973)
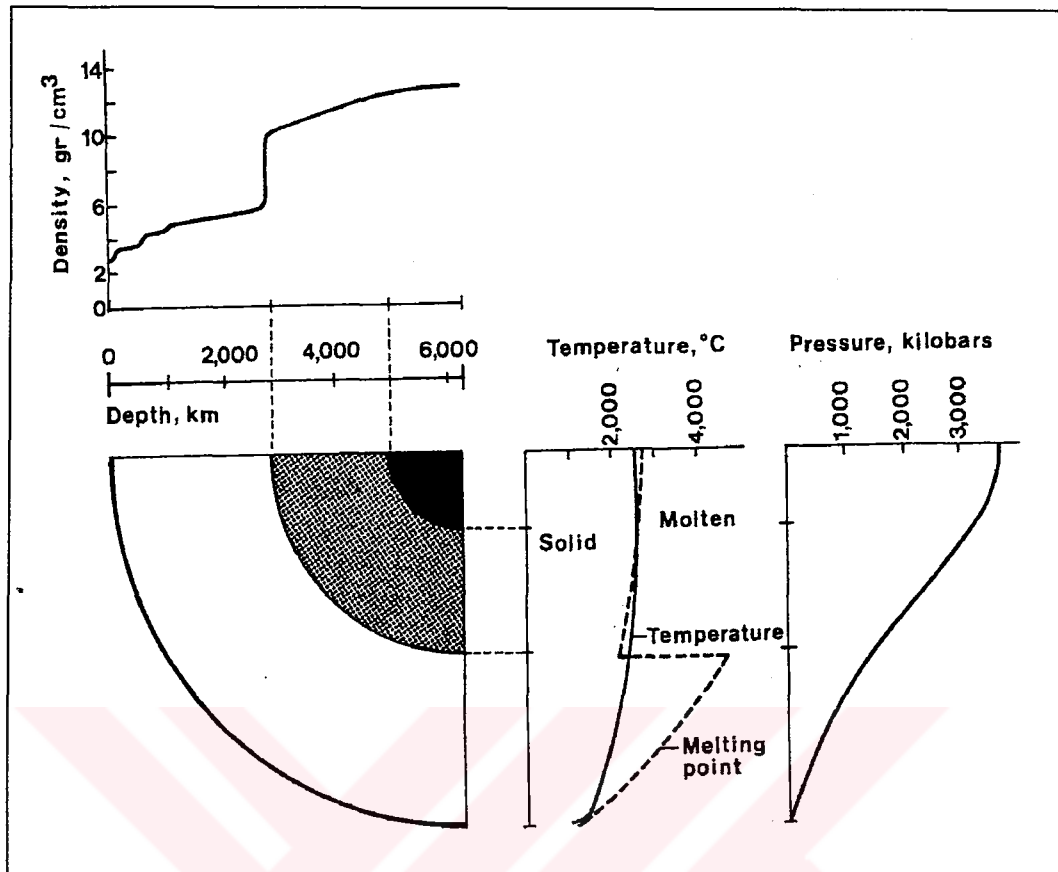
Figure 2. 3 Variation of different physical character of the earth (After McAlester, 1973 and Stacey, 1969)

2.2.1. Strength of the lithosphere

Several researchers estimated the upper limit for the strength of the lithosphere as a function of depth based on the results of laboratory measurements on the mechanical properties of the rocks. They have noted the strength of the Earth can not be greater than the strength of the rocks of which it composed (Brace and Kohlstead, 1980; Kirby, 1980). These analyses divided the lithosphere into either two or three rheological regions. In the uppermost part where the temperature and lithostatic pressure are relatively low, frictional sliding on pre-existing fractures govern the mechanical behaviour. At greater depth due to increasing temperature and pressure, plastic deformation controls the strength. Between these two regions, brittle and plastic processes interact in a transitional zone. The resulting profiles or strength envelopes plot maximum rock strength

7

versus depth, as illustrated schematically in Fig. 2.4 for oceanic and continental lithosphere composed of a layer of crust rock overlying mantle rock (Chen and Molnar, 1983). The strength envelopes reflect the experimental observations that frictional strength increases approximately linearly with increasing pressure and is relatively insensitive to temperature, while plastic strength decreases rapidly with increasing temperature but is relatively insensitive to pressure.
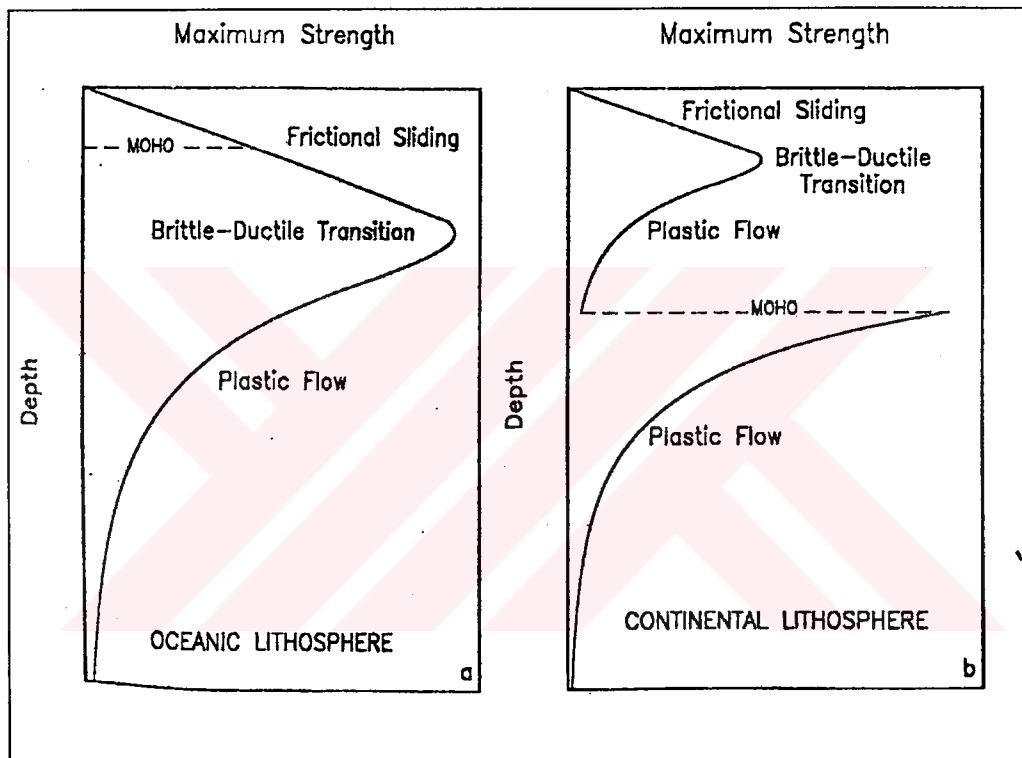
Figure 2.4 Schematic illustration of maximum rock strength as a function of depth
(After Brace and Kohlstead, 1980)

2.3. Tectonic plate movements

It is stated in the literature that the Earth crust is made up 8 main tectonic plates which are: Eurasian, Indian, Pacific, Antartic, African, Nascan, North and South American plates. It is also added that these tectonic plates move by heat energy concentrated under the lithosphere; but this hypothesis is not yet to be

explained completely (MCAlester, 1973). The main tectonic plates of the Earth are illustrated in Fig. 2.5.

2.4. Types of earthquakes

Earthquakes could be defined as chaotic motions of the earth's crust in different seismic waves form. An earthquake begins with a shock at a certain depth below the Earth surface, which is named focus or hypocenter. The characteristic features of an earthquake is shown in Fig. 2.6.
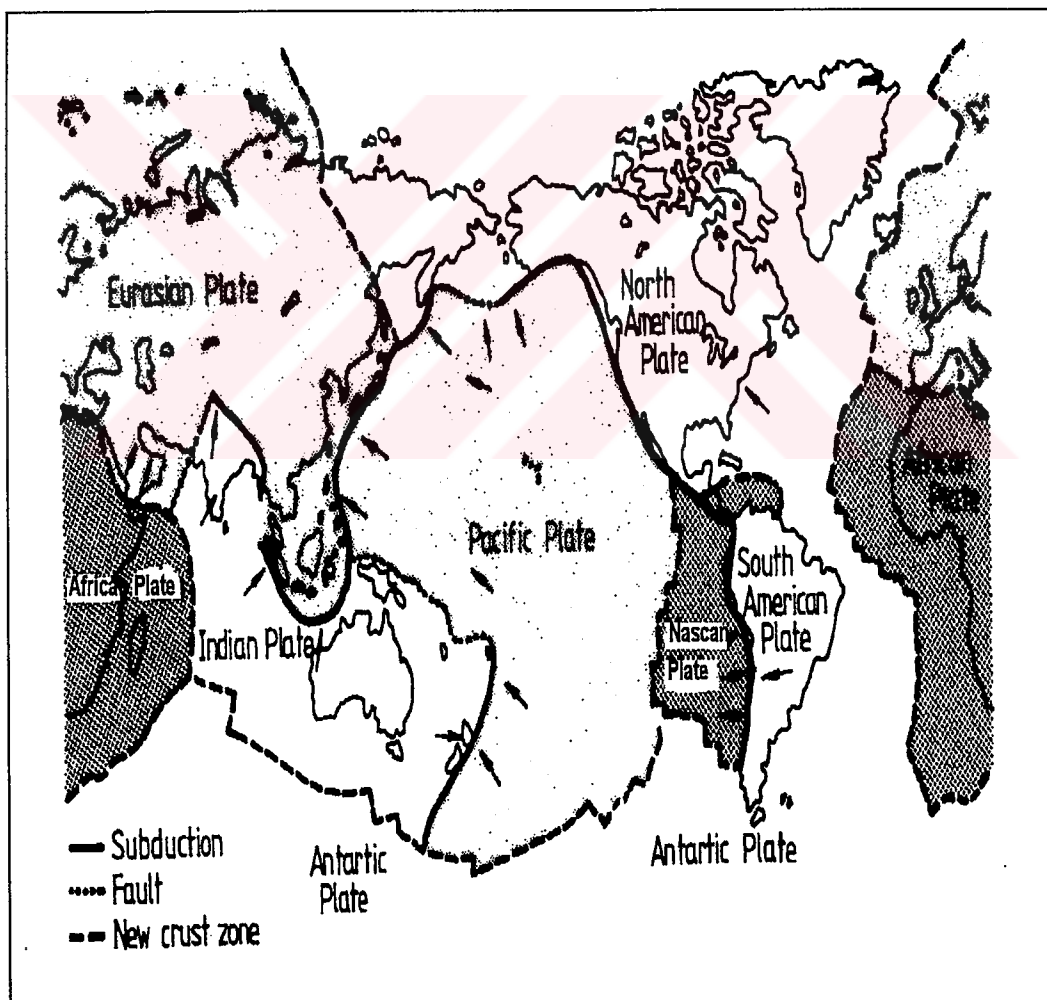
Figure 2.5 Main tectonic plates of the world (After Nur in Jaeger and Cook, 1976)

2.4.1. Earthquakes according to their mechanical causes

A classification of the earthquakes according to their mechanical causes has been made by Scheidegger (1975) who remarks the following classes:

i. Tectonic earthquakes; these are the strongest and most frequent earthquakes. They are caused by sudden break of the rock layer along fractured surfaces, called faults.

ii. Collapse earthquakes; these are earthquakes of low intensity that take place in zones of underground cavities and mines, and are due to collapse of these.

iii. Volcanic shocks; both volcanic eruption and earthquakes are phenomena that seem to have the same tectonic origin. The explosions of gases during eruptions can give birth to earthquakes that generally affect small surfaces and have low intensities.

iv. Earthquakes generated by explosions; man has often produced explosions, especially underground nuclear ones, capable of generating ground motions that can be felt at certain distances.
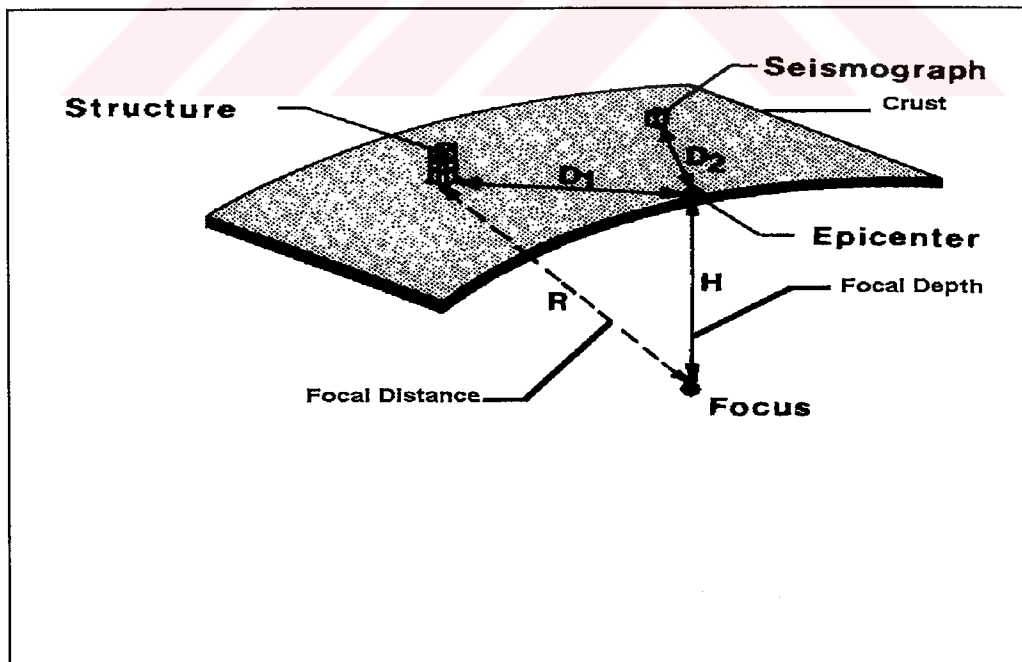
Figure 2.6 Characteristics of an earthquake

2.4.2. Earthquakes according to their focal depths

According to criterion of the focal depth that the earthquake occurs is classified into 3 groups:

i. Normal or surface earthquakes (shallow focus earthquakes) focal depths range in between 5 and 70 km,

ii. Earthquakes with focal depths range from 70 km to 300 km,

iii. The third group is the deep earthquakes whose focal depths are greater than 300 km and can reach up to 700 km.

2.4.3. Earthquakes induced by artificial disturbance

The water, at high pressure, lubricates the fracture plane. Therefore the friction between two adjacent plates decreases, and favourable conditions for an earthquake can appear. That makes evident the importance of the presence of subterranean water with respect to the earthquake mechanism.

This phenomenon has been related to increase of seismicity in some moderate seismic zones due to man's activity such as injection of water in deep wells, or the impounding of water in man-made reservoirs. For example this phenomenon has occurred in Denver in the early 1960's (Jaeger and Cook, 1976).

Many other earthquakes that took place in the proximity of dams existing in different zones of the world are considered to be a consequence of induced seismicity. Such examples may be the earthquakes of Montey Dam in France in April 1963 (Barbat and Canet, 1989).

2.5. Mechanism of tectonic earthquakes

The strongest and the most common earthquake in Earth's crust are tectonic type which are often dangerous and hazardous due to their closeness to the Earth's surface. The shallow focus earthquakes are also included in this classification and most of them are originating from the seismogenic faults.

On the other hand, the structure of the Earth's crust on which earthquake originate is very complicated. It is neither perfectly elastic nor homogeneous and isotropic and it is not perfectly continuos medium. Besides this, the Earth's crust is cut by deep and great faults, and just at these places great earthquakes often occur

11

(e.g. San Andreas fault, North Anatolian Fault Zone). It is also known that the weak earthquakes (the crust fractured at shallow depth) to a certain extent are random, but most of earthquakes of $M_S>6$ (magnitude scale=M_S) occur without doubt on the main tectonic belts (active faults) stated previously.

2.5.1. Types of faults

The four main types of fault related to the tectonic earthquakes are classified in the following groups (Fig. 2.7).

    a. Normal faults, which correspond to zones where the Earth's crust is in extension; one of the blocks separated by the fault moves downwards.

    b. Thrust or inverted faults which correspond to compressed zones;

        -Under thrust faults: one of the interacting plates thrusts under the other, which generally is a continental plate.

        -Over thrust faults: the upper of the two blocks moves upwards.

    c. Strike-slip faults, which involve horizontal relative displacements between the two sides of a fault.
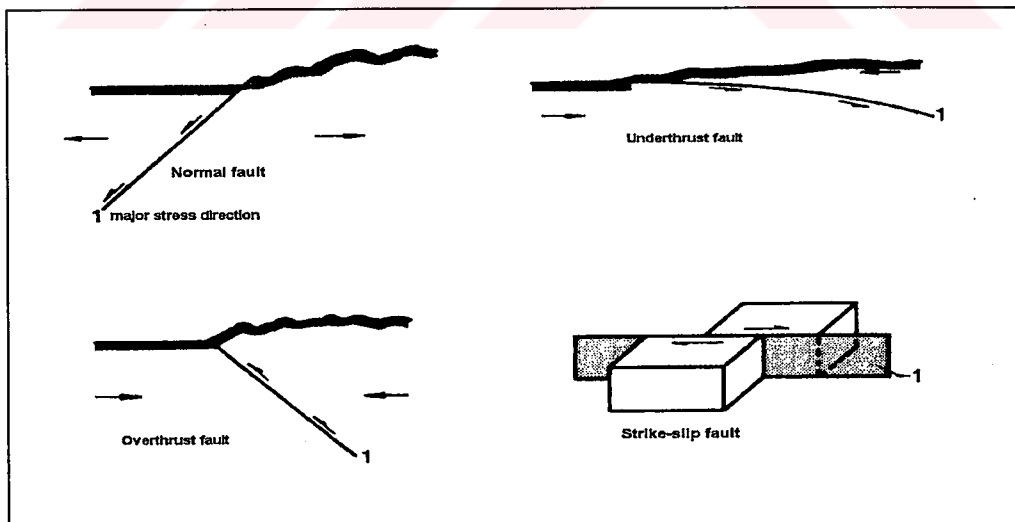
Figure 2.7 Types of faults

2.5.2. Reid's theory

The mechanism of the tectonic earthquake has not completely been explained by now. The most widely accepted theory by the researchers has been developed by Reid in 1906 (Tao and Zhang, 1990), and is named elastic rebound theory. Reid's (Tao and Zhang, 1990) investigations are dedicated to the study of San Andreas fault which was a strike-slip (transcurrent) fault. The mechanism, according to Reid's theory is illustrated in a simple configuration in Fig. 2.8.

Its physical meaning can be summed up as follows:

-   Because of the heterogeneity of rock mechanical properties, the zone of displacement and stress are assumed to be imaginary lines cross the fault (Fig. 2.8a). Around the locking area or the fault ends stress will concentrate to a high degree, and a great strain energy will be accumulated (Fig. 2.8b).
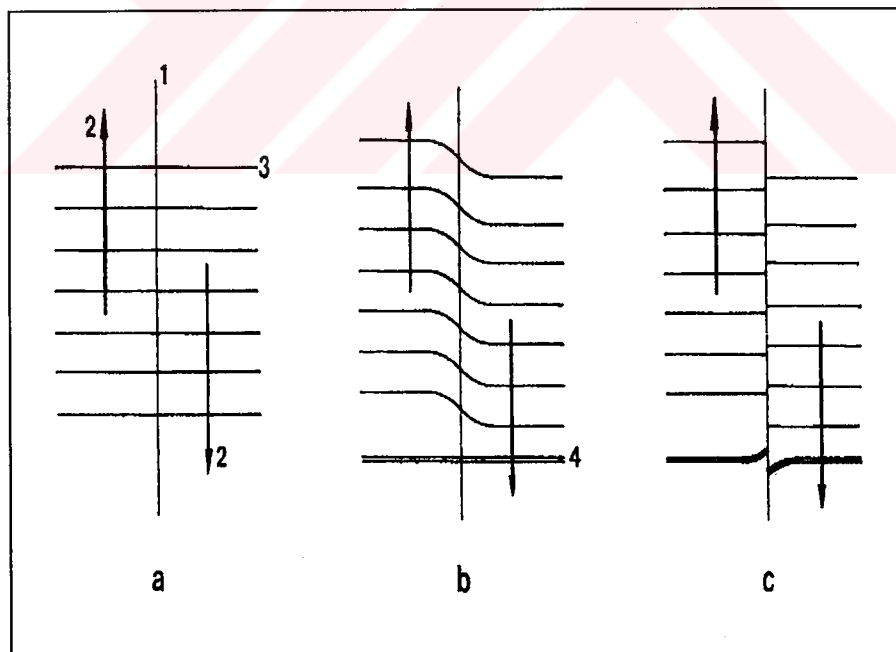
Figure 2.8 The Mechanism of tectonic earthquake (After Tao and Zhang,1990) (a) unstrained state; (b) strained state; (c) situation after the seismic phenomenon; (1) fault line; (2) direction of motion; (3) imaginary lines; (4) road.

- If the continental drift continues, the crust layers will reach stresses and strains that will exceed the material strength, causing a rupture along the fault, starting from a weak point. The accumulated strain energy will be produced and an earthquake occurs. The situation after this rupture is shown in Fig. 2.8c. The focus of the earthquake may be defined as the weakest point at which the first rupture occurs (Fig. 2.9).

- Stress recovery and transition occurs after the first shock because of the viscosity, plasticity, and the internal friction of rocks. The visco-elastic strain energy accumulated in rocks are gradually transmitted into elastic strain energy, and another shock is caused when the stress reaches a new static frictional strength. The after shocks usually release a small part of accumulated elastic strain energy. The tectonic stress field is again disturbed by the after shocks and stress recovery begins again. Repeating this kind of process, aftershocks will continue after a main shock. When considerable stress in the rocks surrounding the fault is released by the main shock aftershocks will disappear.
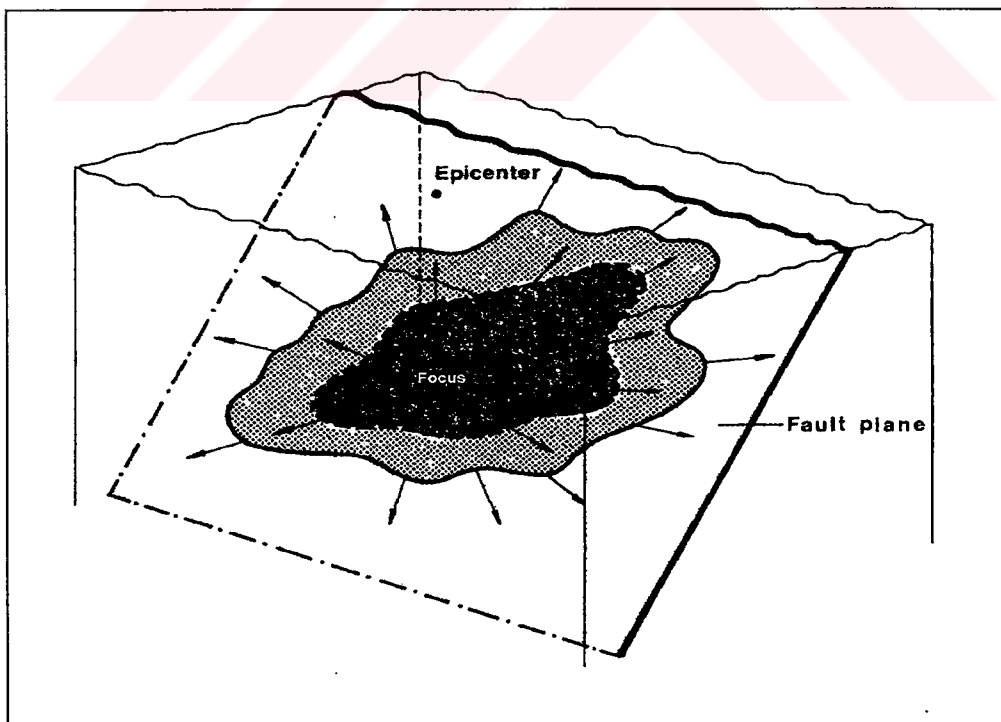
Figure 2.9 The focus of the earthquake (After Bolt,1981)

14

2.5.3. Earth seismic zones

The most important seismic zones of the Earth spotlighted by these epicentres. The coincidence of these seismic belts with the boundaries of the seismic plates can be noticed by comparing Fig. 2.5 and 2.10. One can concluded that both the active volcanoes and the earthquake epicentres are situated in the proximity of the tectonic plate boundaries. That demonstrates that the causes of earthquakes and volcanic eruptions are closely related with the general tectonic process of the world especially with the active faults.

The three main seismic belts of the Earth are identified in Fig. 2.10: the Circumpacific belt, the Transasiatic belt (Himalaya-Iran-Turkey-Mediterranean-Southern Spain) and the Mid Atlantic Belt.
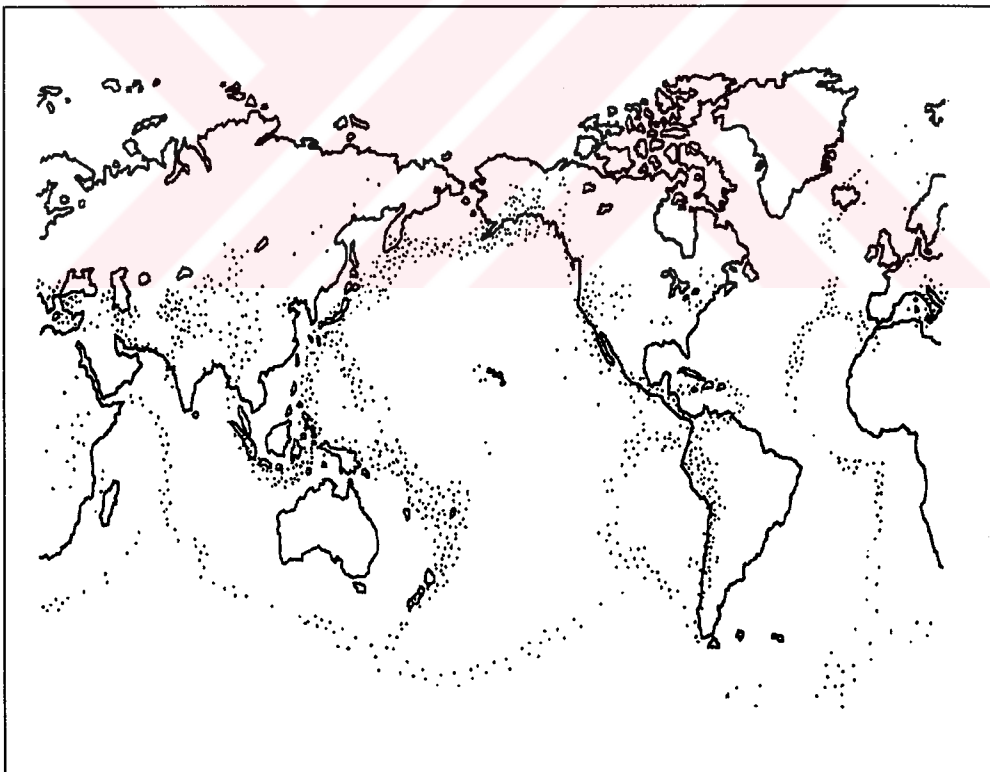
Figure 2.10 Epicentres of the principal earthquakes occurred in the mid 20th century (After Barzagni and Dorman, 1969)

2.6. Ground motion

2.6.1. Seismic waves

The displacement d(t), velocity v(t) and acceleration a(t) of the ground motion generated by the theoretical rupture of a fault at one point are illustrated in Fig. 2.11. It can be seen that the displacement is an impulse type of function. If the acceleration function is multiplied by mass of inertia, the load function can be obtained with the similar shape of acceleration function.

As the rupture propagates along the fault, a record of ground motion produced at certain distance will consist of a combination of elemental waves of the type is shown in Fig. 2.12.
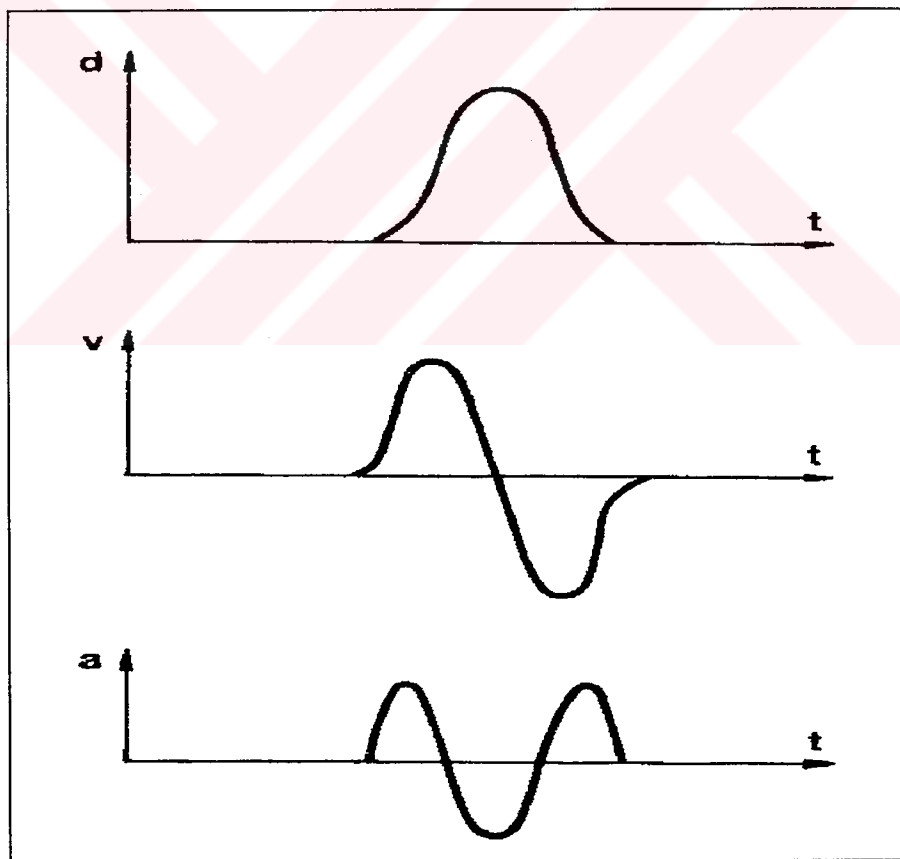
Figure 2.11 Seismic waves by theoretical rupture of a fault
(After Clough and Penzien, 1975)

16

Three types of seismic waves can be distinguished in the Earth's crust shown in Fig. 2.12 as follows:

- Body waves, that propagate through the Earth's mass.
- Surface waves, that propagate through the Earth crust.
- Free oscillations, which are produced only during very strong earthquakes and can be defined as vibrations of the Earth as a whole.

The body waves can be subdivided into primary waves (P) and secondary waves (S). (P) waves are condensation -refraction waves that involve volume changes; can travel across the solids and fluids. (S) waves are shear waves and do not imply volume changes; can not travel across a fluid part of the Earth.
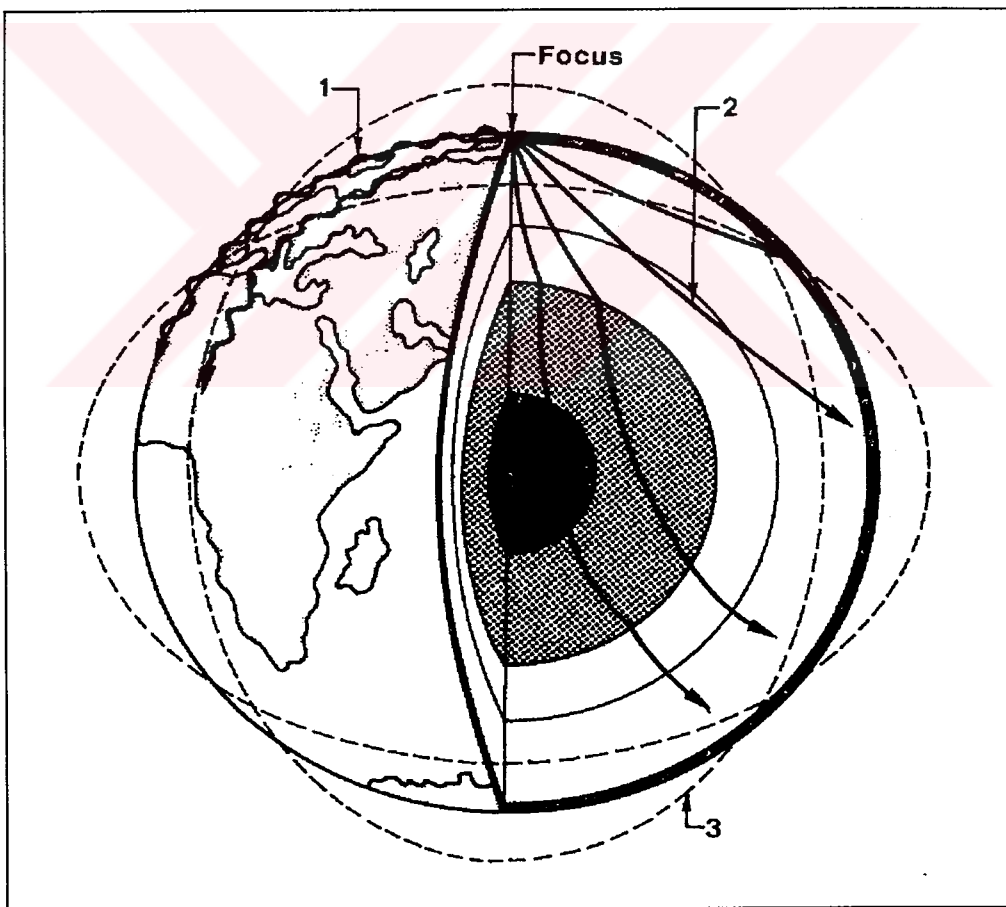
Figure 2.12 Types of seismic waves (1) surface waves; (2) body waves; (3) free oscillations (After McAlester, 1973)

There are two kinds of surface waves or P waves - Rayleigh waves (R) and low waves (L). R waves produce, as P waves do, volume changes, L waves propagate, the same as S waves, with a horizontal translation of the particles, normally in the direction of the wave motion.

The seismic waves reflect and refract when they hit an Earth discontinuity. This involves changes of the velocity of the waves. Fig. 2.13 illustrates these changes of velocity for both P and S waves. It can be noticed that P waves velocities vary between 7.5 and 13 km/s. But at the crust it may be considered that the P waves velocity is 7-8 km/s and that the S wave velocity 4-5 km/s. The surface waves have lower velocities 0.5-5 km/s, depending very much on the nature of the crossed Earth layer.
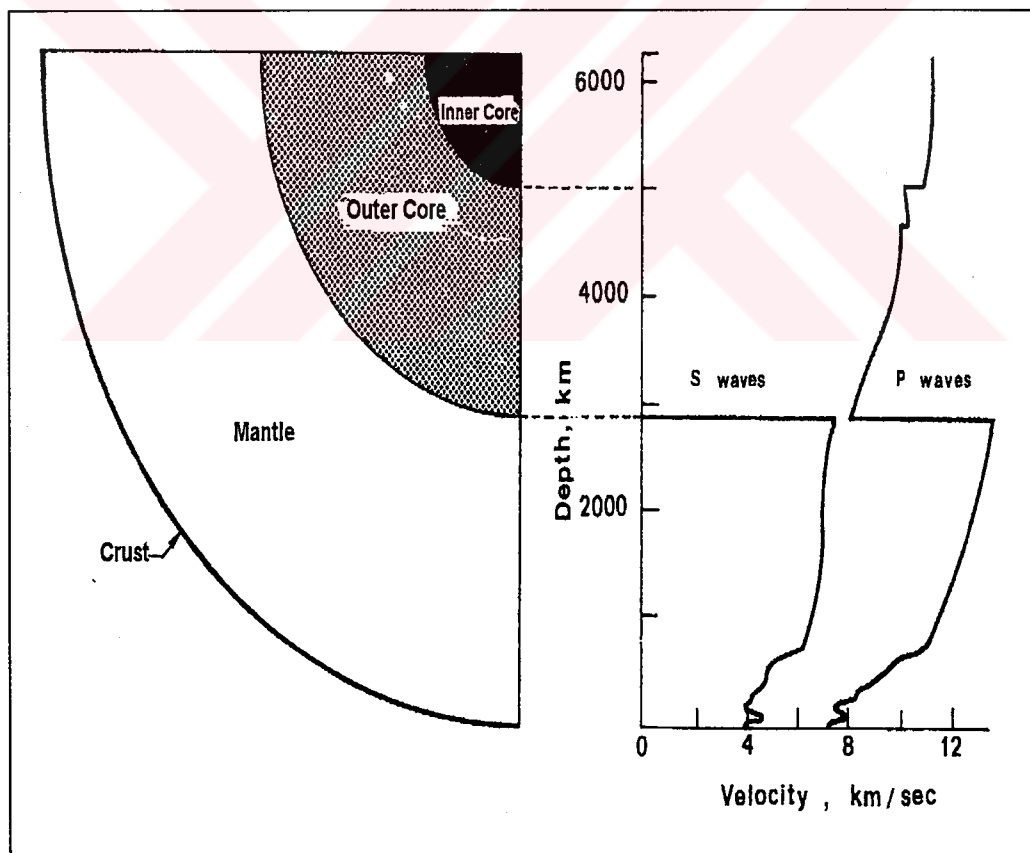
Figure 2.13 Variation of the velocity of P and S waves with the depth
(After McAlester, 1973)

From the elasticity theory, it can be deduced that the propagation velocity of the P waves is

$$v_p = \sqrt{\frac{\lambda + 2G}{\rho}} \qquad (2.1)$$

and that of the S waves is

$$v_s = \sqrt{\frac{G}{\rho}} \qquad (2.2)$$

where;

λ and G are Lame's coefficients,

v_p and v_s are the P and S waves velocity respectively,

Their expressions are:

$$\lambda = \frac{\gamma E}{(1-2\gamma)(1+\gamma)} \qquad (2.3)$$

$$G = \frac{E}{2(1+\gamma)} \qquad (2.4)$$

where E is Young's modulus γ is Poisson's ratio. The ratio of the velocities of the P and S waves is then:

$$\frac{v_p}{v_s} = \sqrt{\frac{2(1+\gamma)}{1+2\gamma}} \qquad (2.5)$$

Admitting for Poisson's ratio a mean value γ=0.25 equations (2.5) provides.

$$\frac{v_p}{v_s} = \sqrt{3} \qquad (2.6)$$

thus this equation(2.6) result demonstrating that P waves travel at higher velocity as compared to that of S waves.

2.6.2. Accelograms

The seismic ground motions symbolised as Q consist of a combination of P and S waves; the difference in the arrival time of P and S waves can practically be observed in some accelograms as a result of the difference of velocity between these two types of waves. In Fig. 2.14 the arrival times of the different types of waves are indicated.
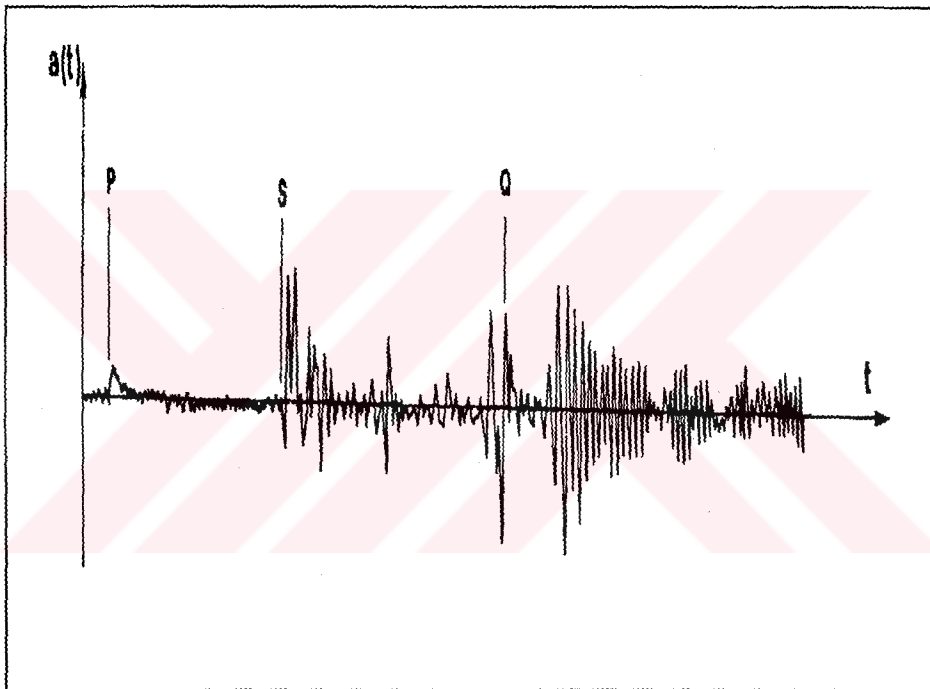
Figure 2.14 Kermadec earthquake , June 1957 (After Richter, 1958)
a(t)= acceleration of ground motion (m/s^2)

2.7. Seismic scales

Seismic study includes the effects of an earthquake upon structures and living beings and is related to the destructive potential of the ground motion. For this purpose, various scales have been established by measuring the intensity of earthquakes. The general intensity scale named as Mercalli Intensity Scale which is arranged by Richter (1958) with the scale consists of 12 intensity degrees is given in Table 2.1.

Table 2.1 Description of the modified Mercalli Intensity Scale
(After Richter, 1958)

D	Effects of earthquakes upon persons, structures and objects.
I	Not felt.
II	Felt only by persons placed favourably, especially on upper floors of tall buildings
III	Felt indoors by many people. Duration can be estimated.
IV	Felt indoors by many people. Outdoors is less perceptible. On the upper floors wooden walls and frames crack.
V	Felt outdoors by most of the people. Unstable objects displaced or upset. Direction estimated. Liquid disturbed. Pendulum clocks affected.
VI	Felt by everyone. Persons walk unsteadily. Windows and glassware break. Books and wall pictures fall down. Furniture moved or overturned. Weak masonry structures crack. Small bells ring.
VII	Difficult to stand. Noticed by drivers. Damage of weak masonry structures. Weak chimneys break at roof line. Cracks in ordinary masonry structures. Large bells ring. Fall of plaster, cornices, architectural ornaments, etc. Small slides of sand or gravel.
VIII	Car driver rendered more difficult. Partial collapse of ordinary masonry structures. Damage of good masonry structures, not design to resist seismic forces. Seismic designed masonry structures not affected. Fall of stucco and of some masonry walls. Fall of chimneys, towers, monuments, elevated water tanks, etc.
IX	General panic. Weak masonry structures destroyed. Ordinary masonry structures heavily damaged, sometimes collapsed. Good masonry structures seriously affected. General damage of the foundations of structures. Frame structures if not bolted, shifted off foundations. Cracks within the ground. Upon alluviated areas sand and mud spouts. Sand craters can appear.
X	Most masonry and framed structures destroyed, together with their foundations. Serious damage of dams, dykes, embankments. Large land slides. Rails bent slightly.
XI	Rails bent thoroughly. Underground pipelines completely out of order.
XII	Destruction nearly total. Large rock masses displaced. Objects thrown into the air.

2.7.1. Magnitude scale

While the previously described intensity scales were subjective, the magnitude provides an objective parameter of the seismic ground motion. The most popular objective scale is certainly the Richter (1958) one.

According to the definition given by the Richter (1958) the magnitude M is a dimension that measures the energy of an earthquake in the focus, and is expressed as the common logarithm of the seismic amplitude, given in microns at 100 km from the epicentre by a standard Wood-Anderson seismograph. The magnitude, M (in ergs), is correlated with the energy, E, in ergs of the earthquake by the expression:

$$LogE = 11.8 + 1.5M \qquad (2.7)$$

Rothe (1968) gives a graphic presentation of the equivalent energy Ee of different earthquakes measured in TNT tones, related to their magnitude M with two nuclear bombs has been included (Fig. 2.15).

The seismic moment M_o is a measure of earthquake power, which depends only on its source mechanism

$$M_o = K_S A\bar{u} \qquad (2.8)$$

where K_S is the shear stiffness (MPa/m), A is the fault plane area (m^2) and $\bar{u}$ is the relative displacement (m) between the two sides of the fault. A relationship can be established between the magnitude and the seismic moment (Jaeger and Cook, 1976).

$$LogM_o = 19.9 + M \qquad (2.9)$$

2.8. Occurrence frequency

The frequency N of earthquake phenomena is defined as the number of seismic of magnitude M, or greater that can occur in a unit of time. As stated in the definition, there is a close relationship between frequency and magnitude M:

$$LogN = A - bM \qquad (2.10)$$

where A and b are constants for a given zone. Kaila and Narain (1970) give values of these coefficients for different Earth zones.
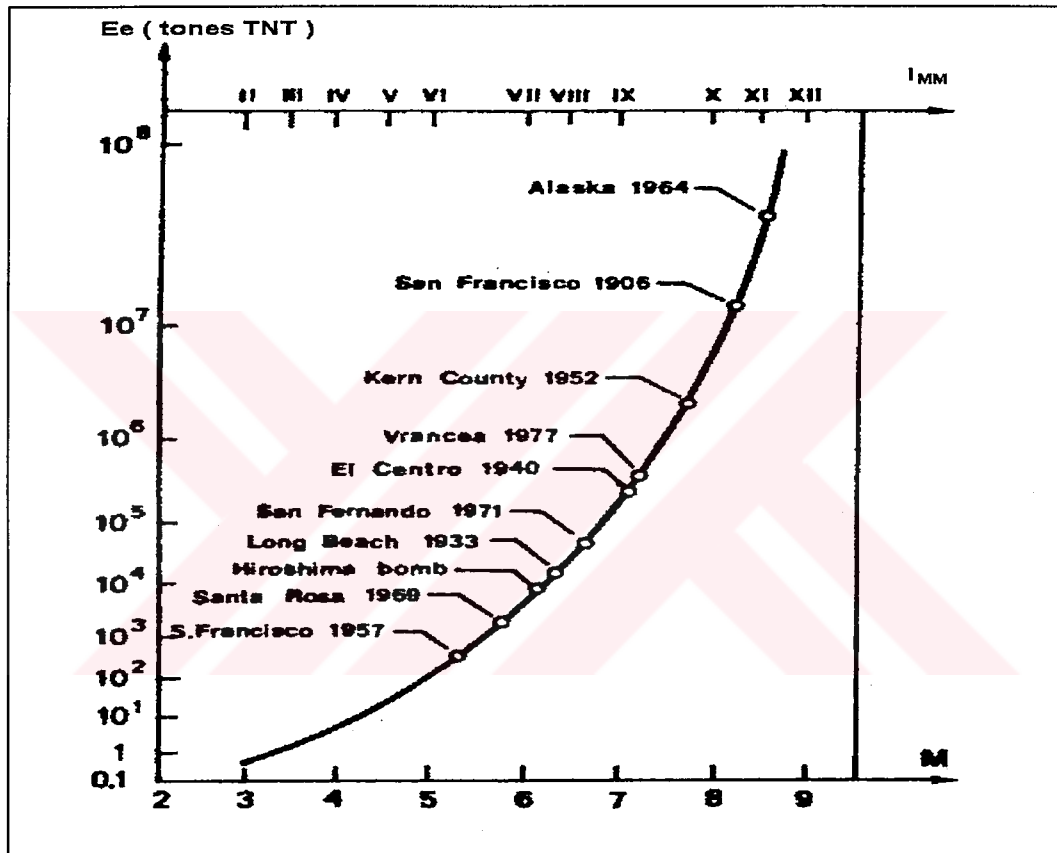
Figure 2.15 Epicentre energy (in TNT tons)- magnitude relation
(After Rothé,1968), I_{MM} = Modified Mercalli Intensity Scale

2.9. Seismic zone maps

Seismic zone maps represent a synthesis of the seismic data of an Earth or an area. The definition of the seismic activity by the help of mapping is one of the important subject of the seismology that provides data for earthquake engineering.

The most important data in connection with earthquakes, that must characterise their complete definition are the following:

- Data related to the fault- position, type, rupture surface.
- Data on the epicentres- location.
- Data describing the focus- depth, mechanism.
- Data on kinematics of the ground motion- displacement, velocity and acceleration records, or at least their amplitudes, predominant frequency.
- Duration of the main shock.
- Risk period and occurrence hour.

Certain investigations, have to be performed in order to build up the seismic risk map of a zone. They can be classified in the following groups:

i. Geological and geotechnical studies: They provide geologic maps of the zone under observation; in this respect the maps of the tectonic plates are particularly important. Moreover the dynamic properties of the earth's crust rock and soil layers are analysed.

ii. Seismological studies: The main objectives of these studies are to obtain seismic records in the area under analysis and perform their statistical process. Besides, they are meant to describe of maps containing the necessary information; epicentres maps; maps of data obtained directly from seismic catalogues; maps of the risk period; maps of the focal mechanism.

iii. Engineering and seismological studies: The effects of previous earthquakes upon structures and living beings of the area are analysed.

2.10. Earthquake prediction

2.10.1. General concept

Due to the destructive effects of the strong seismic motions and to their influence on living beings, it has became necessary to anticipate the seismic phenomena by reducing the seismic risk. Thus, it is necessary to predict the future seismic events in an expected area.

2.10.2. Time prediction

a. Subjective phenomena: this is the prediction of earthquake by monitoring the changes in the behaviour of animals (such as frogs, snakes, rats, dogs, pigeons). These activities are generally are organised in Japan and China under a scientific investigations.

b. Objective phenomena: The stages before the earthquake have been divided into three. After the earthquake an additional stage follows (Bolt, 1981). For the earthquake precursor the variation of five physical parameters have been observed by Bolt (1981). These are P wave velocity, soil Level modification, radon emission, rock resistivity and earthquake number. Their variation before, during and after an earthquake is indicated in Fig. 2.16.

2.10.3. Statistical prediction of characteristics of earthquakes

i. Empirical relations: Statistical analyses of the characteristics of observed earthquakes made possible empirical relations for the calculation of the magnitude and of the occurrence time of future earthquakes. Dambaru (Barbara and Canet, 1989) has developed an empirical relation by which one may calculate the magnitude M of an earthquake with respect to the mean radius r, in km, of the Earth zone affected by crust deformations in 1966.

$$M = 1.96 Log r + 4.45 \qquad (2.11)$$

Tsubakova (Rikitake, 1976) gave a linear relation which allows the establishment of the time t_e that remains until the occurrence of an earthquake of magnitude M, calculated up from the moment when important deformations are observed in the region

$$Log t_e = 0.79 M - 1.88 \qquad (2.12)$$

where the time t_e is calculated in days.

ii. Statistical studies: The statistical models constitutes a very powerful tool which can provide data on the characteristics of the future earthquakes useful in the numerical definition of the expected seismic actions. The

statistical distributions (Weinbull, log- normal, poison, etc.) are widely used in the prediction of earthquakes, with acceptable results.

	1st stage	2nd stage	3d stage		4th stage
	increase of the elastic deformation	rock fracturing	unstable deformations in the fault zone		stress decrease
P wave velocity					
soil level modification				earthquake	
rock resistivity					
radon emission					
earthquake number					
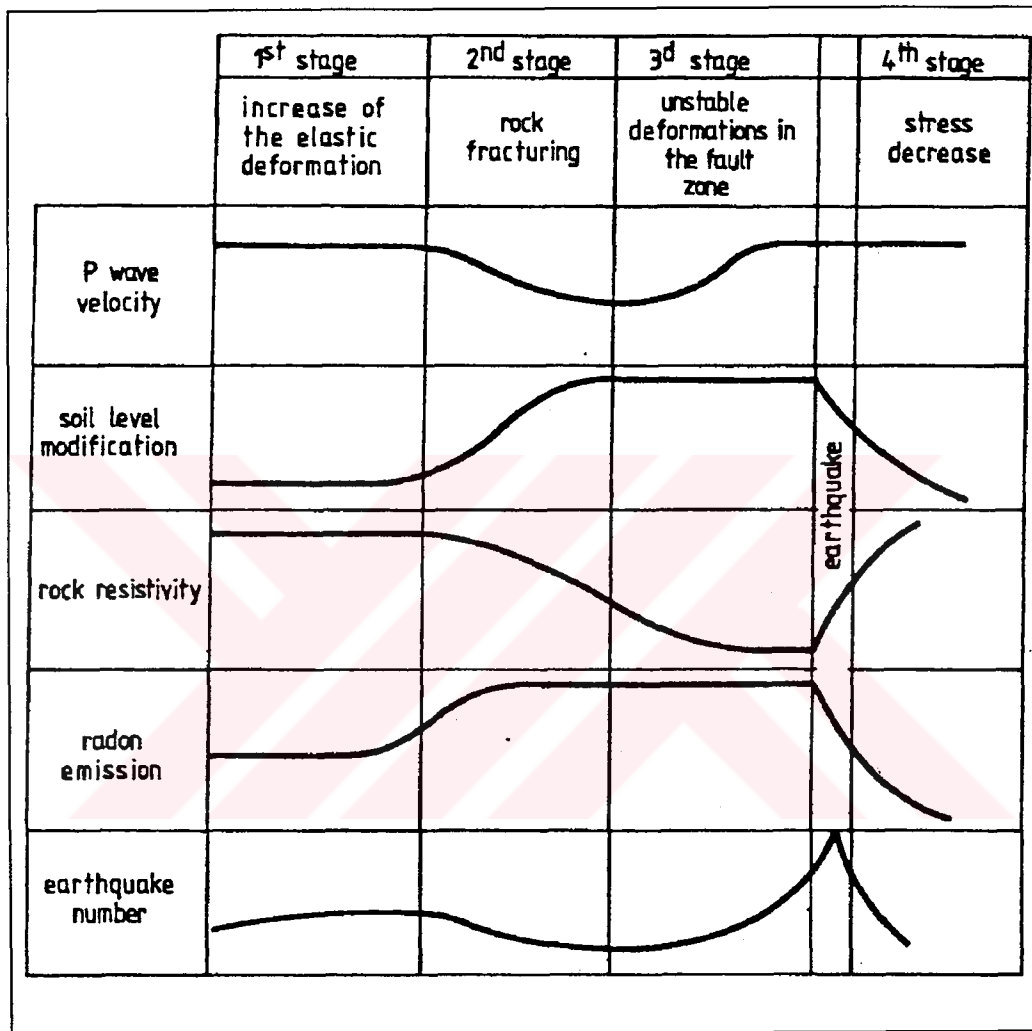
Figure 2.16 Physical parameters used in the seismic prediction (After Bolt,1981)

CHAPTER 3

A LITERATURE SURVEY ON THE PREVIOUS FRICTIONAL STUDIES
FOR THE SHALLOW FOCUS EARTHQUAKES

3.1. Introduction

The various aspects of the tectonic earthquake, (particularly shallow focus)
are widely investigated in the literature. Shallow focus earthquakes which are the
most common type of tectonic earthquakes are considered to be unstable sliding on
pre-existing faults. The investigations on the unstable sliding of faults is important
for the earthquake forecast because one can infer which fault or fault segment is
susceptible to cause seismicity based on the obtained results.

The strength of the upper part of the crust, mostly brittle region, is
governed by frictional strength along faults (Kohlsted et al., 1995). In other words,
the frictional sliding phenomena is the characteristic feature of the brittle structure
of the crust. Thus, experimental studies on the sliding behaviour of faults have been
gained much attention in understanding the mechanism of the shallow focus
earthquakes.

The first theory on how the sliding mode of the fault causes the earthquake
has been developed by Reid in 1910 (Tao and Zhang, 1990) which is called elastic
rebound theory. After Reid's theory, Bridgman (1936) has suggested the jerky
motion and sudden shear stress drops that accompany the shearing of rocks at high
normal stresses (approximately greater than 2 MPa) might be a possible mechanism
for the generation of earthquakes. Subsequently, Brace and Byerlee (1966)
elaborate on Bridgman's (1936) suggestion and propose that the stick-slip may be a
possible mechanism of earthquake occurrence. In addition to this, creep and
thermal softening instability have been also suggested as mechanism of earthquake
(Stesky, 1978). Recent studies also reveal that the sliding and/or sliding-rate
dependence of frictional strength plays an important role in the mechanism of

earthquakes (e.g. Ruina, 1983; Dieterich, 1994). Stability analyses of the fault model have been conducted at different material properties and load conditions in order to establish rate- and state- variable constitutive laws for the definition of different frictional regimes of seismogenic faults by many authors (e.g. Ruina, 1983; Linker and Dieterich, 1992; Hobbs and Brady, 1988; Dieterich, 1994).

Although there are numerous investigations on understanding the shallow focus earthquakes due to active fault (creeping) or locked fault segment (stick-slip), the mechanism of this phenomenon has not been fully understood.

In this chapter, a brief discussion of the mechanism of the shallow focus earthquakes investigated in the literature is included initially. Then, slip instability and variable frictional constitutive laws with the view toward the prediction of earthquake mechanism are reviewed extensively. Scope of the thesis is stated at the last section of the chapter.

3.2. Unstable sliding due to stick-slip

Motion on some part of the fault surfaces (such as North Anatolian Fault Zone (NAFZ) or San Andreas fault) can take place suddenly to produce earthquake. During this sudden slip, shear stress is relieved and fault surfaces may then remain locked together until, at a later stage slip takes place suddenly again. Such sudden motion on pre-existing faults in the Earth is similar to the sudden motion that has been observed during frictional sliding between rock surfaces in the laboratory experiments (Byerlee, 1970).

Since the suggestions by Bridgman in 1936 (Dieterich, 1972) and Brace and Byerlee (1966) that stick-slip friction on sliding interfaces provided an explanation for earthquake, much experimental study has been done on the examination of the detailed frictional behaviour of fault and rock in the laboratory. Within this view, the stick-slip phenomena will be discussed in this section. The concept of stick-slip explaining the earthquake mechanism is explained by Bro (1992) as follows:

i. The stick-slip phenomenon is easily observed from the standard direct shear test. During a direct-shear test, the shear load may drop with a

28

remarkable amount. The instability can be explained by asperity fracture or stick-slip. If stick-slip is the cause, the shear is accompanied by a reduction in the friction angle and a rapid acceleration of the sliding block, followed by deceleration. The elastic strain energy that was stored in the loading system, becomes unbalanced when the friction angle drops from its static value to its dynamic value. Depending on the load levels, friction angles, shearing rate, the shear load drop can vary from a small up to a significant proportion of the peak load. Continued shear, results in gradually reduced shear stress oscillations.

ii. This phenomena can be explained by an example of sliding block on an inclined table. If a smoothed faced block is placed on a smooth inclined surface, the block will start sliding at an inclination that is equal to the static friction angle. The angle of the plane at which the block velocity remains slow but constant is the dynamic friction angle. These two angles form the basis of stick-slip analyses. The transition from the static to dynamic friction angles is sudden; it is commonly approximated by a step function.

iii. The stick-slip model can also be explained by a massless shear spring model (Fig. 3.1). The shearing process starts with no shear load and a constant average velocity V_{avg}. At some spring extension, the force in the spring reaches a maximum value (F_s) as shown in equation (3.1). Upon reaching the maximum value of load, the previously immobile block starts moving and the friction angle drop to its dynamic value.

$$Fs=(Fn+mg) \tan\phi s \qquad\qquad (3.1)$$

in which

    Fs = Shear force (kgf)

    Fn = Applied normal force (kgf)

    m   = Mass of the Block (kg)

    g   = Gravitational Acceleration (m/s^2)

    ϕs = Static Friction Angle (°)
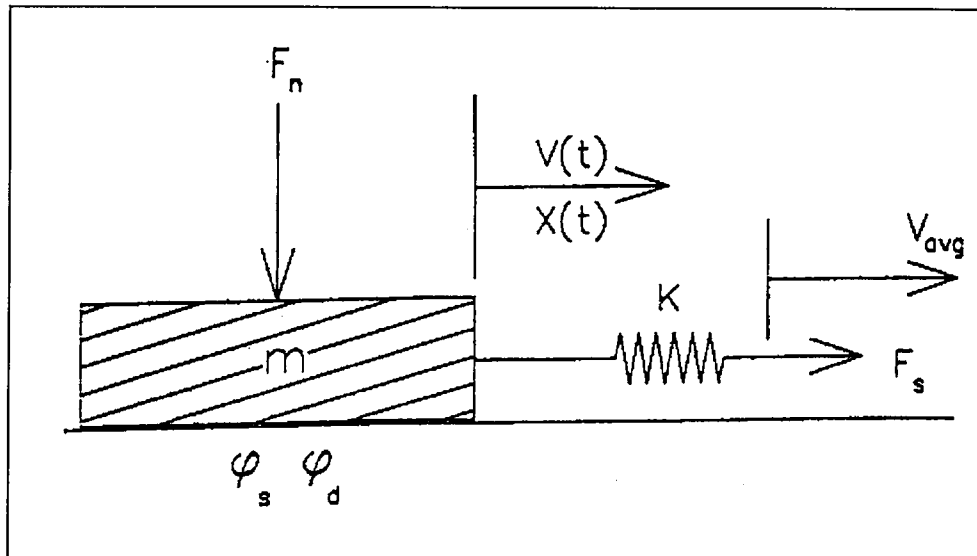
Figure 3.1 Direct shear stick-slip model (After Bro, 1992)

The force imbalance created by the reduced friction angle accelerates the block along the plane of sliding. As the block moves, the shear force diminishes, the block decelerates and finally comes to rest. Once the block stops, the static friction angle re-establishes, and with time the cycle is repeated. The dynamic potion of the stick-slip is defined by the second-order differential equation. The formulation and solutions of the governing equation is presented in Bro's (1992) article as follows:

$$\ddot{X}(t) + A^2 X(t) + B(t) + C = 0 \qquad (3.2)$$

where as:

A^2 = K/m,

B = -KVavg/m,

C = Fn+mg tanϕd - Fso,

K = Shear spring stiffness (kgf/m),

m = Block mass (kgf),

g = Gravitational acceleration (m/s^2),

V_{avg} = Average velocity (m/s),

Fn = Applied normal load (kgf),

Fso = Shear force on the block at the start of the slip (kgf),

30

ϕ_d = Angle of dynamic friction (°),

X(t)   = Position of the block measured from the start of slip (s),

t   = Time measured from the start of the slip (s),

with a solution:

$$X(t) = \frac{C}{A^2}Cos(At) + \frac{B}{A^3}Sin(At) - \frac{Bt+C}{A^2} \tag{3.3}$$

$$V(t) = -\frac{C}{A}Sin(At) + \frac{B}{A^2}Cos(At) - \frac{B}{A^2} \tag{3.4}$$

Slip ceases when velocity becomes zero and the static friction angle is re-established. This condition occurs at:

$$t = \frac{2}{A}Tan^{-1}\left(-\frac{AC}{B}\right) \tag{3.5}$$

From the block displacement and the average velocity (Vavg), the shear force can be calculated from the expression:

$$Fs(t) = F_{SO} - K(V_{avg}t - X(t)) \tag{3.6}$$

$$Fs, min = Fn\,Tan(\phi s) + 2\frac{Ks}{A^2}\left[C + \frac{B}{A}Tan^{-1}\left(-\frac{AC}{B}\right)\right] \tag{3.7}$$

3.3. Instability due to thermal softening

Some authors have stated that the thermal softening could be the earthquake mechanism. Stesky (1978) showed that during sliding there is an increase in temperature at sliding surfaces. In steady sliding experiments using granite or sandstone samples at room temperature, the friction coefficient is observed to decrease when slip velocity increases (Dieterich, 1978). This lead to the idea that kinetic friction could be less than static friction of the surface because the temperature rise during rapid sliding may lower the strength of the material. At higher temperatures (approximately >300 °C), however the friction coefficient is observed to increase as slip velocity increases (Stesky, 1978). This seems to be the

31

semi-brittle field (300-400 °C) corresponding to the onset of plasticity in quartz. The increase in friction shows the stable sliding.

It has been proposed that this mechanism of thermal softening may be mechanism for deep-focus earthquakes (Orowan, 1960). Earthquakes still occur to a depth of about 700 km. At depth of this order the instability may be caused by thermal softening as suggested by the above authors.

There are at least two reasons why this mechanism can not explain the instability that may occur during sliding between rock surfaces at room temperature. First reason is that, the examination of the surfaces of brittle materials after sudden slip has shown that wear particles produced during sliding in experiments at room temperature are produced by the brittle fracture of the rocks (Byerlee, 1970). Secondly, there is no evidence to indicate that the temperature during sliding has been high enough for melting to occur.

From the investigations on the thermal softening instability it can be stated that thermal softening does not appear to be important factor at temperatures up to 300 °C for brittle sliding. On the other hand, sliding surface within the brittle and semi-brittle fields at high slip rates causes frictional heating and hence, this results in a reduction in friction due to the surface melting or pore fluid expansion. The high slip-rate phenomena correspond to the co-seismic (instant of the earthquake occurrence) deformation (slip rates of $0.1-2$ ms^{-1}). The study of this phenomena is important for relating earthquake magnitude to fault sliding modes.

3.4. Instability due to creep

Some researchers claimed that the two surfaces of the rock slip steadily at a relative velocity equal to the load point velocity (sliding rate). This sliding mode is usually referred to as stable sliding in the laboratory and it is an analogue of fault creep (Byerlee and Summer, 1976). The creep theory which is originally proposed by Ishlinski and Kragelsky (1944), reveals that static friction is a function of the time of contact between surfaces. The model for this theory is that when the block is at rest, the junction at the point of contact between the surfaces deform by a creep mechanism so that the area of the junctions increase with time. During rapid

sliding, the time of contact is so small that junction growth does not occur; so that the force required to shear the mobile block is lesser than the block which is at rest.

An objection by Byerlee and Brace (1968) to the creep theory is that, the force required to shear the junctions is determined not only by their size, but by the shear strength of the material as well. If the compressive strength of the material is high, so that junction growth is inhibited. Thus, it should make no difference whether the junctions are large and weak or small and strong, the friction should be the same in both cases.

A test of this theory for rocks was made by Byerlee and Brace (1968). In their experiments, cylindrical specimens of granite with saw cut surface oriented at an angle of 30° to the axis of cylinders were subjected to confining pressure. Frictional sliding on the saw cuts was studied as a function of the rate. In each experiment, sliding was by violent stick-slip. At the largest loading rate, the time of stationary contact between sudden slips was several minutes; at the slowest loading rate, several hours. It was found that there was no correlation between the force required to initiate sudden slip and the time of stationary contact between surfaces. And this observation is contrary to what the creep theory would predict, the instability in these experiments must be due to another mechanism.

The effects of the period for which surfaces are in stationary contact under high normal stresses have been studied by Dieterich (1972), using a fine - to medium - grained sandstone. He has found that the friction characteristics are found to be determined primarily by surface finish and only weakly related to the type of rock.

3.5. Stable sliding (creep) to stick-slip transition

At very low normal stress, stable sliding occurs without stick-slip. As normal stress is increased, a smooth transition from creep to stick-slip occurs. Byerlee (1970) has found the transition, at normal stress, range from a few bars to about 15 bars in their experiments. Brace and Byerlee (1970) have shown that the transition stress (normal stress) depends quite strongly on the rock type, temperature and amount of gouge present. Scholz et al. (1972) have objected this

and they stated that the variation in the transition stress depends quite on sliding surfaces.

From Dieterich (1972) experiments, stick-slip was observed for all rock samples at all normal stresses, 2 to 85 MPa, only if there was an accumulation of gouge.

Byerlee and Brace (1968) found the magnitude of the stress drop to be independent of the stiffness of the test arrangement in stick-slip experiments on finely ground surfaces of granite at high confining pressures. This suggests that the coefficient of dynamic friction is independent of the displacement between the two surfaces. It is difficult to explain how the coefficient of friction drops suddenly from its value and then remains constant. Byerlee (1967) proposed that when two surfaces are contact, the asperities become locked together and at high normal stresses, sliding can only occur in brittle manner. This could account for the apparently abrupt change in the coefficient of sliding friction from its static value to dynamic value.

The transition from creep to stick-slip has also been observed at the field studies, particularly at San Andreas fault. The transition from creep to stick-slip is observed at the north and south part of the fault (the creeping process is seen in the central part of the fault). This can be due to increase in normal stress moving from the centre to south or the north; this may be due to a change in lithology or some other fault characteristics. On the other hand, the value of the transitional stress is much larger for actual faults than for the investigated specimen in laboratory.

It can be also concluded that if a creeping fault is closer to stick-slip (In other words, in episodic mode) or transition stress level, a major earthquake can occur there at any time; since the shear stress required to cause stick-slip is nearly the same as that required to cause creep or stable sliding. This is observed at the faults near to the San Andreas fault.

As far as the above discussions are concerned, the creeping zone or transition zone from creep to stick-slip occurs in the brittle part of the Earth crust. The transition level from creep to stick-slip may be said a qualitative rather than quantitative because the exact point for the transition could not be predicted by the

previous investigators. They've mentioned that with polished or ground surfaces of brittle materials up to 300 °C temperature, the sliding is stable if the normal stress is low (this is not a quantitative value), but unstable if the normal stress is high. As the previous investigations have not reveal out the stress at which the transition takes place, the exact depth that the earthquake originates can not be predicted at present. The experimental studies on this subject have to be correlated with the field measurements in order to be certain on the transition stress between unstable and stable sliding of natural seismogenic faults in the Earth crust.

3.6. Fault and variable friction laws

For a fault to exhibit unstable slip (seismicity), the sliding resistance must decrease with displacement. In other words, the frictional surface or gouge layer, the temperature and the rate of sliding; Even a small changes in the coefficient friction are important in determining stability. Previous analysis indicates that slip weakening is a critical condition for unstable or seismogenic slip (Stesky et al., 1974; Tse and Rice, 1986). Thus, many laboratory experiments have focused on understanding the evolution of the coefficient of friction with either slip displacement or slip rate and with the state of the surface (e.g. Tullis, 1986; Beeler et al., 1994).

The analyses of frictional sliding of rock and fault, and rupture nucleation performed by Dieterich (1972, 1978, 1981, 1994) have led to a new focus in geophysics and rock mechanics: the resulting rate- and state- dependent frictional laws have given some hints for the study of seismogenic faults. The behaviour in which the friction decreases with sudden increase in load point velocity (assuming that the velocity at application point is equal to the system sliding) is called velocity weakening. If the behaviour in which the friction increases from the nominal steady state value with increasing sliding velocity (load point velocity) it is called velocity strengthening. This variation of friction during sliding can yield a dynamic instability noticed by a sudden shear stress drop and seismic slip for velocity weakening; for the velocity strengthening the model yield a stable sliding which can also be named as aseismic slip. The details of this frictional law will be discussed in the section of 3.6.1.

3.6.1. Rate- and state- dependent friction laws

In this section, the rate- and state- dependent (or Dieterich-Ruina rate- and state- variable friction laws) constitutive laws will be discussed in order to define the different frictional regimes of the tectonic faults. These laws are derived from laboratory fault model experiments (velocity-stepping tests). For better understanding of these constitutive laws, the general observations from the typical velocity-stepping experiments (see Fig. 3.3) are summarised as follows:

i. At the beginning of the experiment, the coefficient of friction, μ, evolves a steady state value depending on the nominal slip velocity, V_O, at a constant normal stress, σ, and fixed load point velocity (assume that it is slip velocity of the system, V_O).

ii. After reaching the steady state conditions a step increase in load point velocity is imposed. In response to an imposed step increase in velocity, the resistance to sliding increase suddenly from steady state value μ_1 an amount "a" but then decays to steady state friction value μ_2 an amount "b" (see Fig. 3.2) as sliding proceeds with the increased load point velocity, V_1, . As it can be seen from Fig. 3.2 the decay roughly follows an exponential with characteristic displacement noted as Dc.

iii. The response of the coefficient of friction to a step decrease in load point velocity is fairly symmetric to that observed in response to a velocity increase.

The constitutive equations of Dieterich-Ruina (Tullis, 1988) which is the most commonly used formulation of the velocity dependent behaviour of the frictional sliding experiment are given as follows:

Shear stress τ is normalised by normal stress σ to give

$$\mu^* = \frac{\tau}{\sigma} \tag{3.8}$$

where μ^* is the constant reference value of the coefficient of friction (Steady state coefficient of friction)

Equation (3.8) has the transition dependence of velocity increase

$$\tau = \mu * \sigma + a\sigma \ln\!\left(\frac{V}{Vo}\right) + b\sigma \ln\!\left(\frac{\dot{\theta}}{\theta *}\right)$$ (3.9)

where;

a is the amplitude of friction due to the sudden step increase of load point velocity effect (see Fig.3.2)

b is the amplitude of friction due to the sudden increase of load point velocity delayed effect (see Fig 3.2)

"a" and "b" constitutive parameters those obtained from the experimental study

θ is scalar variable that represents the state of the sliding surface (it will be explained in detail in the following paragraph)

$\theta*$ is constant reference value (steady state value of θ)

Vo is constant load point velocity

V is the load point velocity
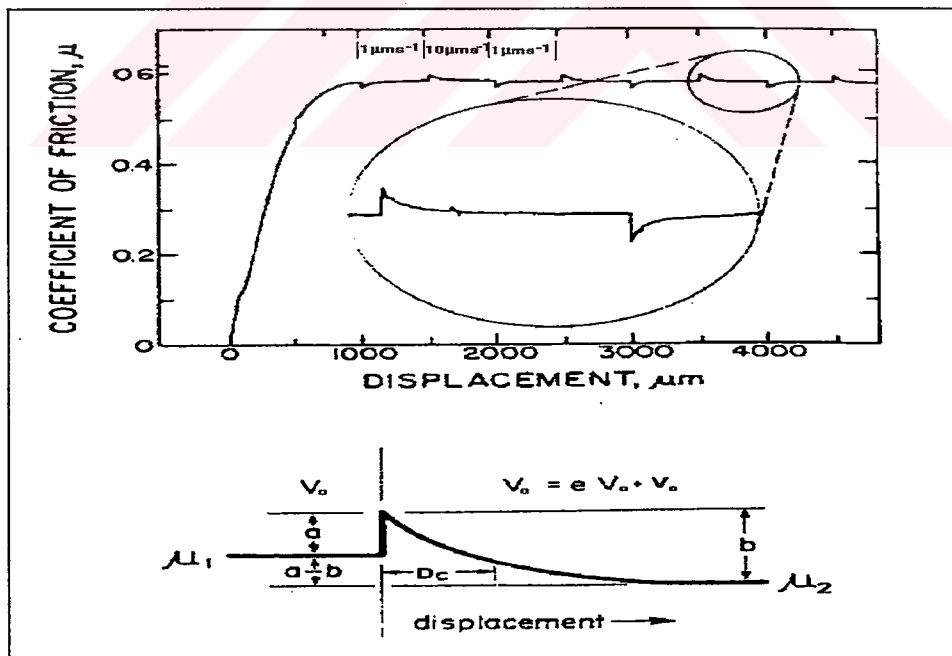
Figure 3.2 Data from typical velocity-stepping test (e is step increased in velocity)

The variation of θ is governed by evolution laws which have been proposed in two forms:

i. The variation in θ with slip, δ, at fixed normal stress:

$$\left(\frac{\partial \theta}{\partial \delta}\right)_{\sigma=constant} = \frac{1}{V} - \frac{\theta}{D_c} \qquad (3.10)$$

and

$$\left(\frac{\partial \theta}{\partial \delta}\right)_{\sigma=constant} = -\frac{\theta}{D_c} \ln\left(\frac{\theta V}{D_c}\right) \qquad (3.11)$$

Where;
δ is the slip or displacement (shear displacement)
Dc is the characteristic decay distance (see Fig. 3.2)
V is the load point velocity

ii. At steady state $\frac{d\theta}{dt} = 0$, and both equations (3.10) and (3.11) yield

$\theta^{ss} = \frac{D_c}{V_o}$ (where θ^{ss} is the steady state of the sliding surface)

The solutions of θ under the condition of constant load point velocity are:

$$\theta = \frac{D_c}{V_o} + \frac{\theta^{\bullet} - D_c}{V_o} \exp^{\frac{\delta^{\bullet}-\delta}{D_c}} \qquad (3.12)$$

and

$$\theta = \frac{D_c}{V_o} + \frac{\theta^{\bullet} V_o}{D_c} \exp^{\frac{\delta^{\bullet}-\delta}{D_c}} \qquad (3.13)$$

where;
δ is the shear displacement
$\delta^{\bullet}$ is the shear displacement
$\theta^{\bullet}$ is the steady state value of θ

V_0 is the constant load point velocity

Dc is the characteristic decay distance

For a fault to exhibit unstable slip (seismicity), the sliding resistance must decrease with displacement. The simplest representation of this behaviour is the slip weakening model. Furthermore, for a fault to exhibit repeated unstable slip, some healing process must also take place. The rate- and state-dependent friction laws not only yield slip weakening, whenever the stress is greater than some reference value, but also result in time-dependent healing of the fault, whenever the shear stress is less than that reference value corresponds to steady state sliding.

These constitutive equations (from (3.10) to (3.13)) involving sliding history (θ) and velocity have been used by many authors in order to analyse and explain experimental rock friction behaviour and to simulate many aspects of seismicity on faults in the Earth (e.g. Dieterich, 1978,1979; Ruina, 1980,1983; Weeks and Tullis, 1985; Beeler et al., 1994; Cox, 1990; Boatwright and Cocco, 1996).

One of the most important aspect of these equations is the prediction of the unstable sliding of fault model under constant normal stress conditions in laboratory. However, these equations can not be used to explain the frictional behaviour after the onset of instability. These laws can be applied to model which has a load point velocity less than 100 μms^{-1}; may not be accurate at higher slip rate (Weeks,1993)

3.6.2. Frictional behaviour of seismogenic faults

Since the idea that seismic instabilities can be modelled and predicted based on the frictional sliding experiment results, the earthquake mechanism has been extensively exploited by numerous workers considering the rate- and state-dependent constitutive equations mentioned in section 3.6.1. Some of the investigations will be briefly discussed in the following paragraphs.

The behaviour of fault within the brittle and semi-brittle fields are studied and these fields are characterised by the rate- and sate- dependent friction parameters "a" and "b" (see Rice and Ruina, 1983). In the relatively low

temperature (approximately >300 °C) Brittle field, a-b value is negative and friction is velocity weakening. This gives rise to abrasive wear, unstable sliding and stick-slip behaviour. For the semi-brittle field (approximately 300-400 °C), a-b is positive and friction is velocity-strengthening, This leads to plastic flow, adhesive wear and more stable sliding.

The slip rates effect on the frictional sliding of the fault (rock) is also investigated by the previous researchers. The slip rate phenomena is classified into low and high slip rates according to the field observation of the earthquake fault motion (Spray, 1989). The low slip rate phenomena correspond to post- (after the earthquake), inter- or pre-seismic (before the earthquake) deformation. This equates with the movement at or less than the plate tectonic slip rate for active faults (e.g. San Andreas Fault rate is 30-32 mm/yr and North Anatolian Fault Zone is 100-110 mm/yr (Kiratzi, 1993)) and somewhat faster than this for most laboratory experiments, but still at considerably less than co-seismic slip rate, slip rates Of 0.1-2.0 ms^{-1} during the earthquakes, (Spray, 1989). The load point velocity (sliding rate) classification in seismogenic fault is shown in Fig. 3.3.
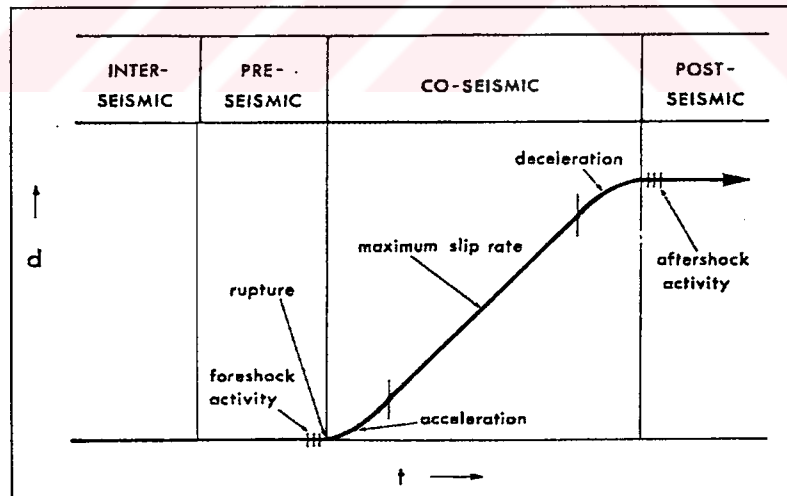
Figure 3.3 Idealised sliding velocity in seismogenic fault (After Spray, 1989)
d=load point velocity in μms^{-1}, t=time in second

The study of slip rate processes is critical for understanding earthquake prediction (Tullis, 1988). On the other hand, the study of high slip-rate processes is important for relating earthquake magnitude to rock type and fault sliding or fault surface conditions. The works of Scholz (1990) which consider gouge evolution, are concerned with essentially brittle-field effects where a-b is negative; whereas the works of Chester, (1988) deal with brittle and semi-brittle phenomena where a-b can be negative or positive. At higher slip rates (i.e. during co-seismic slip), the dependence of the frictional resistance on velocity becomes less apparent and some workers claim that friction becomes independent of velocity (e.g. Okubo and Dieterich, 1986).

Tse and Rice (1986) modelled the process of strain release on vertical strike-slip faults to show how the depth dependence (brittle or semi-brittle zones) of the friction influences the phenomenology of earthquake mechanism. They have showed how progressive slip can penetrate in the aseismic (velocity strengthening) section of the fault due to failure of the seismic part of the fault segment dynamically. They have showed the post-seismic slip on the steady inter-seismic slip. Scholz (1990) discusses the depth variations of frictional behaviour and fault segment creep, identifying the stability transitions at different depths.

Weeks (1993) has mentioned that an instantaneous change in slip velocity, from V_0 to V_1 causes a change in the frictional resistance in the form of $\Delta\mu = a\ln\left(\dfrac{V_1}{V_0}\right)$. As he has considered only one state variable "a", he has used the equivalent version of the constitutive equation (equation (3.14) from Rice and Tse (1986)):

$$\frac{d\mu}{dt} - \frac{a(V)}{V}\frac{dV}{dt} = \frac{V}{D_c(V)}\left[\mu - \mu^{ss}(V)\right] \qquad (3.14)$$

Here the state variable and parameter "b" have been eliminated and steady state dependence of friction on velocity is written explicitly. In equation (3.14), μ is coefficient of friction, V is slip velocity at the sliding surface, "a" is the strength of the instantaneous velocity dependence, D_c is the characteristic length associated with evolution toward steady state (see Fig. 3.2) and μ^{ss} is the steady state coefficient of friction. Values of D_c, a and μ^{ss} depend on velocity (V).

41

On the other hand, Chester (1988, 1994) incorporated temperature into the so-called Dieterich-Ruina constitutive law which was built on laboratory observations showing that frictional strength depends both on slip rate and on the recent history of sliding. In adding temperature, Chester (1994) retained the rate and state- dependence of the earlier law:

$$\mu^{ss} = (a-b)\ln\left(\frac{V}{V_o}\right) + \mu^* + \frac{aQ_a - bQ_b}{R}\left[\frac{1}{T} - \frac{1}{T^*}\right]$$ (3.15)

where Qa and Qb activation energies in kJ/mol, T is temperature in Kelvin, R is gas constant.

The steady state velocity dependence of friction in fixed temperature is:

$$\frac{\partial\mu^{ss}}{\partial\ln V} = a - b$$ (3.16)

such that positive values of a-b indicate "velocity strengthening", and the negative values of a-b indicate "velocity weakening". The steady-state temperature dependence (at fixed slip rate) is most conveniently given in terms of inverse temperature:

$$\frac{\partial\mu^{ss}}{\partial T^{-1}} = \frac{aQ_a - bQ_b}{R} = \left(a - b\frac{Q}{R}\right)$$ (3.17)

such that positive values indicate temperature weakening, and negative values temperature strengthening (Chester, 1994).

Blanpied et al. (1995) have studied the sliding on faults in the continental crust at hydrothermal conditions at elevated temperatures and under the pressures of aqueous pore fluids. They've measured the strength, sliding behaviour and friction constitutive properties of faults at hydrothermal conditions on granite with simulated gouge. They've performed velocity stepping experiments at temperatures of 23 to 600 °C, pore fluid pressure of P_{H_2O} = 0 (dry) and 100 MPa (wet), effective normal stress of 400 MPa, and sliding velocities V_0 of 0.01 to 1 μms^{-1} (approximately 0.32 to 32 mm/yr).

Linker and Dieterich (1992) have performed frictional sliding tests concerning the velocity and stress change. In the first type, step changes in load point velocity are imposed and the normal stress is held constant for the duration of the test. This is the standard velocity stepping test that has been performed by other workers (Dieterich, 1979, 1981; Ruina, 1983; Weeks and Tullis, 1985). The slip rates are ranged from 0.05 to 2.0 μms^{-1}, and the imposed changes in slip rate increase are one decade. Their observations are consistent with the other workers. As all the workers have observed in response to a step increase in load point velocity, the shear stress rapidly increases and then decays to a new, steady value as sliding proceeds. The decay to steady state shear stress roughly follows an exponential with a characteristic displacement, Dc, of about 1 to 2 μm.

The other test that Linker and Dieterich (1992) have performed is normal stress step tests consisting of a step change in normal stress during sliding at fixed load point velocity of 1 μms^{-1}. They have observed that sudden normal stress step significantly affects the coefficient of friction for one rock type at one nominal normal stress and one slip rate (specifically westerly granite at a normal stress of 5 MPa and a slip rate of 1 μms^{-1}).

The same type of stress variation experiments have been also conducted by the other authors (e.g. Hobbs and Brady, 1985; Lockner et al., 1986 and Olsson, 1988). The experiments of Hobbs and Brady (1985) have been conducted on gabbro, the experiments of Lockner et al. (1986) have been conducted on westerly granite with a layer of gouge, and the experiments of Olsson (1988) have been conducted on welded tuff. Lockner et al.'s (1986) experiments are performed at a normal stress of 50 MPa, while those of Olsson's (1988) are performed at 2 to 6 MPa.

Boatwright and Cocco (1996) have modelled the lateral variations in fault friction using a rate- and state- dependent friction law. They have prepared a phenomenological classification according to the modelled fault frictional properties. They have also tested this frictional model by comparing the seismicity and co-seismic slip for the 1966 Parkfield, 1979 Coyote Lake, and 1984 Morgon Hill earthquakes.

Some of the investigators has stated that whatever the fault and whatever the fault location, stresses in the Earth crust acting on the faults vary with the time suddenly or in an increasing mode.

A stress perturbation which means the variation of the field stress (regional nominal stress) are termed as the co-seismic stress by the previous researchers (e.g. Dieterich, 1994). These are generally occurred by aftershocks of the large scale earthquakes.

Significant geologic and artificial (induced) events which could change the value of the field stress often change the rate of earthquake occurrence. Examples to this, include earthquake associated with magma intrusion, changes of effective stress related to impoundment of reservoirs and fluid injection into deep wells, nuclear bombs (Jaeger and Cook, 1976). Mavko et al. (1985) have investigated the effects of the nearby earthquakes of San Andreas fault. They have stated that the earthquake around the San Andreas fault has an immediate effect on creep rates and co-seismic change in normal and shear stress. In this case even the change in normal stress exceeded the change in shear stress by at least a factor of 2.

3.7. Scope of the thesis

From the literature review, it is revealed out that the major focus in the laboratory studies and numerical simulations have been to describe the problem of the earthquake mechanism of the tectonic type under constant stress boundary conditions. In other words, the most of the investigations are on studying the frictional behaviour of the earthquake faults with depth dependence parameters such as normal stress (at different normal stress level but constant during test period), hydrothermal and temperature conditions and other parameters. Most of the proposed model for understanding earthquake mechanism are depended on constitutive rate- and state- dependent parameters which are closely related to sudden (step) changes of sliding rate of the fault.

On the other hand, the effects field stress (sudden change in the regional field stress) on the earthquake fault mechanism have not been investigated in detail. However, the side effects, the lateral variations of friction and shear strength due

to sudden changes of field stresses, are similarly important as well as the frictional variation depth.

In this study, it is aimed to predict the shallow focus earthquake mechanism by experimental and numerical approaches. In the light of the above cited facts; it is clear that the study covering the missing or overlooked points, in the field of shallow focus earthquake mechanism, is required and important for the prediction of earthquake. Therefore the following items are studied:

i. The effect of co-seismic type of field normal stress variations on the seismogenic fault model. It is performed in two groups:

- The effects of stepwise normal stress change on the seismicity of faults.
- The effects of functional normal stress change on the seismicity of faults.

ii. The effect of sudden change of simultaneous normal and shear stresses on the seismogenic fault surface in functional form.

iii. Estimation rate- and state- dependent empirical parameters of this model. They are compiled from the results of the velocity-stepping experiments.

To conduct the above studies, a computer controlled direct-shear test apparatus is developed and fabricated and also validation of the new apparatus is checked by the direct-shear tests according to ISRM standards (Brown, 1981).

In order to support the experimental fault model results, the numerical simulation with the distinct element method is used extensively. At the final stage of this study, an approach to predict the shallow focus earthquake mechanism is established according to phenomenological and stability criteria.

CHAPTER 4

COMPUTER CONTROLLED DIRECT-SHEAR APPARATUS

4.1. Introduction

The importance of rock friction as a controlling factor of fault seismicity has been pointed out by many researchers. Notwithstanding the considerable amount of laboratory work on this subject, much is still not understood about the parameters affecting rock friction, and a number of recent studies have been directed toward delineating possible sources of variations in friction experiment as mentioned in previous review chapter.

Most testing machines in common use for frictional studies have serious design drawbacks which limit their utility and introduce difficulties in comparing results obtained with different methods.

The two methods in common use for frictional studies at high normal loads (up to 800 bars for triaxial) are the triaxial test and the direct shear test. The triaxial test has the advantage of allowing the application of very high normal loads, but is limited to small samples and small displacements. Furthermore, the configuration of a small jacketed sample within a pressure vessel physically prohibits very detailed measurements of the sliding process. Sliding displacement is not measured directly in triaxial experiments, but is indirectly from piston displacements made outside the pressure vessel.

Although the direct shear test in its many forms is the configuration used most frequently for friction studies in engineering rock mechanics, it is used less frequently for geophysical rock friction studies, principally because the samples are unconfined and hence the maximum stress that can be reached is limited by the compressive strength of the rock. In practice, the direct shear apparatus produces internally consistent and reproducible results.

On studying the literature, it is also noted that the standard direct shear and triaxial techniques are remarkably crude for the determination of strength parameters, stick-slip and creep behaviour of rock faults. When conducting these tests, it is generally unsatisfactory to maintain the required confining and normal pressure on the specimen with a standard testing configuration. On the other hand, computers are playing an ever- increasing role in numerous sectors of laboratory testing equipment, whether it is being in the design or execution laboratory, in-situ tests, automatic data acquisition or control and statistical treatment of data, etc.

Since the intention of this study is to make detailed investigation on the frictional sliding behaviour of discontinuities surfaces, representing the seismogenic earhquake faults in the laboratory, an attempt is made to develop a computer controlled direct-shear apparatus capable of operating at desired experimental conditions and yet to avoid as much as possible the difficulties described above.

4.2. Developed computer controlled direct-shear apparatus

4.2.1. General aspects

In general, direct-shear apparatus developed to full fill the research objectives and requirements should have at least the following characteristics, namely;

   i. the model or specimen being tested,
   ii. the testing system, and
   iii. the monitoring system.

During a typical laboratory test, for example, in a direct shear test, the cylindrical or any other shaped specimen prepared from a type of rock is subjected to axial load by means of a suitable hydraulic ram. It is also subjected to increasing shear load by means of a hand operated hydraulic ram or by means of a motor through a reduction gear box. The magnitude of these loads and displacements are monitored throughout the test.

In the simple experiment described above, only two parameters (load and displacement) can be monitored. In general, the test specimen, the testing system and the monitoring system can have a variety of forms. The monitoring system;

47

also called a data-acquisition system become very elaborate depending on the number of components involved.

Fig. 4.1 shows a block diagram of the overall testing layout. Basically, it is divided into the loading system and data monitoring system. The specimen or fault model under study is mounted on the loading frame. The loading frame and its associated control system are utilised to apply the required loads to the specimen. During the experiment, the independent (controlled) and dependent (specimen or model response) variables are recorded by the data monitoring system. Transducers associated with the loads (axial and shear) sense these controlled variables. Strain transducers (LP or LVDT) mounted on the specimen sense its behaviour under applied loading conditions. Electrical signals (analogue output) from these transducers are connected into a signal conditioning unit, the outputs of which are monitored by both a data acquisition control card via a computer. Experimental data and control system is thus available in both analogue and digital form, allowing the investigator to monitor and control the experiment while it is in progress and to have data in convenient form for analysis after the experiment is successfully completed.
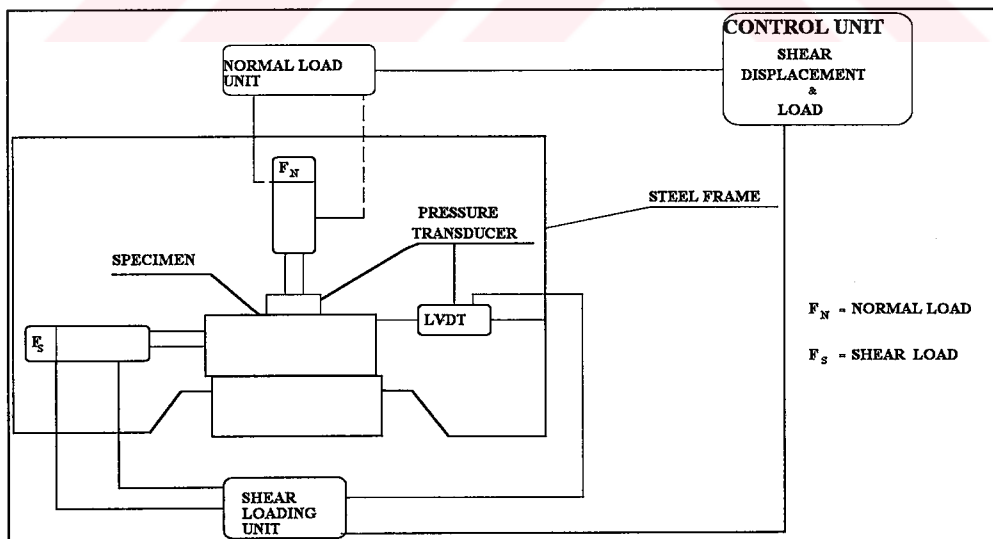
Figure 4.1 The main parts of the developed direct shear apparatus

48

4.2.2. Loading frame

The apparatus consists of vertical and horizontal loading actuators, reaction frames and shear box fixtures. Fig. 4.2 shows assembly of this equipment and Fig. 4.3 presents the general photographic view of the apparatus. A loading frame is required principally for reacting forces imposed upon the specimen by the hydraulic actuator and mechanical actuator (shear force) driven by an electrical motor. The hydraulic ram is mounted at the centre of the loading frame and oriented so that its line of action is perpendicular to the shear box. The mechanical actuator is placed parallel to the sheared plane in order to prevent rotational and buckling movement of the specimen. The present loading frame is capable of applying load up to 25 tons in compression. The stiffness of the system is capable of carrying this load without any distortion and deflections.

The designed shear box fixtures for the specimen housing is flexible to be simulated for the desired specimen size easily. The specimen is placed into two halves box. The maximum dimension of lower box is designed include the specimen up to 400x400x100 mm in size. It is bolted to 600x400x10 mm steel base plate which is guided through rollers between steel base and brace steel frame along the shear movement of the box. Fig. 4.4 shows this system which remarkably decreases the friction caused by steel to steel environment.

The axial load ram is constrained to the rotation about horizontal axis in line with the shear, rotation about the horizontal axis transverse to the shear. Those constraints are assured by connecting the axial load ram to a fixed upper reaction brace which acts on the top of the upper shear box. Thus, the top specimen block is constrained to the two degrees of freedom, plus a third, which is translation in the direction of shear.

The spherical seat between the shear box (lower and upper) and load actuators accommodate slight misalignment in both directions. Fig. 4.5 shows the general layout of the loading rams and shear box fixtures.
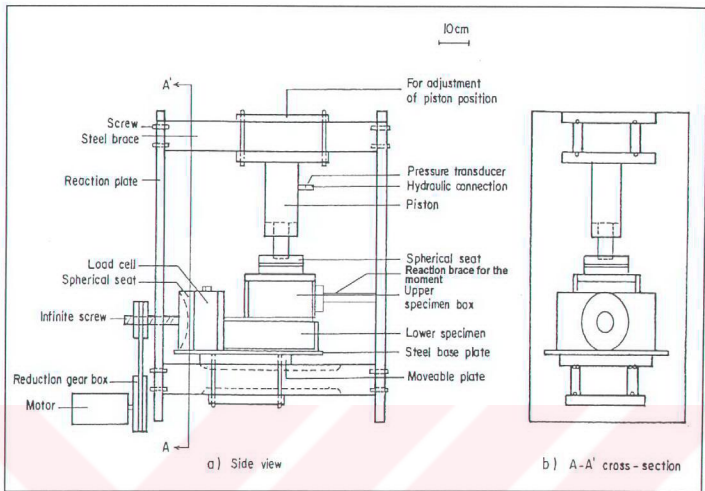
Figure 4.2 The schematic view of developed direct-shear apparatus

Figure 4.3 The general view of the computer controlled direct-shear apparatus
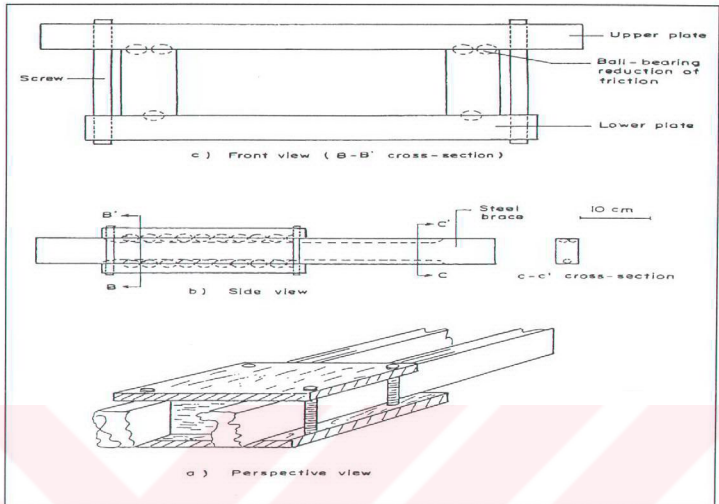
Figure 4.4 The moveable parts of the shear apparatus
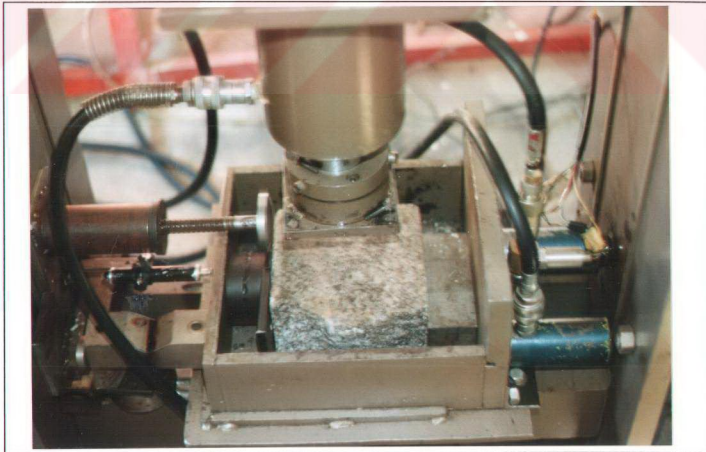
Figure 4.5 General layout of the loading rams and shear box fixtures

4.2.3. Axial loading system

In direct-shear apparatus, usually, the axial loading system is basically supplied by the hydraulic power unit and most of the hydraulic unit incorporate open-loop control systems (Fig. 4.6). In this type of control, the testing unit crosshead is caused to move at a constant rate by use of machine screws or hydraulics according to some pre-set adjustment. Load, strain are subsequently measured by various means (dial gages etc.).

The loading system developed in the present study is considerably sophisticated one. It is technically referred to as an "electro-hydraulic closed-loop servo controlled loading system". A closed-loop control system (Fig. 4.7) offers a number of advantages. It allows the establishment of load, strain, deformation, etc. as the direct primary control parameter and provides an automatic system that will maintain the command environment upon the specimen. The desired axial load is maintained in the range of ±1% sensitivity.
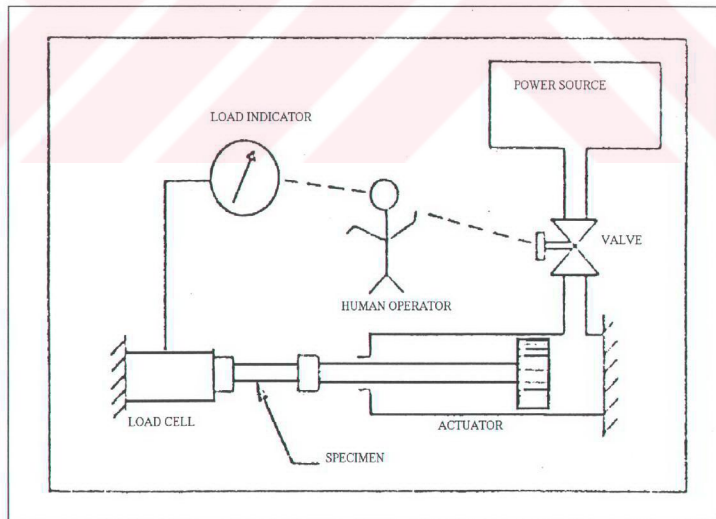
Figure 4.6 Simplified open-loop control system

Up to date many works have been carried out by researchers and better pressure control was achieved by utilising electronic control system. This system enabled the pressure in the hydraulic unit to be monitored continuously by the electronic controller. It was able to control the pressure to within $\pm$ 6.5 % of that required pressure. Baleshta and Dusseault (1988) maintained the pressure to within 0.1 % of that required up to a maximum working pressure of 70 MPa. Recently, more precise pressure control can be achieved by introducing micro computer and feed back control process.
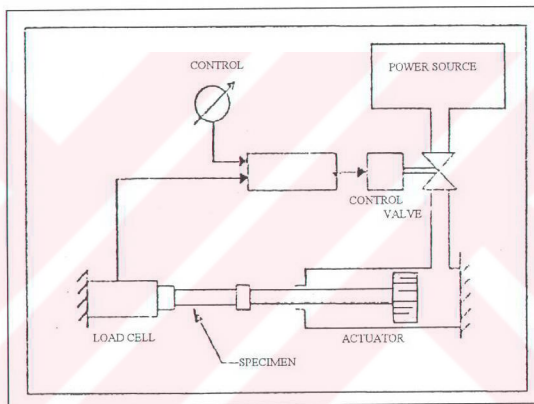
Figure 4.7 Simplified closed-loop control system

As the hydraulic ram can be programmed from the computer, special tests can be readily performed (for example, a sinusoidal input command will impose a cyclic load upon the specimen). This hydraulic ram acts through a pressure transducer whose output is used as the control signal (feed-back) for regulation of axial load by the hydraulic-power unit. Fig. 4.8 and Fig. 4.9 shows the photographic view and flow sheet of this unit respectively. As it is easily seen from this figure, hydraulic tank (40lt) is equipped with a hydraulic pump, electric motor, proportional pressure relief valve, directional valve, check valve, pressure relief

valve and pressure accumulator. The detailed information about these apparatus is given in appendix A.

Hydraulic power supply furnish an adequate flow of clean hydraulic fluid at a constant or variable pressure within reasonable limits of temperature (up to 70 ° C). The prime mover is electric motor which drives a positive displacement type pump. The power supply in this unit has a flow capacity of 30 lt/min. The maximum output pressure is normally up to 250 kgf/cm^2. The temperature of the oil is controlled by passing it through a heat-exchanger cooled by tap water.

Figure 4.8 Photographic view of the hydraulic unit
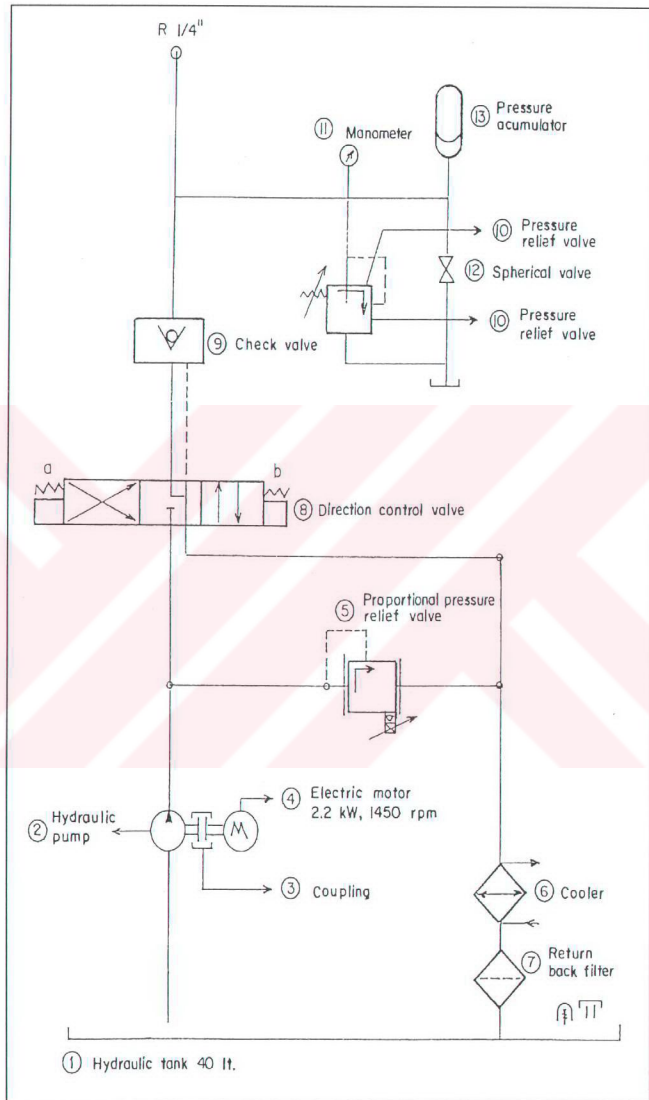
Figure 4.9 The flow sheet of hydraulic unit

The direction of the ram is controlled by the directional valve. This is maintained by sending digital output to the a or b section of the valve from the computer. The regulation of the axial load is supplied by proportional pressure relief valve. This valve has an electronic card which is sensible to analog output from the data-acquisition and control card of the computer. The analog input let the unit release or compensate the overload or less load correspondingly. As it is seen from the flow sheet for overloading or any other undesired condition the unit is preserved by mechanical pressure relief and check valves. The small amount leakage or access pressure due to dilation from the breaking of roughness during shear can be compensated by pressure accumulator.

4.2.4. Horizontal loading system

Some of the testing techniques are based on keeping the shear load constant or stress rate (strain controlled) constant. First technique (constant stress) demands a high accuracy and temperature and humidity conditions, stability of measuring devices over a long time periods (it may take hundred of days). Cruden et al. (1987) point out that such tests can be carried on soils within reasonable period of times, because of the relatively lower viscosity than rocks. Due to high viscosity, the testing duration necessary for rocks will be in order of years; so that such studies can hardly be afforded. He also remarks that it is difficult to choose relationship between normal and shear load yielding measurable deformation without failure. The second technique, i.e. stress rate constant, is better and demands a minimum of time (a few minutes to two or three days) for getting reasonable results in order to predict and model faults behaviour.

In the present design, the horizontal load produces a strain controlled direct shear rate to a lower box via the infinite screw, which is supplied by A.C. motor through a reduction gear box. Two reduction gear boxes (1/25 and 1/280 reduction ratio) are mounted in series or differentially according to required shear rate. This system is powered by A.C. motor. The A.C. motor frequency is controlled by ALTIVAR 5 series 45 2 variable speed controller. It is connected to microcomputer via data-acquisition and control card. The speed control is possible by A/D board from the computer controlling the amount of voltage applied to the motor and indirectly the response speed of the system. The frequency or the revolution per minute (rpm) of the A.C. motor is regulated by analog input (0-10v)

from the computer. The rate of the shear displacement is 0.003 mm/min and 4 mm/min for 0 and 60 frequency values respectively (the relative shear velocity can be varied infinitely between these ranges). This rate is sufficient to simulate the plate tectonic movements (e.g. NAFZ rate is 110 mm/year). The selection of loading rate by mechanical system rather than hydraulic system is for the sake of homogeneous loading requirement. If this is done by hydraulic power unit, fluctuation in the stress rate loading will be caused by long-term loading and instantaneous stress concentration .

4.2.5. Instrumentation

In the sophisticated closed loop testing equipment, the control and data-acquisition process is maintained by electrical connection between the computer and data recording devices. The voltage out of the system is applied to a solid-state switch through 5V relays. The relay and contractors and other electrical accessories are used to start the motor (pump motor and shear motor) and drive the directional control valves. Fig. 4.10 shows the electrical connection of the hydraulic power unit and shear movement motors. The other devices driven by analog input signal are directly maintained form the data acquisition card.

The axial and shear load are measured by pressure transducers. A transducer that is capable of operating within the maximum range (315 bar) of the hydraulic system is chosen yet calibrated in the range within which it is operated. For each different test condition, these transducers were calibrated beforehand. The sensitivity of transducers are 0.1 MPa. For a maximum input voltage into the A/D from the pressure transducer of 5V at a pressure 35 MPa, one count on the A/D converter 1.3 kPa (1 % within the limit of recommended ISRM standard). An example calibration curve for these transducers is given in appendix B.

The horizontal displacement transducer mounted by bonding on to the steel frame and lower shear box, provide measure of the block is relative motion. For the normal displacement measurement four displacement transducers are used. For the shear displacement two displacement transducers are used. All the displacement transducers are linear potentiometer (LP) and linear variable differential type (LVDT). These transducers are also calibrated for each test condition. The sensitivity of linear potentiometer is 12.5± 0.001 mm.
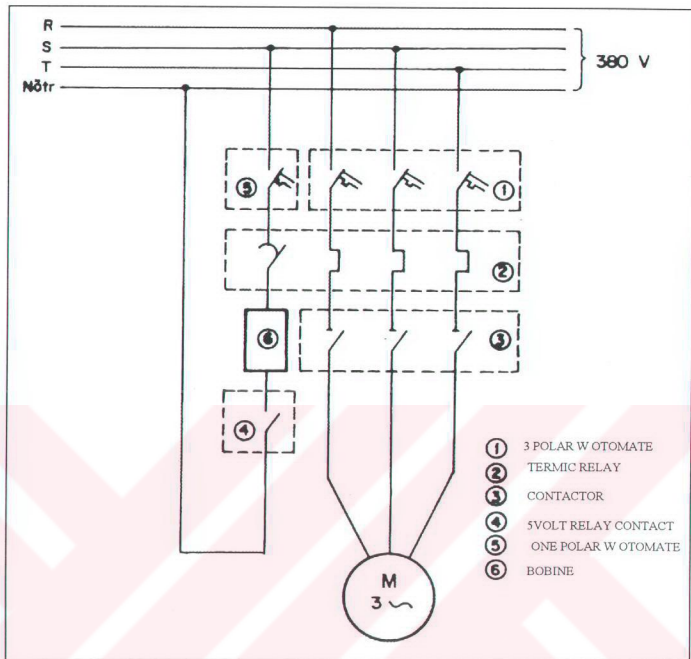
Figure 4.10 Electrical connection of the system motors

R ── S ── T ── Nötr ── 380 V

① 3 POLAR W OTOMATE
② TERMIC RELAY
③ CONTACTOR
④ 5VOLT RELAY CONTACT
⑤ ONE POLAR W OTOMATE
⑥ BOBINE

M 3∿

4.2.6. Data acquisition and control

A typical data acquisition system includes three basic components, namely:

i. the transducer,

ii. the signal conditioner, and

iii. the signal recording and processing unit.

A more complex data acquisition system also includes control component with the function of monitoring and modifying the conduction of the test in some pre-programmed condition. The following includes a brief discussion of the role of each component of data acquisition system.

4.2.6.1. Transducer

The transducer is a device that converts a given quantity such as displacement, pressure or load into a electrical signal. Generally, the transducer produces a change in resistance, output voltage, or output current which is proportional to a physical change within the system being monitored.

4.2.6.2. Signal conditioner

The signal conditioner is a device which is necessary to obtain the best possible signal for recording and further processing. Depending on the type of measured parameter and the form in which a given signal is analysed, a signal conditioner may perform one or more functions, such as amplification, filtering, and excitation of the transducer. The role of a signal conditioner is very important in every data acquisition system since its quality is reflected in the quality of the recorded data.

4.2.6.3. Recorder

The recorder is a device that preserves experimental data from a given test. There are two basic methods of data recording, namely:
    i. the analog method, and
    ii. the digital method.

4.2.7. Analog to digital converter

The analog to digital (A/D) converter establishes the link between the analog signals measured during the experiment and the digitally equivalent signal in the microcomputer. Its role is to convert an analog signal into digital form suitable for processing and storage within the computer. The A/D converter is the major component of digital data acquisition system. The PCL-718 data acquisition card for IBM PC/XT/AT or compatibles is used for data recording and control purposes.

A 12 bit A/D converter is selected for the system to provide an accuracy of conversion at a reference voltage of 200 mV and 60 kHz 10 samples per second. It has 16 analog input (A/I) channel, 2 analog output (A/O) channel, 16 digital input (D/I) and 16 digital output (D/O) channel.

4.2.8. Microcomputer

The IBM PC/AT compatible hardware and software with 512 Kb RAM, 80 MB hard disk is used for the data acquisition and control purpose. In order to increase the speed of calculations, the math co-processor based on the 8087 microprocessor was chosen. It is based on Intel-manufactured 80386 microprocessors.

4.2.9. Electrical stability

In laboratory type measurements, the quality of data depends largely on the electrical stability of the measuring system. Power failures, vibration, acoustic noise, varying temperature, and dust are of the many sources of measurement disturbances generally referred to as "noise". Unfortunately, noise exists in every type of measurement. What is important, however, is the magnitude of the quantities measured. For example, for the measured output signal voltage of 5 V, the noise of ± 5 mV represents only ± 0.1 percent of the measured quantity.

4.2.10. Programming language

A comprehensive I/O driver routines for A/D, D/A, Digital I/O is written in assembly language and accessed through the CALL statement of the interpreted or compiled BASIC. Utility software is included with each PCL-718 for the application programming works. New software in Quick Basic language is developed for the control and data acquisition system by using the card driver. These programmes are developed for each testing conditions and also used for calibration of pressure and displacement transducers. The developed software is given in appendix C.

4.2.11. Data acquisition and control module

Fig. 4.11 shows the flow sheet of the data acquisition and control module. As it is seen from this figure the PC BUS that includes the card board is used to record the measured data and control the systems. The signal from the transducers is passed from signal conditioner module to analog multiplexer and A/D converter; and then it is stored in hard disk or a disk as raw data for further processing or directly send to any program that is used for analysis. At the same time, the digital output is send to hydraulic power unit in order to activate the hydraulic motor and directional valves relay (on/off signal) and also for the direct shear motor relay. The proportional pressure relief valve which is used to control the pressure and the variable speed controller unit which regulates the shear motor frequency are feeded by analog output (0-10V) from the control programme.

The computer controlled shear apparatus enable to control of experimental variables (Load, displacement, etc.) automatically and precisely. A feedback signal representing some experimental condition is generated by transducers and compared with the program signal which represents the desired condition. If a difference exists, a new signal is generated to supply corrective action. However, the response time of complete closed-loop system mainly governs the successful control of the experiment. The sound data also depends on the sensitivity of the used transducer and also noise problem generated from the environment mentioned in the previous section. Anyhow the computer controlled equipment can always give better and precise results than ordinary ones. The compilation and evaluation of these results are easy and accurate.
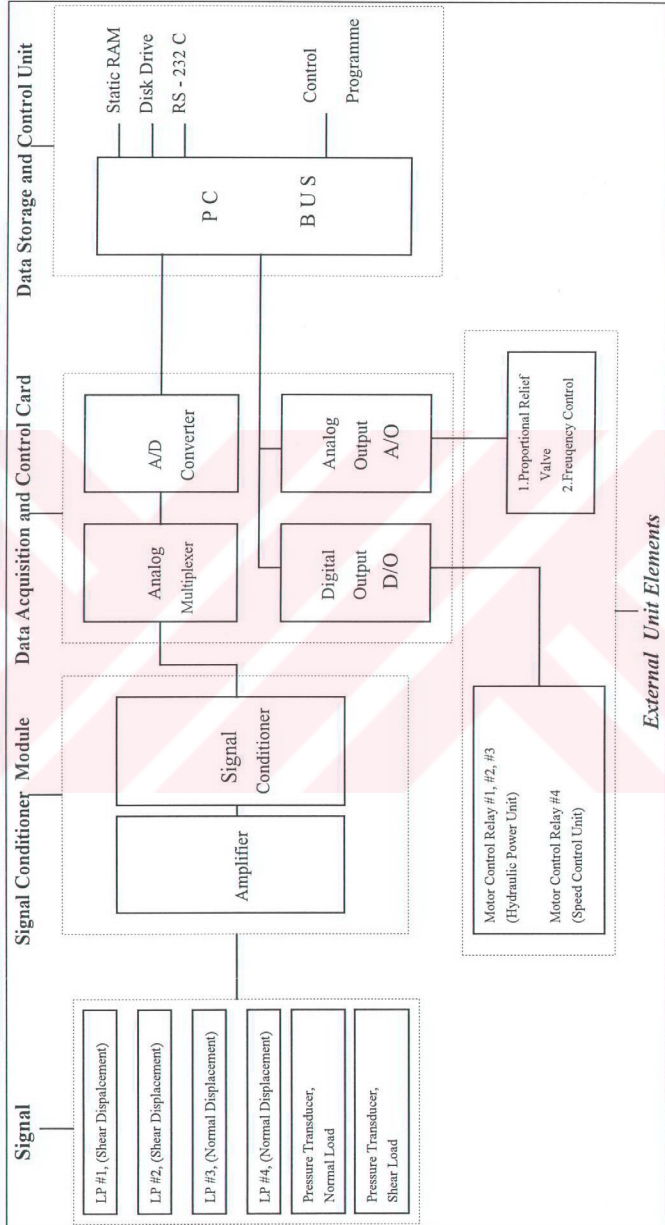
Figure 4.11 Data acquisition and control module

CHAPTER 5

THE EXPERIMENTAL WORK OF FAULT MODEL

5.1. Introduction

Laboratory testing has many advantages compared to field observations in seismology. It is usually not known where an instability may occur, so there are few opportunities to observe precursory phenomena of earthquake faults. Measurements of deformation and stress at the place of earthquake centre are extremely difficult under natural conditions, but the simulation of these boundary conditions is relatively easy.

On the other hand, The laboratory tests should provide reliable data necessary for the prediction of seismic phenomena from an engineering point of view. Therefore, in this study much effort was given for the experimental work. This chapter is not meant to be a complete overview of the laboratory tests results but the aim is to identify and present the principal data which allow the definition of the phenomenological aspects of the shallow focus earthquake mechanism. Thus, a brief description of the specimen preparation and properties of the sample are included initially, followed by the direct shear tests on the saw cut granite specimens. Afterwards, the velocity-stepping tests are given. Then results and interpretations of different tests which are simulations of sudden changes of field stress in different modes are given.

5.2. Specimen Preparation

The specimens are rectangular granite containing a saw cut surface. Granite is chosen, because the nucleation of the shallow focus earthquake is mostly observed in the granitic rock masses under the continental crust (See section 2.2). The granite specimens are cut from the same block sample by sawing machine in order to conduct multiple experiments. Two halves of the specimen were casted

into the upper and lower parts of the shear box using a polyester and sand mixture (Fig. 5.1). Polyester is chosen in stead of cement since it has a shorter curing time (1- 2 hours instead of 21 days) and a higher strength (with the hardness catalisor). Thus in a short period, many test specimens can be prepared for testing. The size of the upper half specimen is 50x60x60 mm. The lower one is 150x150x100 mm in size which is chosen larger than upper specimen for better and easier control of the normal stress.

Figure 5.1 The moulded specimen with polyester-sand mix

The sheared plane is positioned nearly 5 mm above the casted polyester surface. Both parts are tightly bounded prior to testing in order to preserve the mechanical integrity of the specimen. The simulated fault surface area is generally

30 cm^2. Six experiments can be conducted without changing the specimen.(each run results in 1 mm displacement).

5.3. Properties of the granite sample

Along with the frictional properties, some other properties such as uniaxial compressive strength, Young's modulus, Poison's ratio, dry density and friction angle of the sample are also determined in accordance with the procedure given in ISRM standards (Brown, 1981). These are tabulated in Table 5.1.

Table 5.1 The estimated properties of the sample

Name of the sample	UCS* (MPa)	Friction angle (°)	Young's modulus (E) (GPa)	Poisson's ratio	Dry Density (kg/m^3)
Granite	120±6.7	36±7	60±10	0.22	2650

* Uniaxial Compressive Strength

5.4. Experiments conducted

5.4.1. General

During this experimental study four types of frictional sliding tests are performed under the prescribed load and/or strain controlled modes. These are:

i. The standard direct-shear experiment. It is conducted to find the shear strength parameters of the specimen. Besides this the validation of the apparatus is also performed by this experiment

ii. The standard velocity-stepping experiment. It is performed following the sudden velocity changes of the constant load point velocity procedure.

iii. Sudden variation in normal stress. This experiment is carried out in two forms, i.e. stepwise and functional change in normal stress

iv. Simultaneous sudden change in normal and shear stresses.

5.4.2. Standard direct-shear test

This test was carried out in order to measure shear strength parameters as a function of normal stress. The stages given below summarise the testing procedure for this experiment:

i. At first, mounting the specimen in the shear box, the consolidation stage of testing was carried out in order to allow the packing and stabilisation of the rock under normal stress before shearing. The normal load was raised to prescribed value at a standard rate of ISRM (Brown, 1981) of 0.5-1 MPa/sec. The hydraulic power unit with electronic control facility is capable of maintaining normal load within 2% of selected value throughout the test.

ii. Then, the shear loading acting in the plane of shearing was applied through a motor via a mechanical gear drive system up to a displacement more than 10% of the specimen length (generally 10-12 mm). The shear force is applied continuously in such a way as to control the rate of shear displacement. The rate of shear displacement (load pint velocity) is 0.001 mm/sec ($1~\mu ms^{-1}$) during the test period.

iii. For each test specimen graphs of shear stress versus shear displacement and normal stress versus normal displacement are recorded by continuous data acquisition. The average shear stress versus shear displacement graph of the specimen is presented in Fig. 5.2 . From these results the mathematical model is obtained by the regression curve. The slope of the regression line, which means the derivative of the regression equation with respect to displacement results in shear stiffness (Ks) of the system. By the same procedure the normal stiffness (Kn) of this sample can be found from the regression curve equation in Fig. 5.3. The mathematical expressions obtained from the standard direct-shear tests for the shear and normal stiffness are given in equation 5.1.

$$\frac{\partial(\tau)}{\partial(u)} = 0.114 \, (u)^2 - 1.23 \, (u) + 3.158$$

(5.1)

$$\frac{\partial(\sigma)}{\partial(v)} = 57.834(v) + 9.599$$

Where u is shear and v is normal displacement in mm, $\frac{\partial(\tau)}{\partial(u)} = Ks$

(shear stiffness), $\frac{\partial(\sigma)}{\partial(v)} = Kn$ (normal stress), σ is normal τ is shear

stress in MPa.

iv. Graphs of peak and residual shear strength versus normal stress are plotted in Fig. 5.4. Shear strength parameters ϕ_r and C are abstracted from these graphs by means of mathematical formulation of regression curve and are presented in Table 5.2. The mathematical expression for the determination of friction (μ) and friction angle ($\phi = \tan^{-1}\mu$) of the system is given in equation 5.2.

$$\tau = -0.067 \, (\sigma)^2 + 1.94 \, (\sigma) - 7.185$$

(5.2)

$$\frac{\partial(\tau)}{\partial(\sigma)} = -0.134 \, (\sigma) + 1.94$$

Where, $\frac{\partial(\tau)}{\partial(\sigma)} = \mu$

e.g. when the normal stress (σ) is equal to 10 MPa, the coefficient of friction (μ) is 0.6 and the friction angle (ϕ) is 31°.

Table 5.2 Shear strength parameters of the granite

Residual Friction angle $\phi_r, (°)$	Residual Cohesion (C) (MPa)	Ks (MPa/mm)	Kn (MPa/mm)
30-38	0	2-7.5	20-30
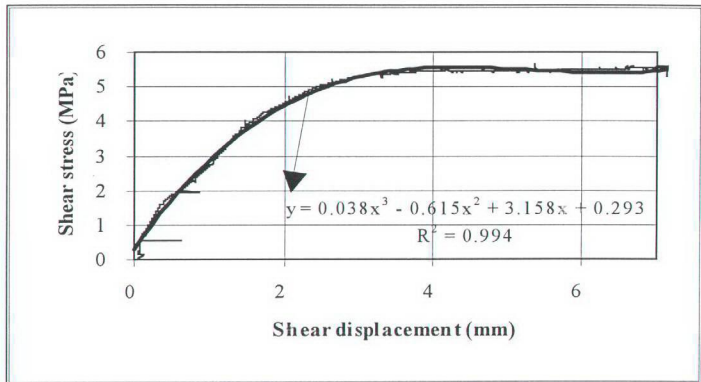
Figure 5.2 The estimation of shear stiffness (Ks)
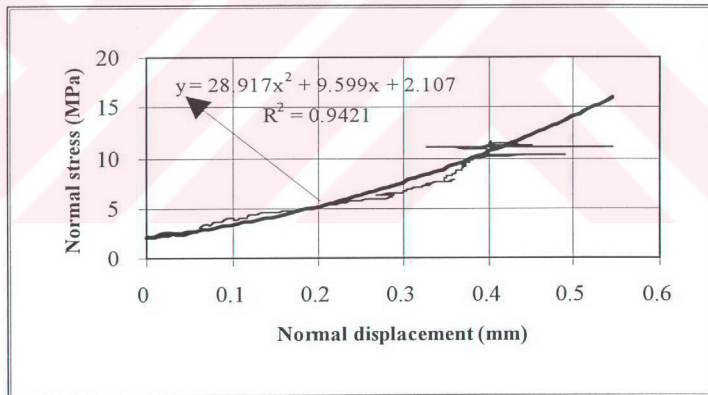
Figure 5.3 The estimation of normal stiffness (Kn)
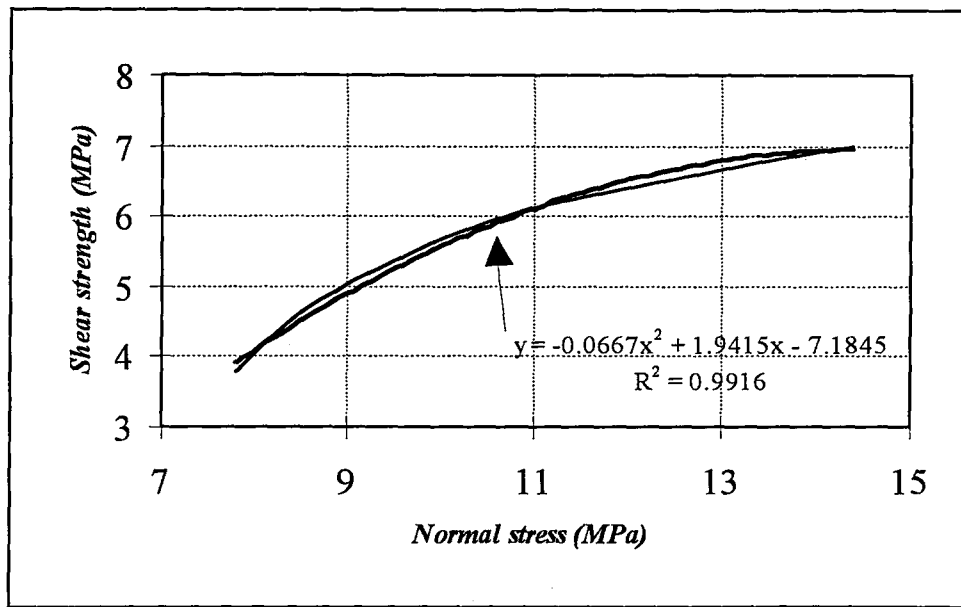
Figure 5.4 The shear strength vs. normal stress

5.4.2.1. The results of standard direct-shear experiments interpretations

The results of direct-shear tests are logical and consistent with each other and consistent with the ISRM standards (Brown, 1981). The obtained graphs show the characteristic of polynomial curve. The shear strength parameters are consistent with the values reported in the literature for the granite specimen (e.g. Jaeger and Cook, 1976). The logical and consistent results with the previous investigations also prove the validity of the new computer controlled direct-shear apparatus.

5.4.3. Velocity-stepping test

Velocity-stepping experiments are performed at normal stress of 5 MPa and displacement rate of 1 μms^{-1}; Small deviations from these values are observed due to experimental conditions. The chosen sliding velocity is classified as regular velocity for earthquake mechanism tests reported in literature (e.g. Logan and Rauenzhan, 1987 and Blanpied et al., 1995). Different categories of sliding velocities for frictional sliding tests are given in Table 5.3. In this table the velocity sequence means the sudden change in load point velocity in descending and than in ascending order.

Table 5.3   Nominal load point velocity and duration under differential load for velocity-stepping experiments (After Logan and Rauenzhan, 1987)

Type of test	Velocity sequence (μms^{-1})	Time under load (hrs)
Regular	20-2-0.6-0.02-0.6-2-20	5
Long term	0.2-0.02-0.002-0.02-0.2	35-40
Short term	200-20-2-2-20-200	0.25

During these experiments, the same nominal stress and sliding rate of the previous authors are used in order to be able to compare this study results with their conclusions. (The same procedure is also followed for the stress change effect tests). On the other hand in the parametric study it is not necessary to take the real stress or velocity into consideration. It is needed to maintain the constant value of the investigated parameter (e.g. normal stress) throughout the set of experiments while other parameters are changing (e.g. sliding velocity; duration).

The overall procedure followed in this test is the same as the direct-shear test. The normal speed was increased at a rate of 0.5 MPa/sec. to a nominal stress of 5 MPa, at first. Just then, shear load is applied at a nominal sliding rate of $1\mu ms^{-1}$. When the system reached the steady state (static) shear stress or coefficient of friction (it is experienced after many runs of the experiment), the sliding rate is stepped by a factor of 10 (Ten fold increase of sliding velocity). After a while the sliding rate was lowered to the nominal value ($1\ \mu ms^{-1}$) again. This procedure can be repeated up to a sliding displacement of 10-12 mm. An example to the sudden increase of slip rate of velocity-stepping test is shown in Fig. 5.5.

The results of the experiments are presented in Figs. 5.6-5.15. From the graphs, the coefficient of friction and its transition parameters, a, b, Dc and Kc are measured as a function of displacement. Besides, the shear stress and its transient parameter A (the direct effect of step changes on shear stress) and B (the evolution effect of step changes on shear stress is also recorded.
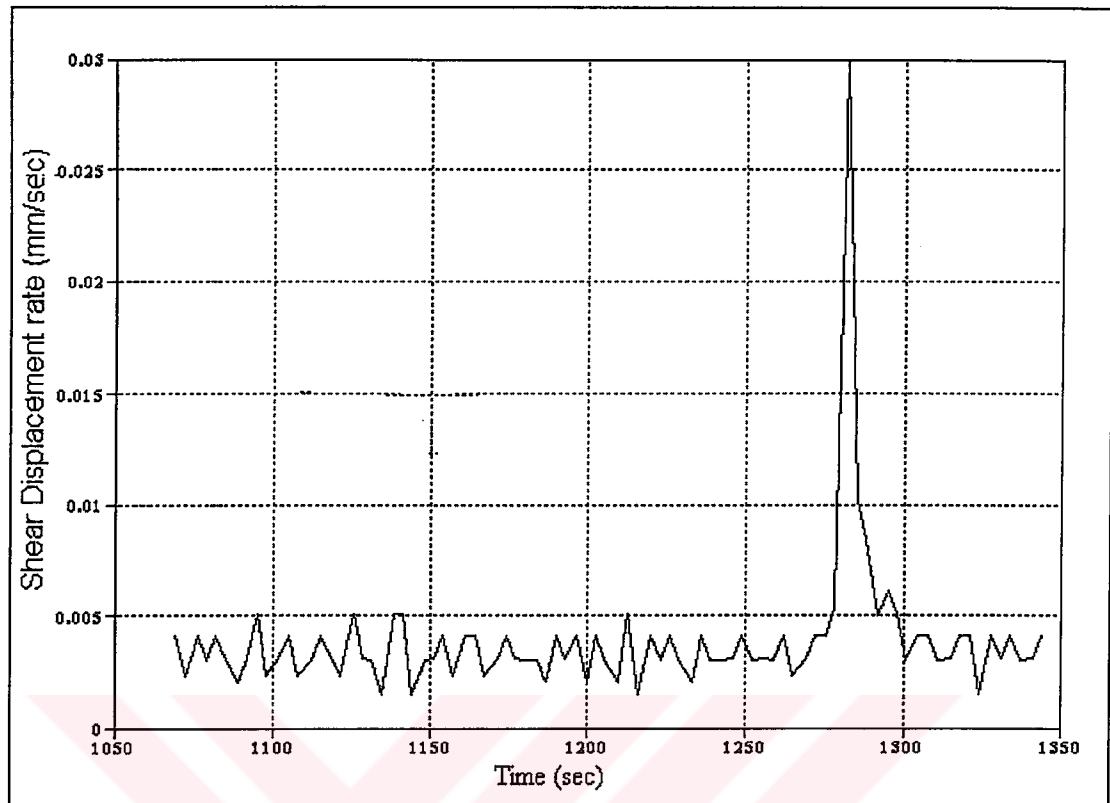
Figure 5.5 The sudden increase of sliding rate during velocity-stepping test

A common feature of the graphs obtained is that, in response to a step increase in load point velocity, the shear stress of coefficient of friction suddenly increases and then decays to a new steady value. (see Figs. 5.6-5.7). In most of the presented graphs, the decay to the steady state roughly follows an exponential path with a characteristic displacement, Dc. In some of the results the new steady state coefficient of friction or shear stress value (after the step change in load point velocity) is lower than the initial steady state. This behaviour is commonly to a velocity-weakening which shows seismogenic behaviour. Most of the graphs of this experiment show velocity-strengthening which means that the steady state values increase to a higher value from it initial value with a step increase in sliding rate. This behaviour resembles the stable sliding (creep) of the faults.
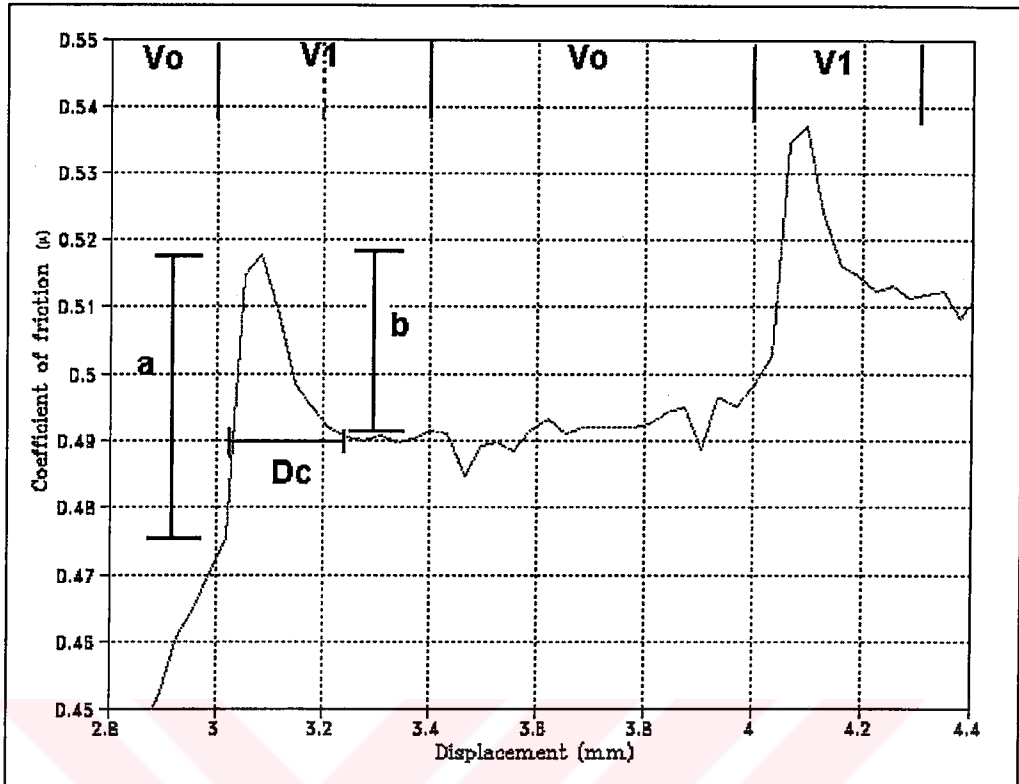
Figure 5.6 The coefficient of friction vs. sliding displacement (granit1)
Vo is the nominal V1 is the increased velocity
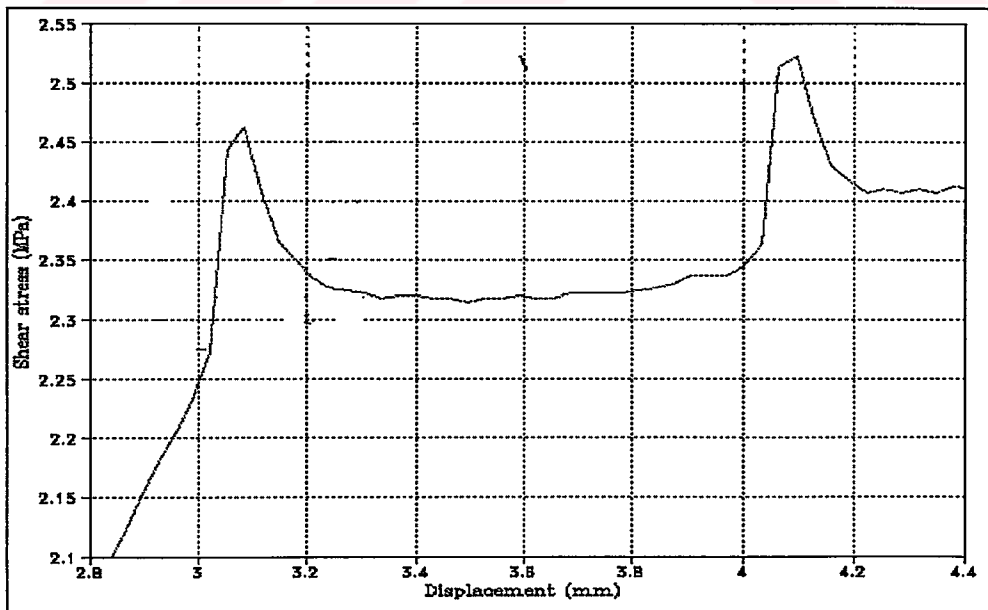
Figure 5.7 The shear stress vs. sliding displacement (granit1)

72
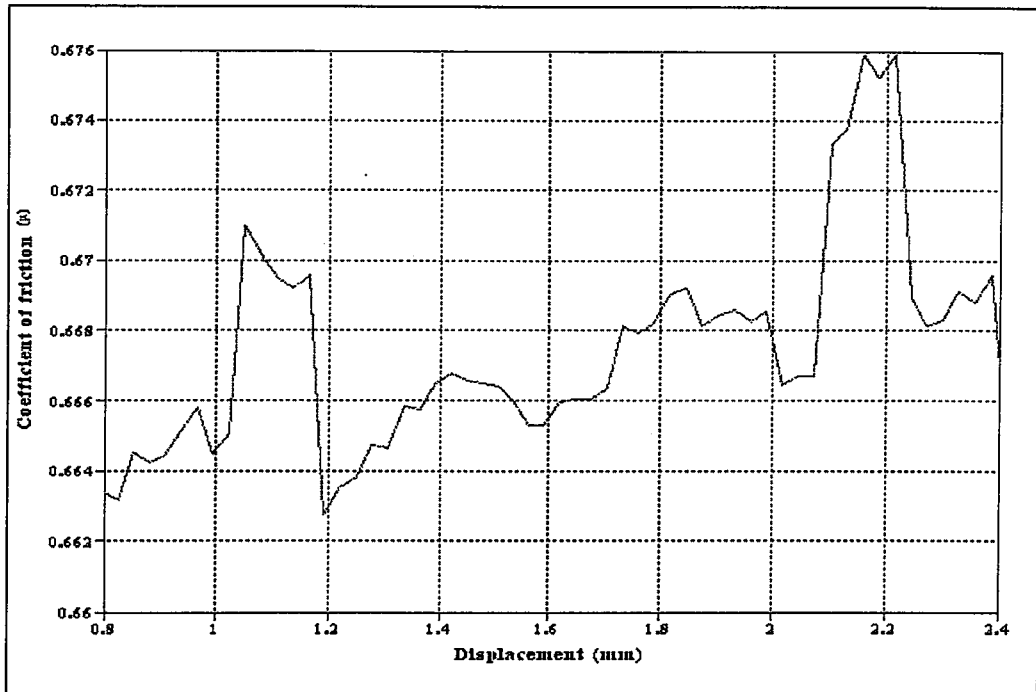
Figure 5.8 The coefficient of friction vs. sliding displacement (granit2)
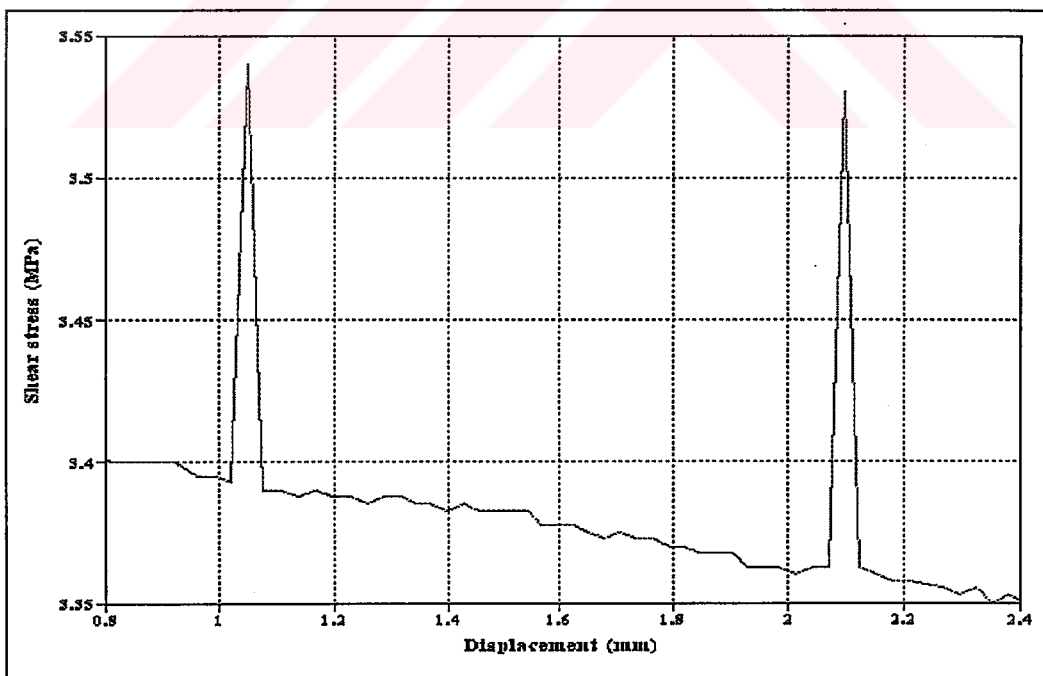
Figure 5.9 The shear stress vs. sliding displacement (granit2)

73
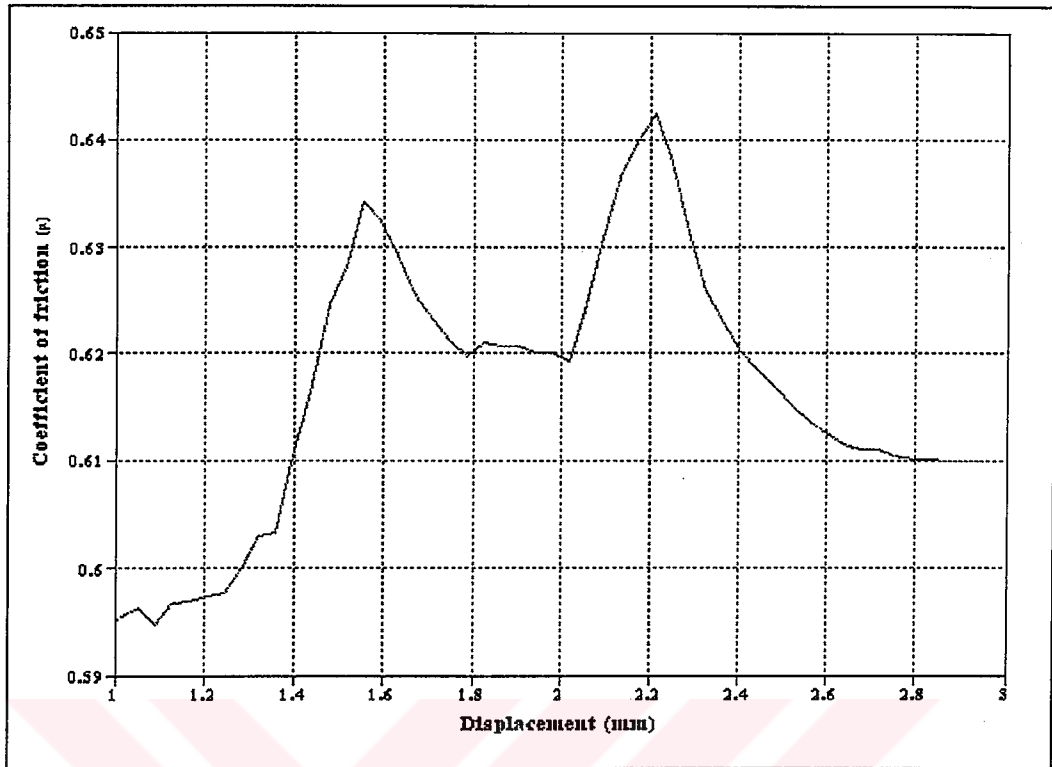
Figure 5.10 The coefficient of friction vs. sliding displacement (granit3)
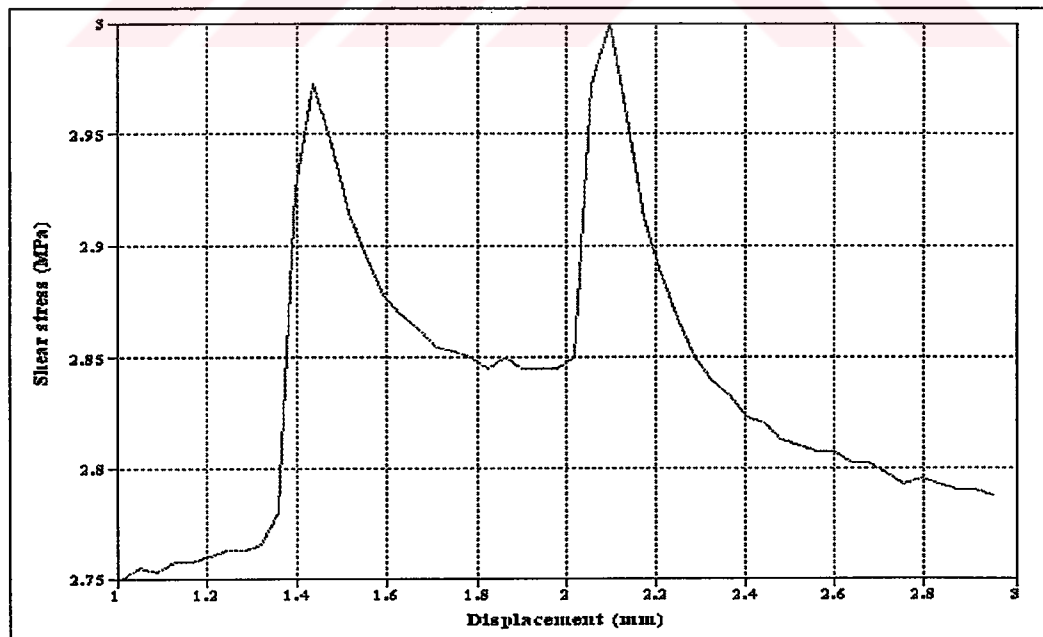
Figure 5.11 The shear stress vs. sliding displacement (granit3)

74
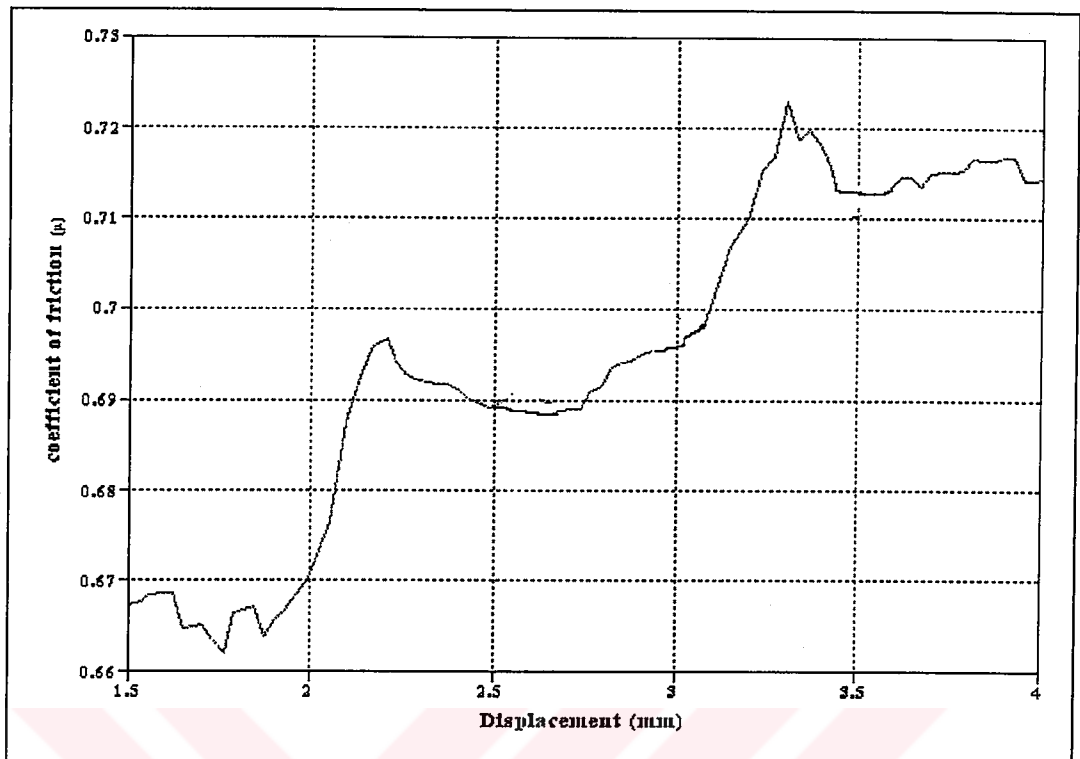
Figure 5.12 The coefficient of friction vs. sliding displacement (granit4)
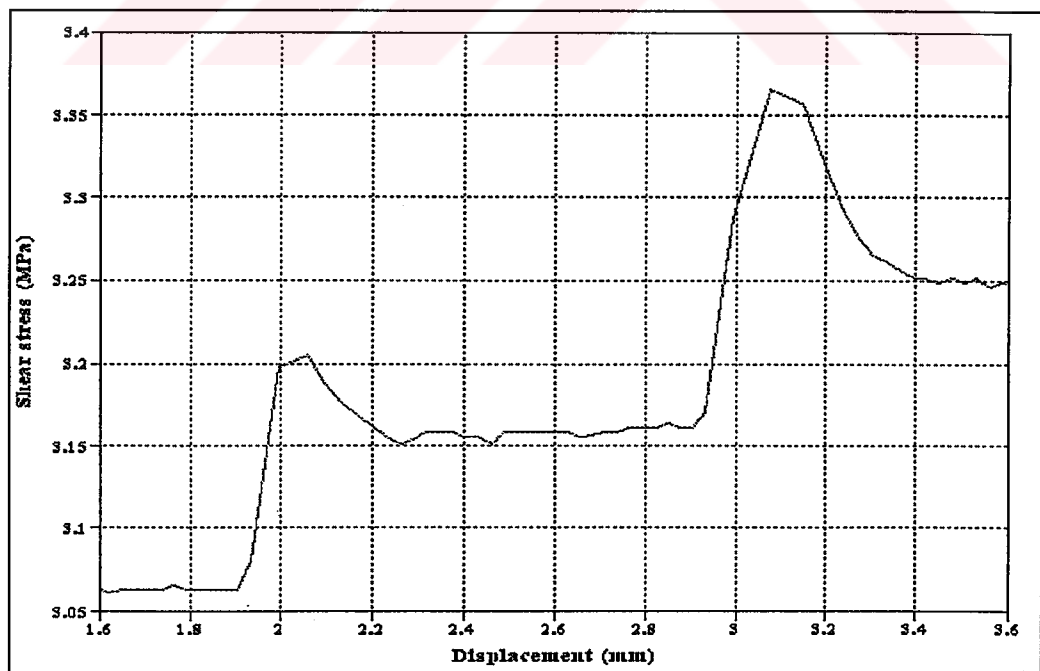
Figure 5.13 The shear stress vs. sliding displacement (granit4)

75
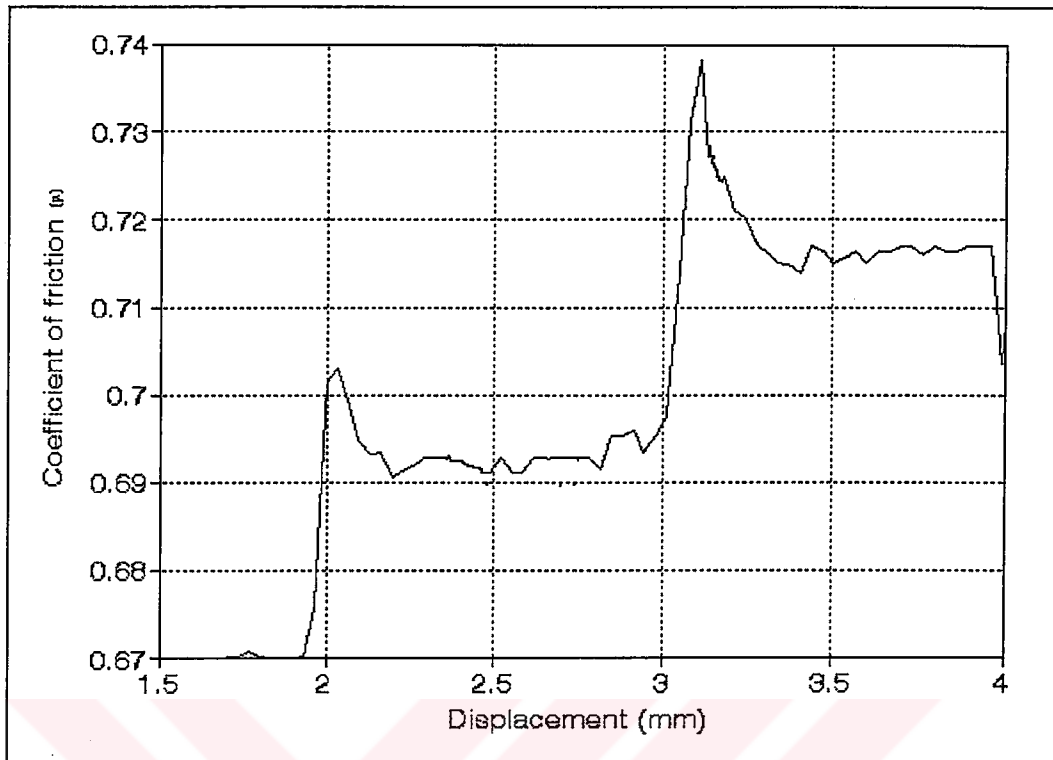
Figure 5.14 The coefficient of friction vs. sliding displacement (granit5)
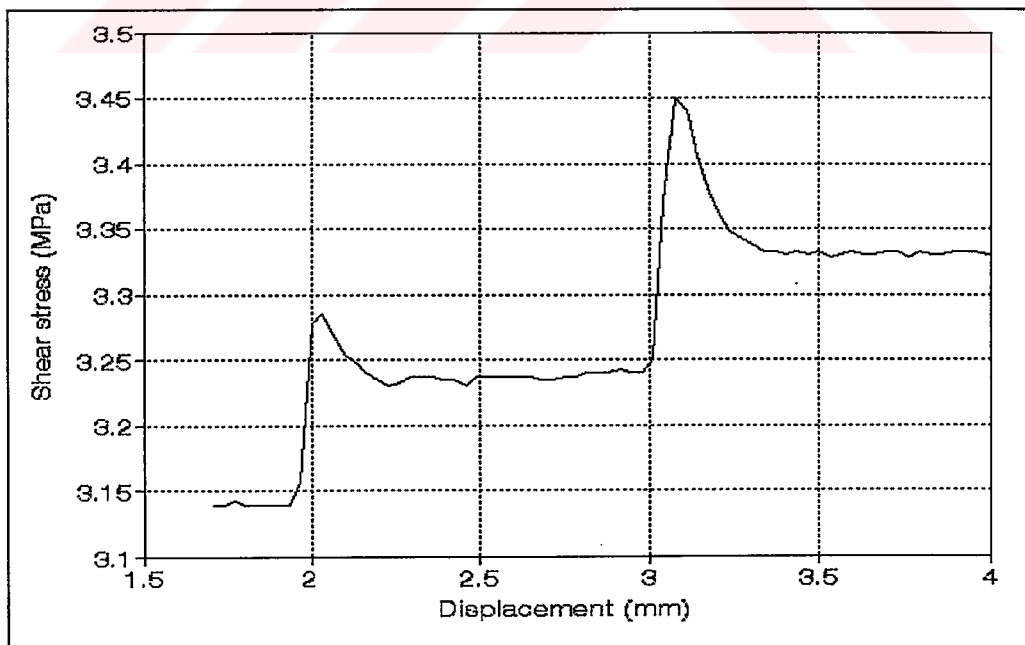
Figure 5.15 The shear stress vs. sliding displacement (granit5)

76

The empirical parameters of the velocity-stepping test are listed in Table 5.4. For each step change in load point velocity a, b, Dc, Δτ and other parameters are determined directly from the experimental graphs under the assumption that a step change in load point velocity results in equivalent step change in slip rate. It is also assumed that in response to an instantaneous step increase in slip velocity, surface state remains constant so that the resulting jump in stress is a measure of "a". With continued sliding at the new slip speed, θ evolves toward a new steady state value that depends on the new slip velocity so that the magnitude of the decay in shear stress is a measure of "b".

Table 5.4 The rate- and state- empirical data from the velocity-stepping test

Specimen Name	a	b	Dc (mm)	Δτ$^\zeta$ (MPa)	Δμ* (b-a)	Kc# (MPa/mm)	σ$^\xi$ (MPa)
Granit1	0.04	0.0289	0.2	-0.05	-0.011	-0.25	4.5
	0.04	0.0244	0.2	-0.07	-0.016	-0.36	
Granit2	0.336	0.0344	0.2	0.004	0.0008	0.02	5
Granit3	0.413	0.0283	0.3	-0.06	0.013	-0.19	4.6
	0.0326	0.435	0.4	0.05	0.011	0.13	
Granit4	0.043	0.0239	0.3	-0.09	0.02	-0.31	4.6
	0.0304	0.0109	0.21	-0.09	0.02	-0.44	
Granit5	0.0270	0.0085	0.2	-0.09	-0.019	-0.44	4.7
	0.0404	0.0213	0.3	-0.09	-0.019	-0.30	
Average	0.037± 0.01	0.025± 0.01	0.26± 0.07	0.054± 0.05	-0.012 ±0.002	-0.27±0.14	4.73± 0.05

* Drop in coefficient of friction Δμ= b-a

Critical stiffness Kc= $\dfrac{\Delta\mu\sigma}{D_c}$

ζ Normal stress

ξ Shear stress drop

5.4.3.1. Velocity-stepping test interpretations

The experimental rate- and state- dependent constants (a, b, Dc, Kc) show variety for the same sample; but this variation is within reasonable limits. The direct velocity affect "a" from this study with the values reported in the literature are given in Table 5.5 for comparison. It can be noticed that the average value of "a" from this study is almost the same value of the granite sample of the previous investigations.

Table 5.5 Empirically determined values of the "a", direct velocity effect,
       (After Kato et al., 1992)

a	Rock type	Reference
0.011	quartzite	Ruina (1983)
0.006-0.008	quartzite (rough surfaces)	Determined by Gu et al. (1984) using
0.003-0.005	quartzite (smooth surface)	the Dieterich's (1981) data
0.2	dolomite, marble	Weeks and Tullis (1985)
0.004-0.0075	granite	Tullis and Weeks (1986)
0.0125-0.0150	granite	Blanpied et al. (1987)
0.027-0.028	granite	METU (1996)

According to the instability theory (see Cox, 1990), the seismogenic faults show instability if the experimental data results in:

i. $K \langle (\frac{\Delta\mu\sigma}{Dc})$ or $K < Kc$ 　　　　(5.1)

where K is the shear stiffness of the sample and loading system, Kc is the critical shear stiffness after the step increase of velocity, σ is the nominal normal stress, and $\Delta\mu$ is the change (this may be drop or increase) in the coefficient of friction takes place over the characteristic displacement Dc.

ii. $\dfrac{\partial \mu^{ss}}{\partial \ln v} = a - b < 0$ (5.4)

Where μ^{ss} is steady state coefficient friction, "v" is the final velocity and "a" and "b" is the empirical values obtained from friction versus displacement graph.

On the other hand, the seismogenic fault always shows stable sliding if Kc ≤ 0, (Cox, 1990).

As far as the above stability criteria are concerned, the experienced velocity-stepping model mostly shows stable sliding. In other words, these experimental results show aseismic (stable sliding) behaviour. The model rarely shows a velocity-weakening (possibly seismogenic zones). Under appropriate loading boundary conditions the slip can accelerate to instability and some of the stored elastic energy can be radiated seismically (see Section 5.4.5).

In addition to the stability criterion, Boatwright and Cocco (1996) have divided the range of possible behaviours into four different regime; strong seismic or very velocity weakening, weak seismic or slightly velocity weakening, compliant or slightly velocity weakening, and viscous or very velocity strengthening. According to this phenomenological classification, the experimental results are compiled and tabulated in Table 5.6. In this table the "A" and "B" values are obtained directly from the shear stress versus shear displacement curves.

The sliding behaviour of the fault model according to stability criteria and the phenomenological classification are supported each other as both of the approach almost indicate the same seismicity type.

Table 5.6 Seismicity types of velocity-stepping model according to phenomenological classification of Boatwright and Cocco, 1996

Specimen Name	A (MPa)	B (MPa)	B-A (MPa)	σ (MPa)	Seismicity	Strain release
Granit1	0.18 / 0.18	0.13 / 0.11	-0.05 / -0.07	4.5	A-B>0 and ≤0.1 some aftershock	creep and forced dynamic slip
Granit2	0.168	0.172	0.004	5	B-A>0 and ≤ .05 weak seismic, inter seismic equation,. Main shocks	creep and intermittent dynamic slip
Granit3	0.19 / 0.15	0.13 / 0.2	-0.06 / 0.05	4.6	A-B>0 and ≤0.1 some aftershock / B-A>0 and ≤ 0.05 weak seismic	creep and forced dynamic slip / creep and intermittent dynamic slip
Granit4	0.2 / 0.14	0.11 / 0.05	-0.09 / -0.09	4.6	A-B>0 and ≤0.1 some aftershock	creep and forced dynamic slip
Granit5	0.13 / 0.19	0.04 / 0.1	-0.09 / -0.09	4.7	A-B>0 and ≤0.1 some aftershock	creep and forced dynamic slip
Average	0.170± 0.025	0.1± 0.06	-0.054 ±0.05	4.68± 0.19	A-B>0 and ≤0.1 some aftershock	creep and forced dynamic slip

In the light of the discussed comments, it can be stated that the overall character of the sliding is aseismic (stable sliding) and includes some aftershocks, creep and forced dynamic slip. Aseismic areas are velocity-strengthening faults regions that slip aseismically but can be driven to seismic events if they are sufficiently loaded by a sudden change (increase or decrease) due to rupture propagation in an adjacent velocity-weakening (seismogenic) area. As this study shows potentially seismic behaviour, the response of the same model is

investigated with the dynamic change of field stress effect at variable modes in the coming subtitles..

5.4.4. Normal stress change

In this study, the behaviour of the fault model is investigated under the stepwise simulation of the sudden change of the field stress. It is assumed that the field stress variation only affects the normal stress. The nominal normal stress is taken as 5 MPa and 10 MPa. Two kinds of stepwise tests are performed.

- At the first set of experiments, a single sudden increase of stress from the nominal stress is applied; after a period of time the normal stress is decreased to the nominal value again (see Fig. 5.17).

- The second set of experiments consist of the variation of the normal stress step in an ascending order from its nominal value, in other words, the repetition of a single sudden increase of normal stress step test with an ascending amplitude ($\Delta\sigma$ %) of 10%, 20% and 40% of the nominal stress (see Fig. 5.22). In this test, it is aimed to simulate the effect of field stress variation with steps from a small magnitude to a higher level in the Earth crust.

Figs. 5.16-5.27 show representative shear and normal stress versus time, shear stress versus shear displacement and coefficient of friction versus shear displacement records. As it is clearly seen from these figures, a step increase in normal stress causes a sudden increase in shear stress. This is due to elastic coupling between normal and shear stress. As the model continued to slide, the shear stress rises further. Eventually, the shear stress versus time path departs from the elastic loading curve and increases asymptotically toward a new value. The asymptotic rise roughly follows an exponential path. The transient effects (at the time of increasing or decreasing the normal stress step) are observed apparently for the higher stress step amplitude (40% of nominal stress) that cause unstable sliding (see Fig. 5.23).

81
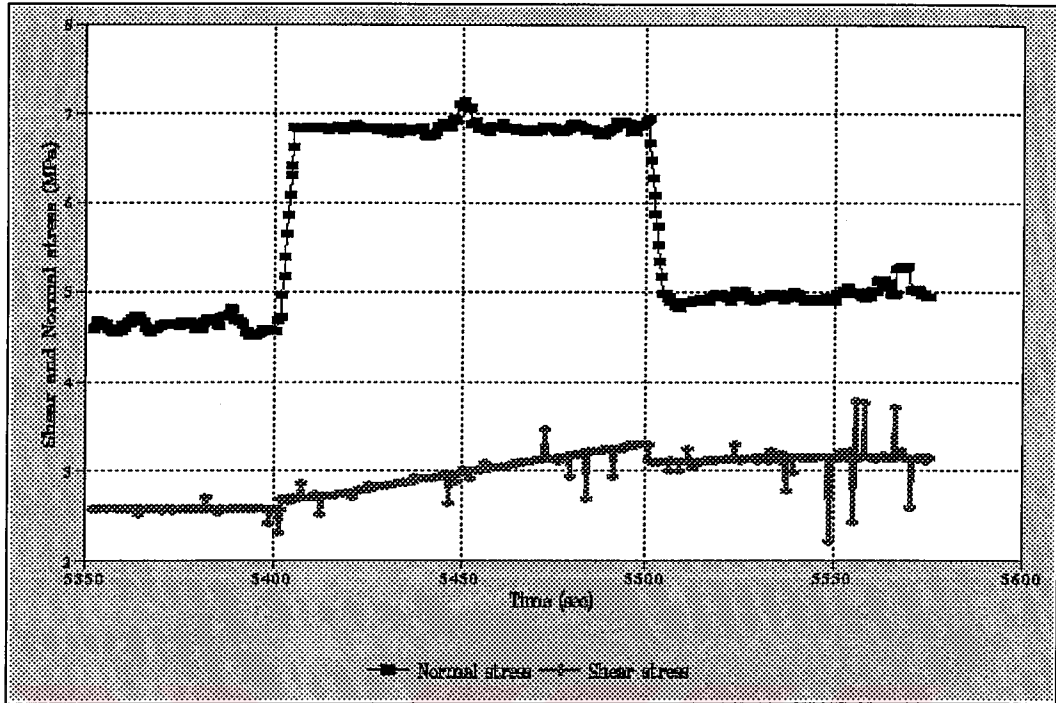
Figure 5.16 The shear and normal stress vs. time for normal stress single step change (Nominal stress is 5MPa)
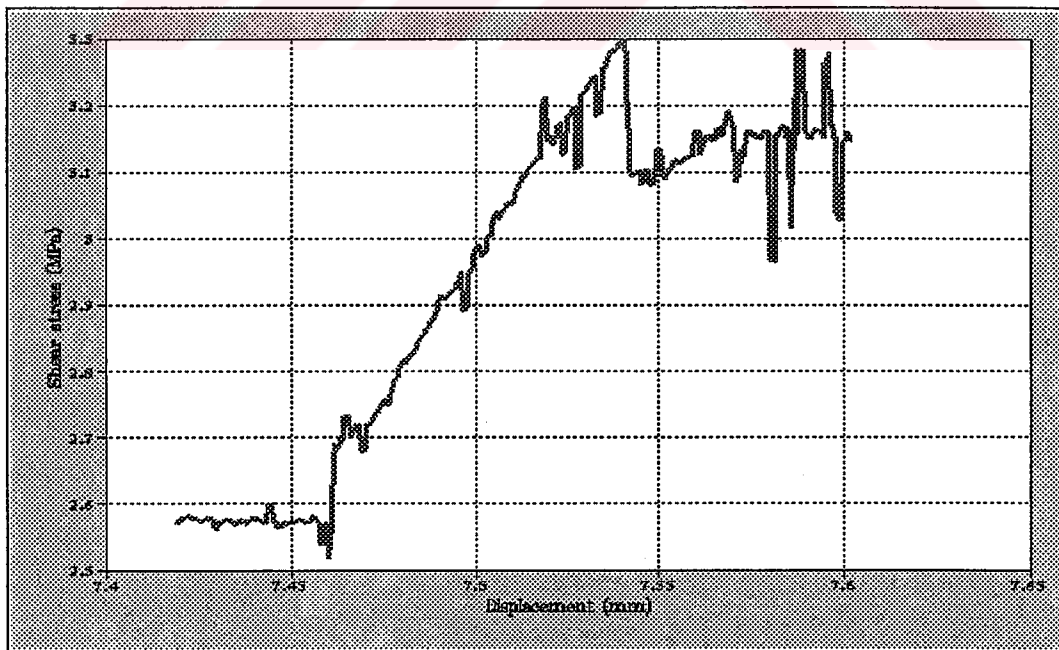
Figure 5.17 The shear stress vs. shear displacement for normal stress single step change (Nominal stress is 5MPa)
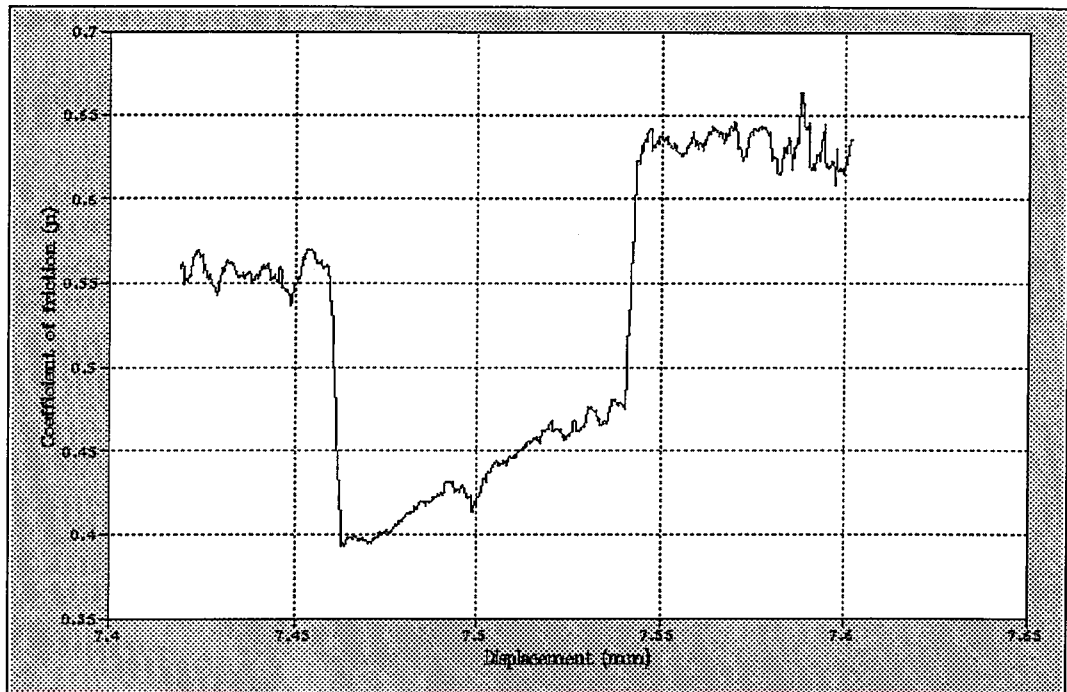
Figure 5.18 The coefficient of friction vs. shear displacement for normal stress single step change (Nominal stress is 5MPa)
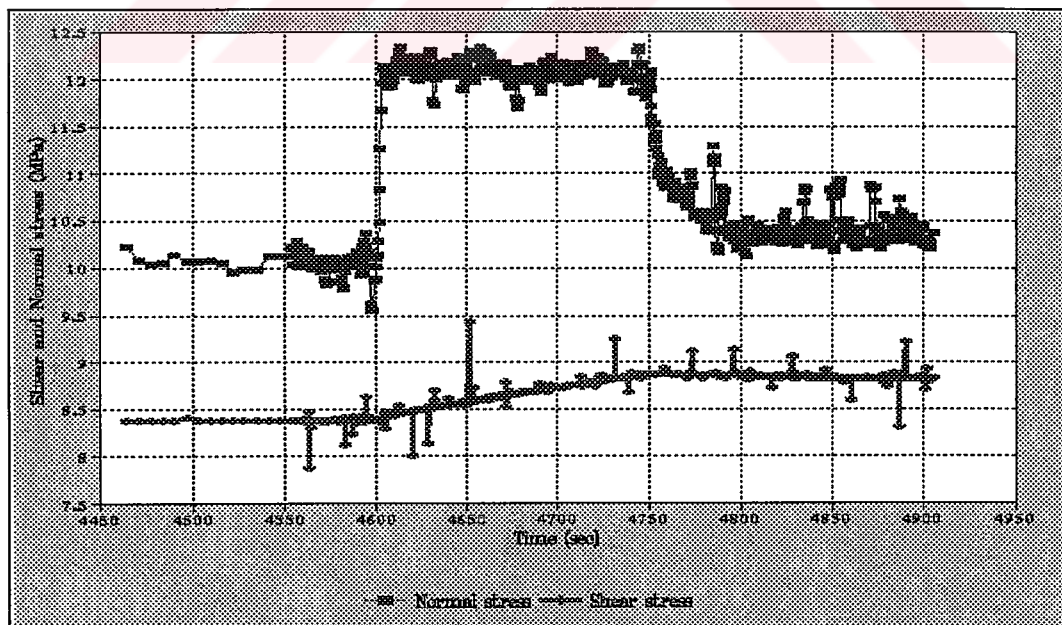
Figure 5.19 The shear and normal stress vs. time for normal stress single step change (Nominal stress is 10MPa)
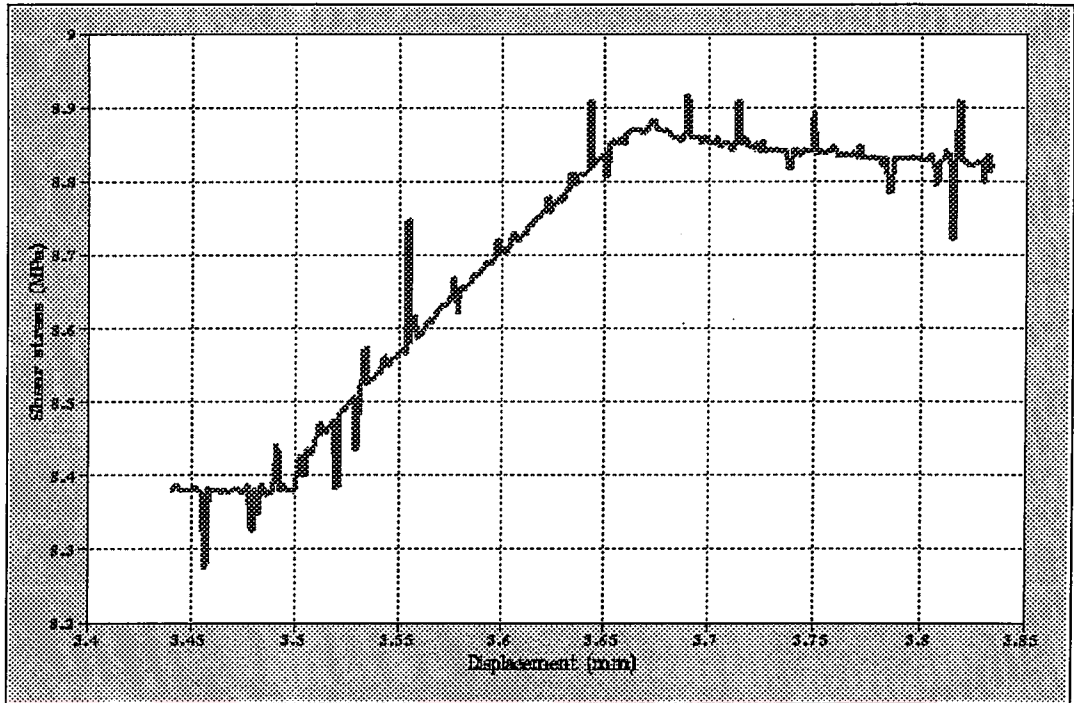
Figure 5.20 The shear stress vs. shear displacement for normal stress single step change (Nominal stress is 10MPa)

Figure 5.21 The coefficient of friction vs. shear displacement for normal stress single step change (Nominal stress is 10MPa)
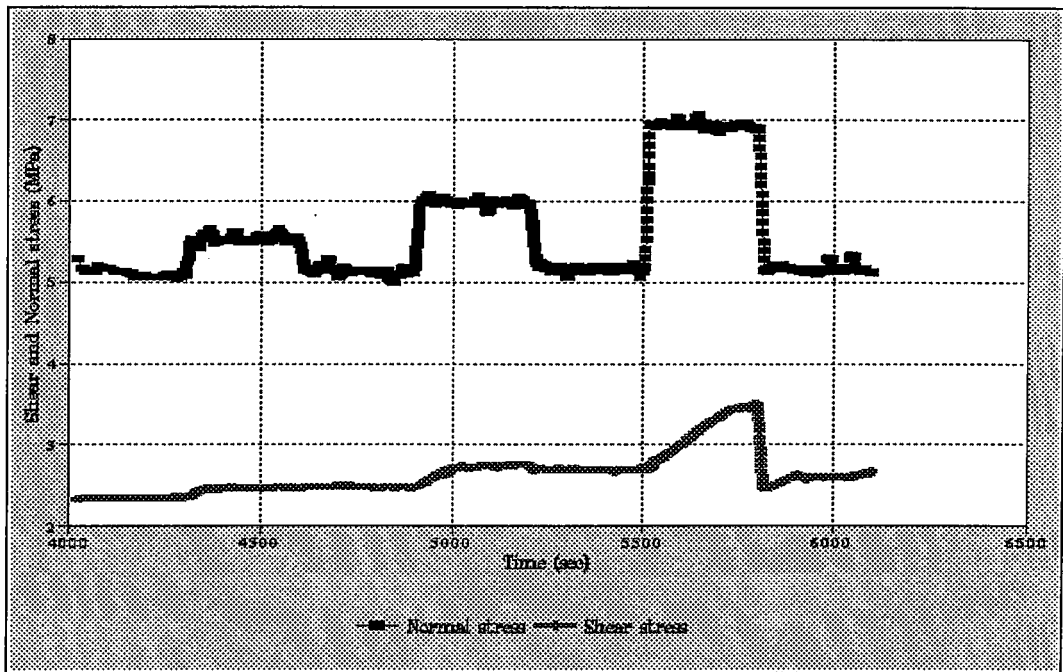
Figure 5.22 The shear and normal stress vs. time for normal stress ascending step change (Nominal stress is 5MPa)
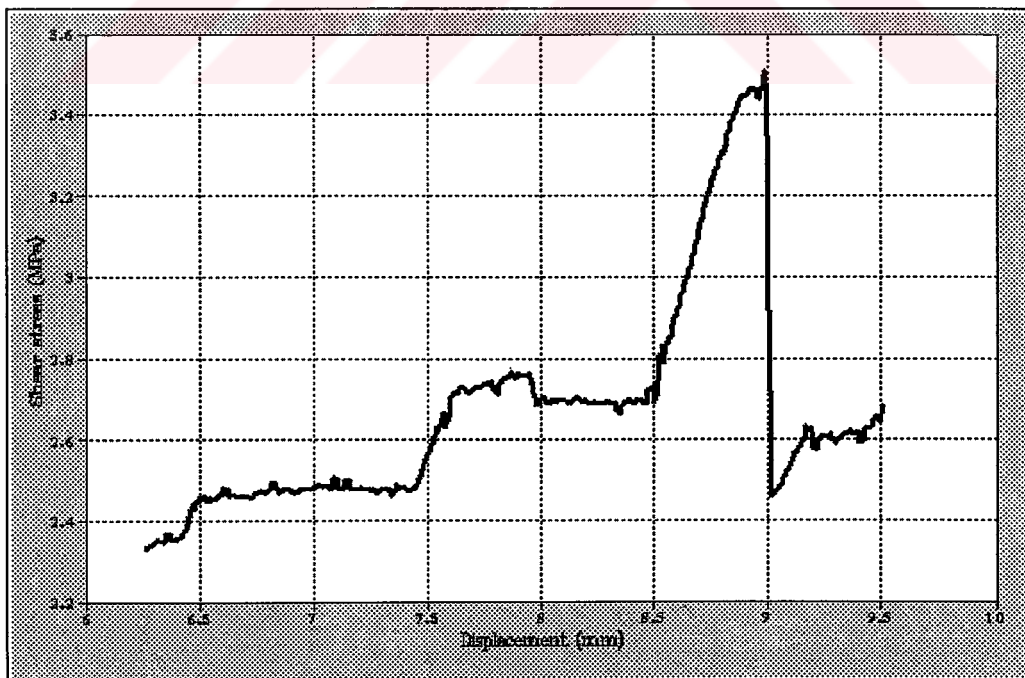
Figure 5.23 The shear stress vs. shear displacement for normal stress ascending step change (Nominal stress is 5MPa)

85
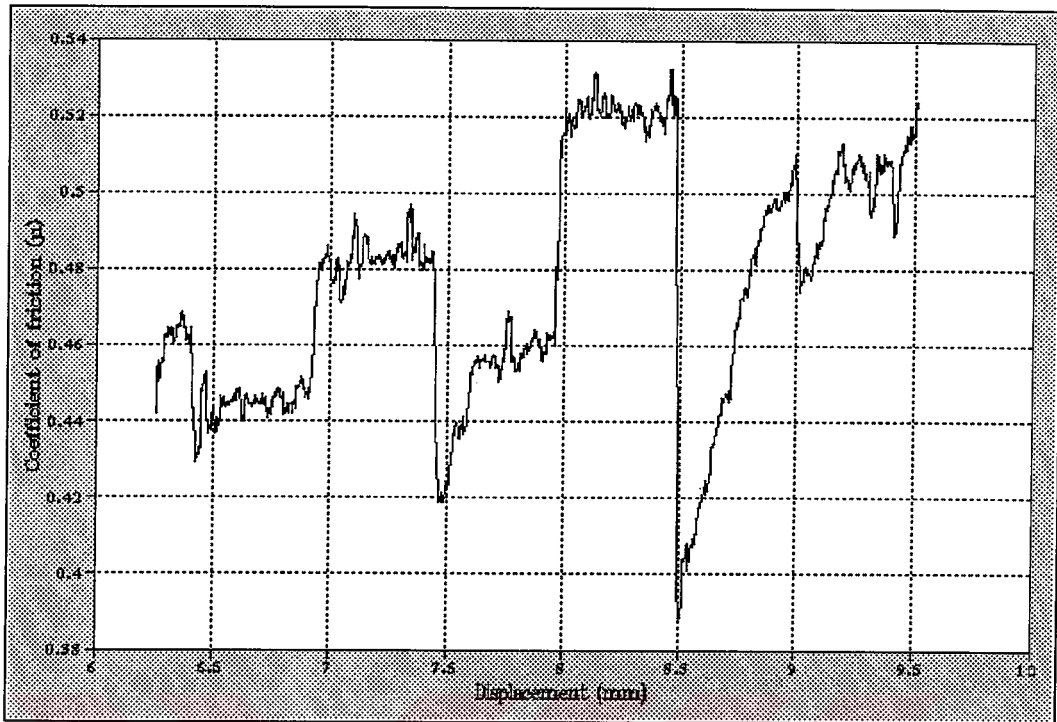
Figure 5.24 The coefficient of friction vs. shear displacement for normal stress ascending step change (Nominal stress is 5MPa)
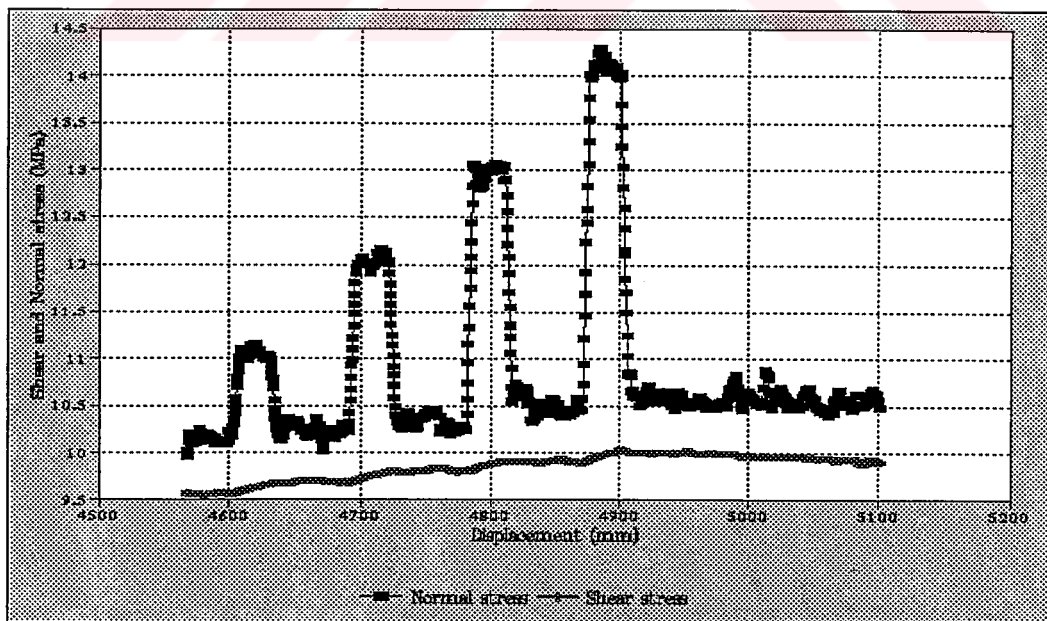
Figure 5.25 The shear and normal stress vs. shear displacement for normal stress ascending step change (Nominal stress is 10 MPa)
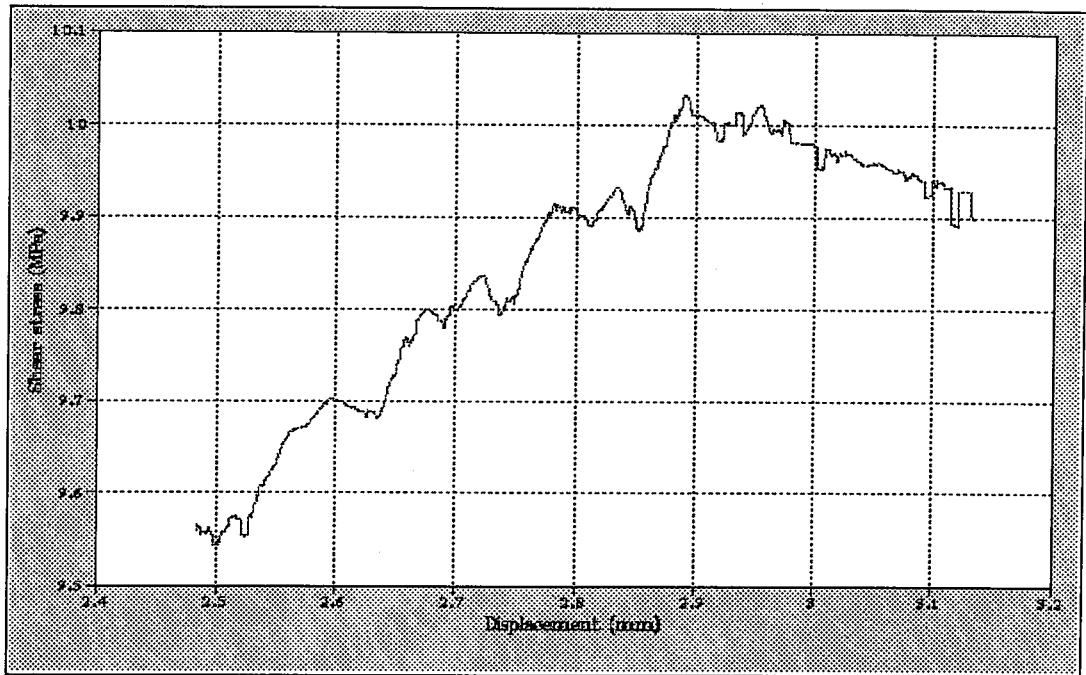
Figure 5.26 The shear stress vs. shear displacement for normal stress ascending step change (Nominal stress is 10 MPa)
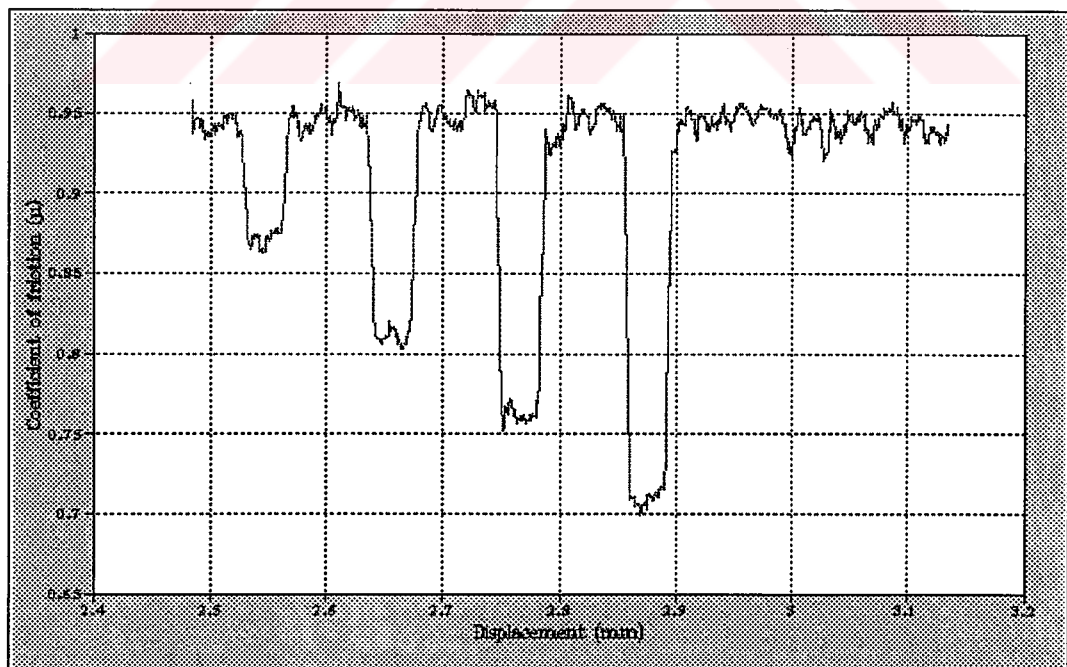
Figure 5.27 The coefficient of friction vs. shear displacement for normal stress ascending step change (Nominal stress is 10 MPa)

The empirical parameters resulted from the normal stress step change test (the shear stress increase ($\Delta\tau$); the steady state coefficient of friction (μ^{SS}) and coefficient of friction increase ($\Delta\mu$)) are tabulated in Table 5.7.

Table 5.7 The empirical parameters resulted from the normal stress step experiment

Specimen Name	Normal stress (MPa)	Normal stress step amplitude ($\Delta\sigma$ %)	Shear stress increase (MPa)	Shear stress increase ($\Delta\tau$ %)	Steady state coeff. of friction (μ^{SS})	Coefficient of friction increase ($\Delta\mu$)	Period (T) (sec)	Contact time (sec)
SP1	5	40	0.6	23	0.56	0.08	100	5400
SP2	10	20	0.44	5	0.84	0.02	200	4500
SP3	5	10	0.08	3	0.46	0.02	300	4500
SP3	5	20	0.27	11	0.48	0.04	300	5000
SP3	5	40	-0.1	4	0.52	-0.02	300	5500
SP4	10	10	0.14	1.5	0.95	0	30	4600
SP4	10	20	0.12	1.2	0.95	0	30	4700
SP4	10	30	0.1	1	0.95	0	30	4800
SP4	10	40	0.1	1	0.95	0	30	4900

5.4.4.1. Normal stress step test interpretations

The main focus in this experimental model is to establish a basis for the parametric study of normal stress variation affects on the behaviour of the seismogenic faults.

The stepwise increment of normal stress results mostly characterise the stress strengthening behaviour of the seismogenic faults. It means that sudden stress change in the normal stress causes the model to gain higher shear strength than the initial steady state. In other words, the new steady shear stress or coefficient of friction increases from the initial steady state values to a higher one after the stress step change in the normal stress.

The parametric study includes the duration (period) and amplitude ($\Delta\sigma$%) effect of the normal stress step on sliding behaviour of the model. From this parametric analysis it can be revealed out that the duration of the sudden change of field stress may be more critical than the magnitude of the sudden change of the field stress (amplitude) (see Table 5.7).

The types of seismicity based on the Boatwright and Cocco (1996) phenomenological classification is tabulated in Table 5.8. The stepwise normal stress change shows stable sliding and no seismicity; rarely, the creep and forced dynamic slip strain release is observed.

Table 5.8 Seismicity types for normal stress step according to phenomenological classification of Boatwright and Cocco, 1996

Sample Name	σ (MPa)	σ ($\Delta\sigma$, %)	B-A (MPa)	Seismicity	Strain release
SP1	5	40	-0.6	A»B none	stable sliding
SP2	10	20	-0.44	A»B none	stable sliding
SP3	5	10	-0.12	A»B none	stable sliding
SP3	5	20	-0.27	A»B none	stable sliding
SP3	5	40	0.1	A-B>0 and ≤0.1 some aftershock	creep and forced dynamic slip
SP4	10	10	-0.14	A»B none	stable sliding
SP4	10	20	-0.12	A»B none	stable sliding
SP4	10	30	-0.11	A»B none	stable sliding
SP4	10	40	-0.11	A»B none	stable sliding

On the other hand , the parametric study at different normal stress levels (5 and 10 MPa) shows that the depth variation effect on the sliding behaviour of seismogenic fault is not clearly observed. Although it is early at this stage to jump sound conclusions, it can be stated that the shear stress variation does not depend primarily on the depth (see Table 5.7). To support this assertion , this type of experiments should be repeated at different nominal normal stress levels.

5.4.5. Functional normal stress change tests

At this model study, the same procedure is applied as the normal stress step test. The only difference is the shape of the sudden normal stress change. When the state of steady state shear stress is reached, the prescribed functional form of a normal stress change instead of stress step is imposed. The simulated stress functions are given in equation 5.6. The analytical and resulted experimental output from the execution of applied analytical sine function of the normal stress variation is shown graphically in Fig. 5.28.

$$F(t) = \frac{P}{2}\left(1 - \cos\frac{4\pi t}{T}\right) + P_i \quad 0 \le t \le \frac{T}{4}$$

or,

$$F(t) = P\left(\sin\left(\frac{2\pi t}{T}\right)\right) + P_i \qquad 0 \le t \ge T \tag{5.5}$$

$$F(t) = P_i \qquad\qquad t < T, \quad t > T$$

where $T = t_f - t_i$ is period in second and $P = P_f - P_i$ is load in kgf, as they are graphically shown below:
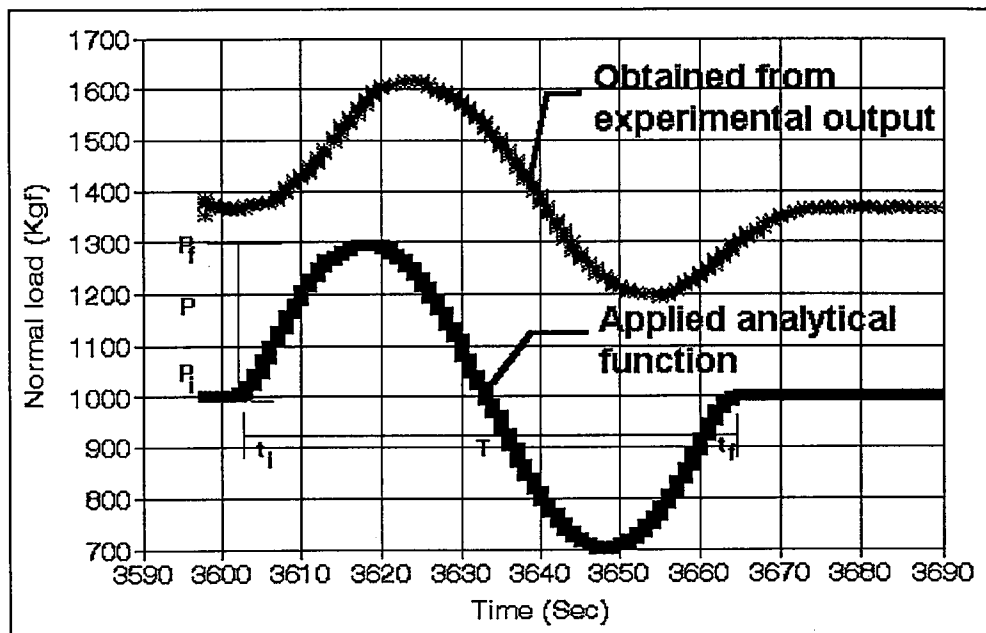
Figure 5. 28 The simulation of normal stress change with sine function

This type functional normal stress change is applied since the most of the aftershock seismicity profile is in this form (see Section 2.6.1). Besides this, the shape effect of stress change is studied by using two kinds of normal stress variation function (sine and cosine and also step function in normal stress step tests).

The sudden change of field stress may occur in different modes in the Earth crust. The magnitude, duration of occurrence or periodic (cyclic) events associated with co-seismic field stress change are well known modes which alter earthquake mechanism. In order to study these affects, the parametric study of the functional normal stress change is applied in three modes. In the first mode, the functional normal stress change is repeated continuously two or three times (cyclic loading conditions). Then, the amplitude ($\Delta\sigma\%$) effect of functional normal stress change is studied extensively at the second mode. The last mode includes the effect of the duration or period (T) of the functional normal stress change (see Fig. 5.28)

The representative graphs obtained from these experiments are given in Figs. 5.29-5.41. The common feature of these graphs is that; the elastic response of a shear stress to the sudden increase in normal stress is observed initially. Then shear stress asymptotically decays to a new value following the decrease of the normal stress change. The coefficient of friction graphs show just the opposite (increase in shear stress corresponds to decrease in the coefficient of friction). The overshoot of the shear stress or coefficient of friction (very high sudden drops of the shear stress or coefficient of friction) at the inflection point of the functional normal stress change is clearly observed (e.g. see Fig. 5.37). Under this stress change level, the functional normal stress change value is under the nominal, the normal stress before the application of the functional normal stress change, normal stress. At this point, sudden drop of the shear stress is very high which is in the range of remarkable seismic stress drop (0.4-10 MPa). The obtained new steady shear stress is below the nominal steady shear stress value.

In the cases of the repeated (periodically imposed) functional normal stress change, the shear strength of the model falls critically at the beginning of this application. Subsequent shear stress changes are very small compare to the first shear change resulted from normal stress change at the start of the functional stress change execution (see, Fig. 5.29-30).

91
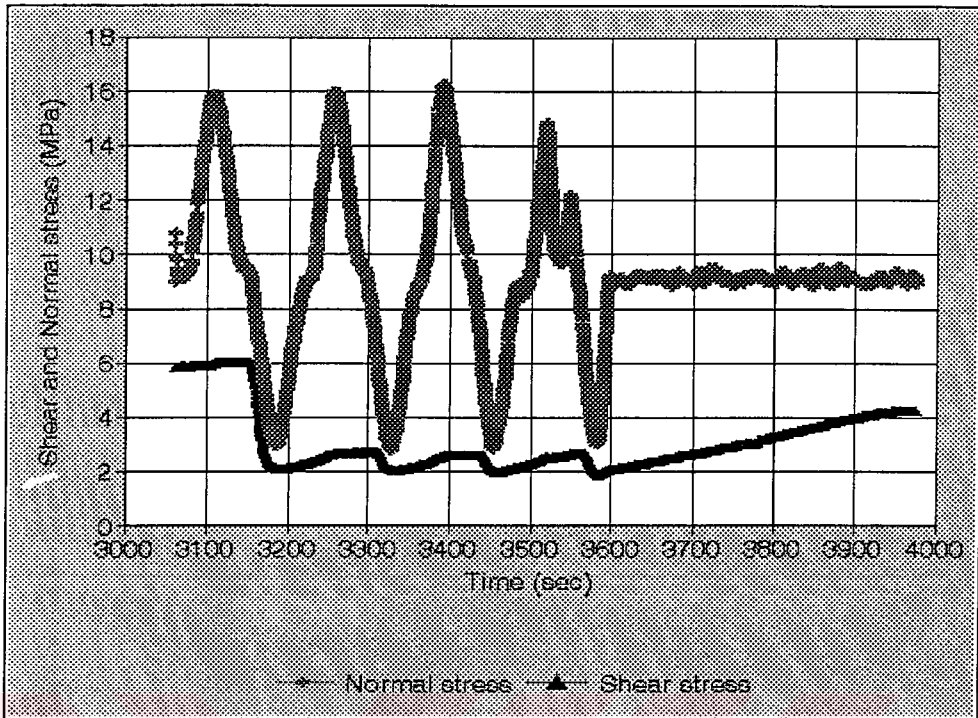
Figure 5.29 The shear and normal stress vs. time for repeated functional normal stress change (Nominal stress is 10 MPa)
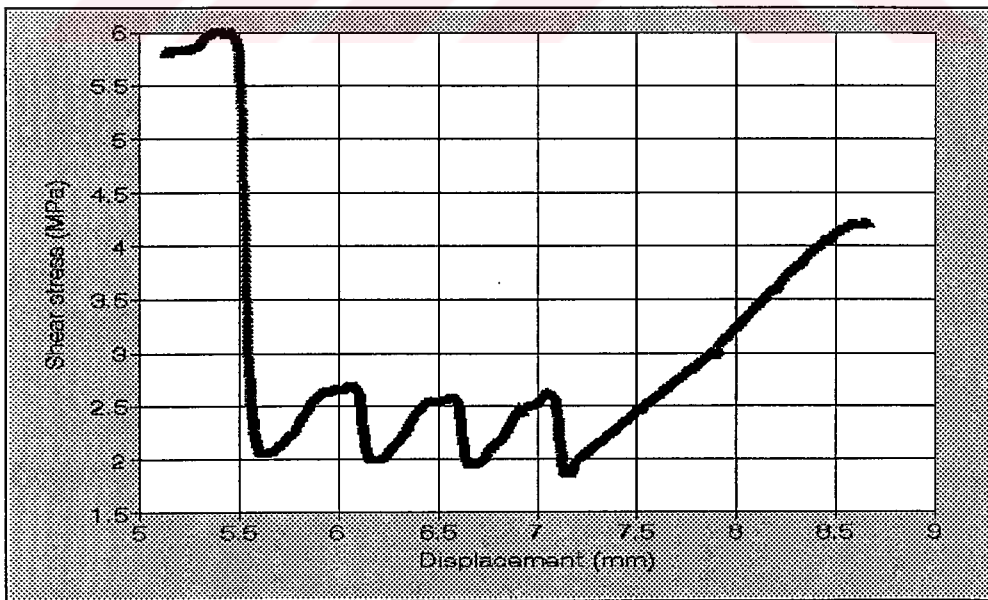
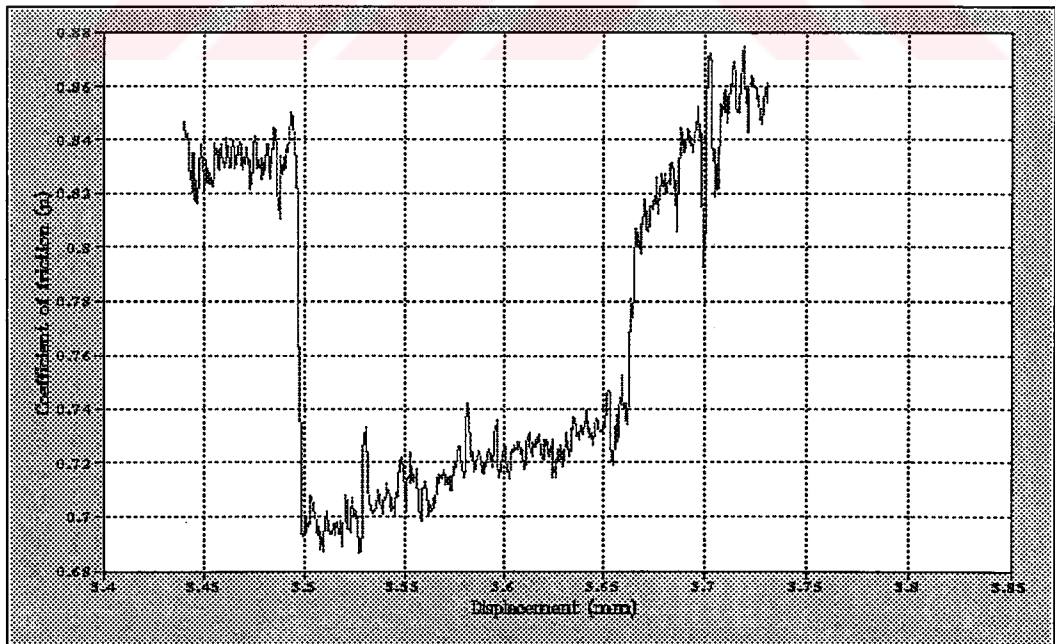Figure 5.30 The shear stress vs. shear displacement for repeated functional normal stress change (Nominal stress is 10 MPa)
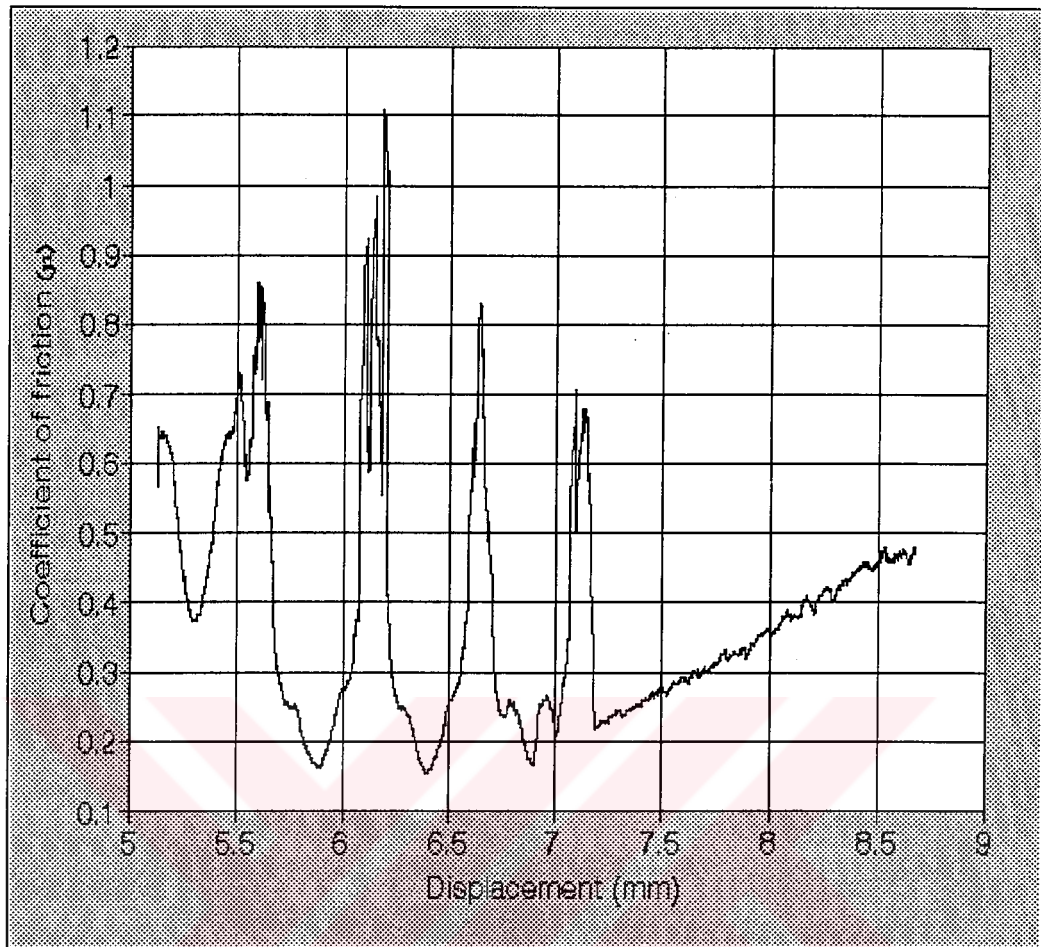
Figure 5.31 The coefficient of friction vs. shear displacement for repeated functional normal stress change (Nominal stress is 10 MPa)

The period of the simulated functional normal stress change effect on the frictional sliding can be clearly observed the Figs. 5.32-5.34. At the same loading and sliding conditions, the function with long period (e.g. T=60 sec) causes more unstable sliding which produces higher stress and friction drop than the shorter period (T= 30 sec).

The parametric study for the amplitude of the functional normal stress change shows the highly effect of this parameter to the sliding behaviour of the model. From the Figs. 5.35-5.36, the amplitude effect (for $\Delta\sigma\%=10$ and $\Delta\sigma\%=40$ of nominal normal stress change in magnitude) of the functional normal stress change can be observed.
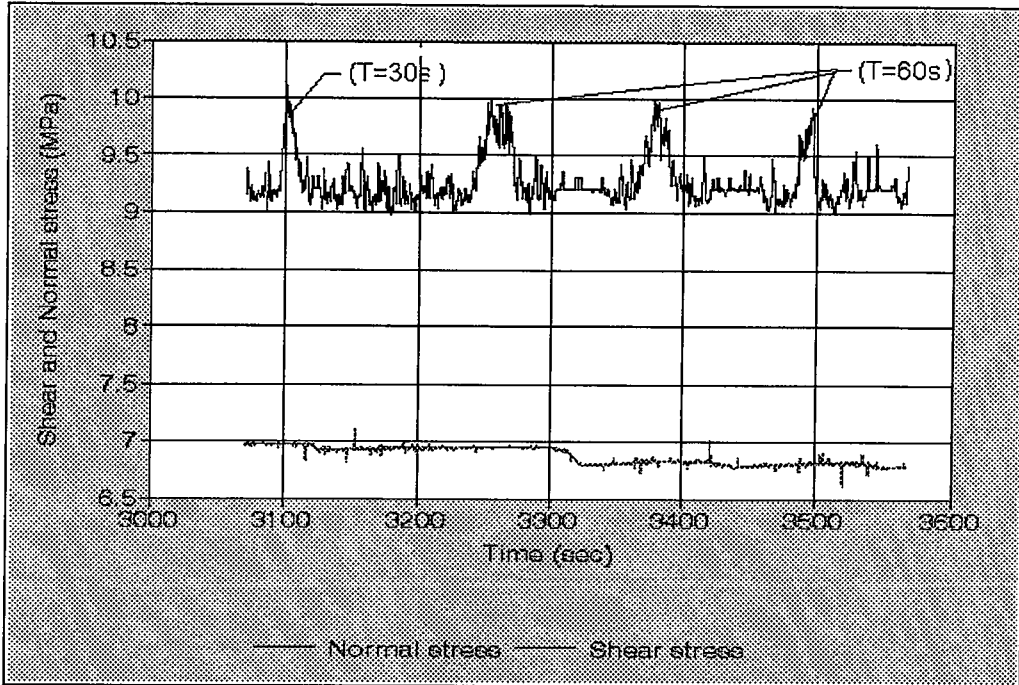
Figure 5.32 The shear and normal stress vs. time for period effect functional
normal stress change (Nominal stress is 10 MPa)
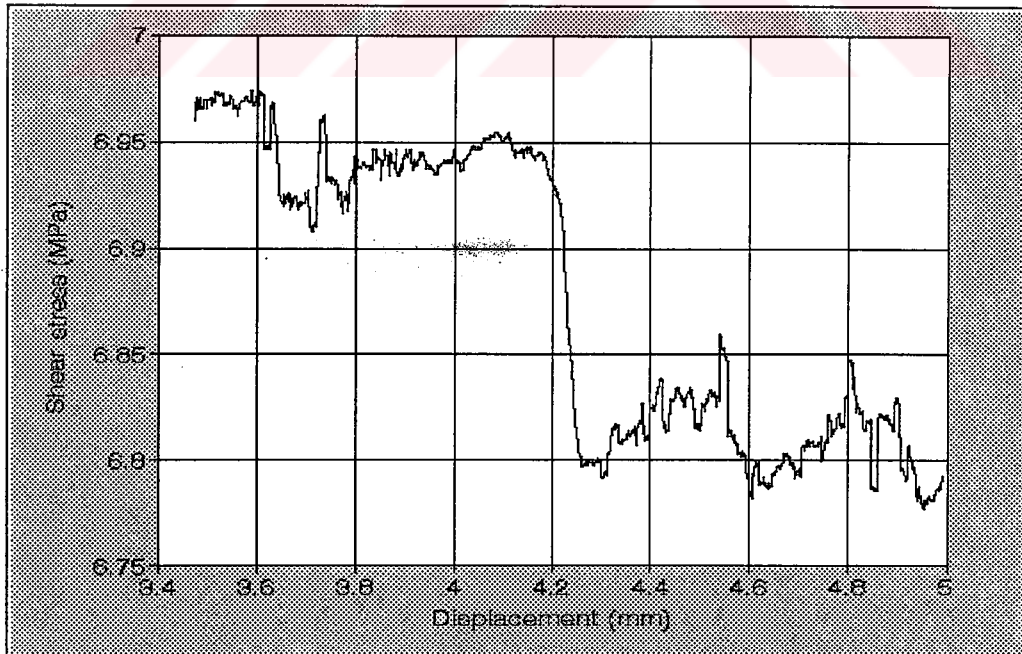
Figure 5.33 The shear stress vs. shear displacement for period effect functional
normal stress change (Nominal stress is 10 MPa)

94
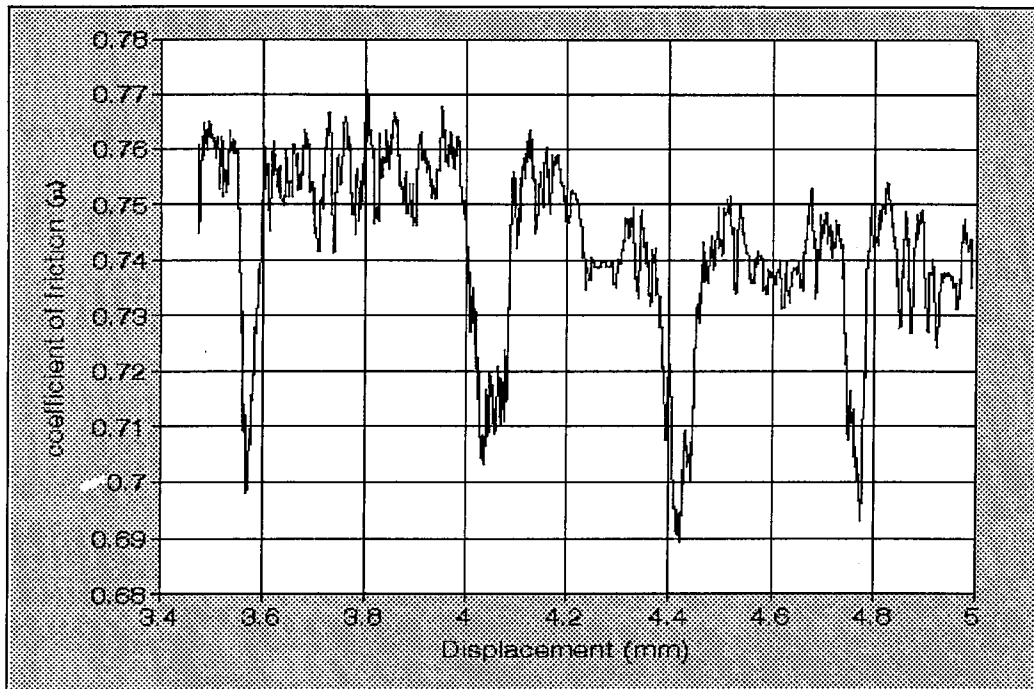
Figure 5.34 The coefficient of friction vs. shear displacement for period effect
functional normal stress change (Nominal stress is 10 MPa)
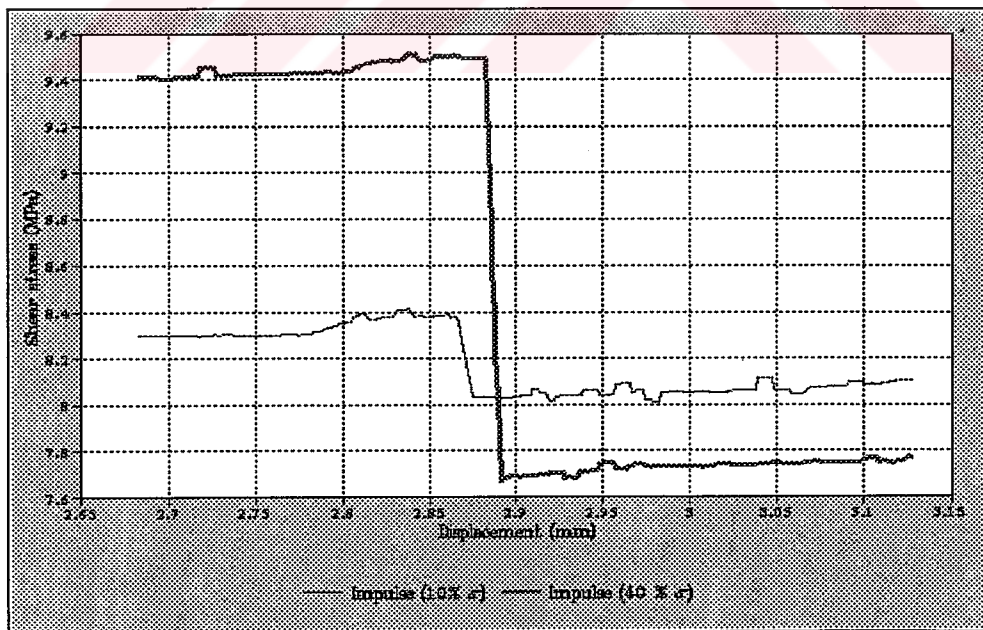
Figure 5.35 The shear stress vs. shear displacement for amplitude effect
functional normal stress change (Nominal stress is 10 MPa)

95
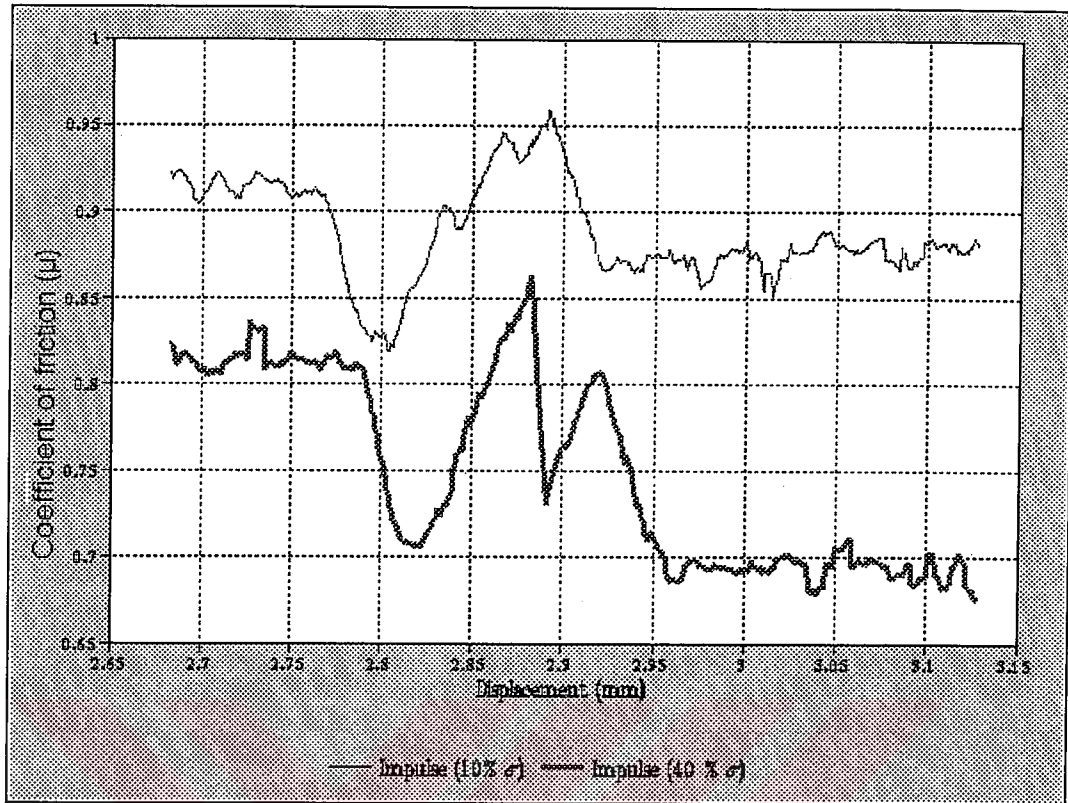
Figure 5.36 The coefficient of friction vs. shear displacement for amplitude effect functional normal stress change (Nominal stress is 10 MPa)

The empirical results of the functional normal stress change (shear stress drop ($\Delta\tau$); the steady state friction (μ^{SS}) and coefficient of friction drop ($\Delta\mu$)) are tabulated in Table 5.9 according to normal stress change amplitude and period.

5.4.5.1. The functional normal stress change test interpretations

The results of this model are consistent within each other. The different graphs show the same characteristic curve under the same stress and strain boundary conditions resulted from the same sample experiments. Some of these empirical parameters will be used for the mathematical modelling of the earthquake fault mechanism in the coming sections.

Table 5.9 The empirical parameters estimated from the functional normal stress

change experiment

Specimen Name	Normal stress (MPa)	Stress amplitude ($\Delta\sigma$ %)	Shear stress drop (MPa)	Shear stress drop ($\Delta\tau$ %)	Steady state coeff. of friction (μ^{SS})	Coefficient of friction drop ($\Delta\mu$)	Period (T) (sec)	Contact time (sec)
S2A2	9	78	3.9	65	0.64	0.43	120	3100
A2B1	5	56	1.25	46	0.6	0.25	20	4600
A22	5	41	1.41	44	0.66	0.22	120	3600
SPP1	10	38	2.56	28	0.91	0.27	60	4600
2A1	5	36	1.74	49	0.70	0.29	60	3600
SPG1	10	32	1.72	19	0.9	0.19	30	4600
SPG2A	10	30	1.05	16	0.74	0.09	60	3100
5SIN1	5	30	+0.1	3.2	0.60	0	60	3600
5SIN6	8.2	30	1.4	19	0.86	0.16	60	4000
5SIN5	6.8	24	1.7	25	0.86	0.24	60	4000
2BS3	5	22	1.4	56	0.51	0.21	60	3600
SG2A2	10	18	0.39	14	0.95	0.08	20	4600
SG2A3	10	15	1.73	18	0.81	0.11	60	4600
SG2B1	10	13	0.26	3	0.91	0.04	60	4600
SG22	8.8	11	0.6	8	0.83	0.06	120	3100
SS5	5	11	0.05	2	0.45	0.01	60	4600
SG2B2	9.2	5	0.14	2	0.76	0.02	60	3100

During this model study, it is observed that when the functional stress change is increased according to the shape of the function, the shear strength of the system also increases following the same kind of curve. When the applied stress change function turns to the level which is below the nominal normal stress value, the overshoot is observed in the shear stress and friction (see Fig. 5.36). This behaviour reveals out that the stress relief is very sensible parameter that affects the seismicity of the earthquake faults.

The sliding rate at the instant of shear stress drop increases to a very high value. This increment can be even hundred times of the nominal sliding rate of the model ($1 \mu ms^{-1}$ increases to $100 \mu ms^{-1}$). This much increase in the sliding rate apparently indicates that the model is in the state of highly strong seismic mode. The change of sliding rate depending on the applied functional stress change amplitude is shown in Fig. 5.37.
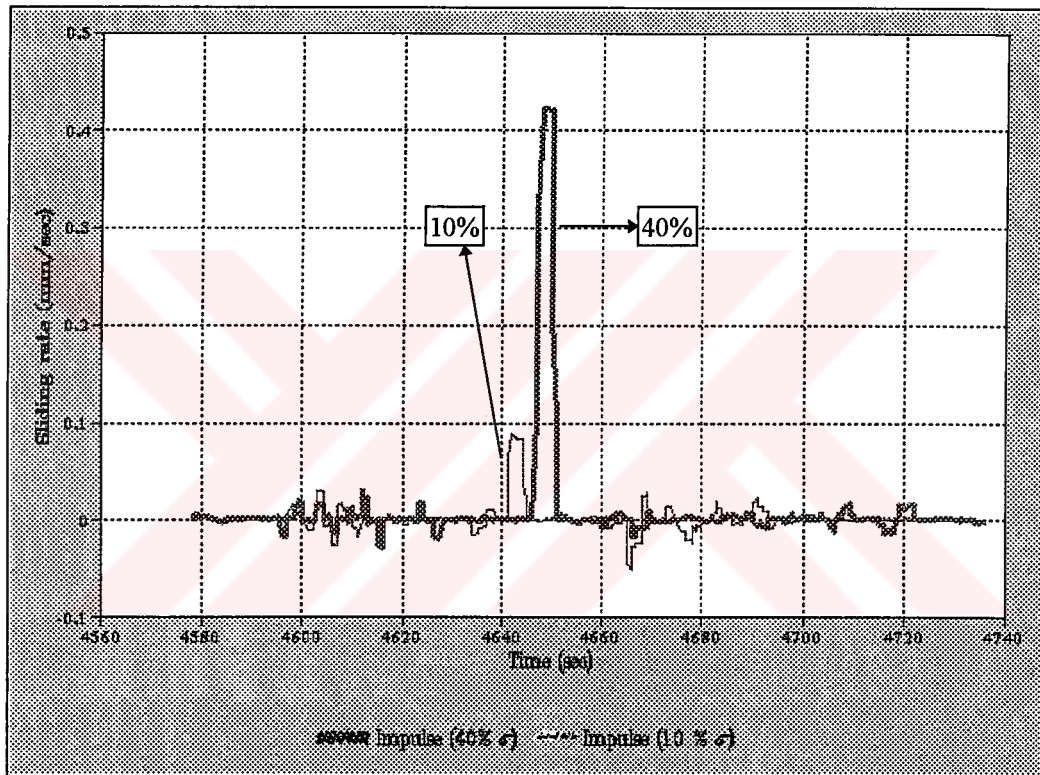
Figure 5.37 The sudden increase in sliding rate according to functional stress change amplitude

From this figure (Fig. 5.37) the effect of the amplitude of the field stress change on the sliding rate is clearly seen. Besides the relief of the field stress, the amplitude ($\Delta\sigma$) of the field stress change is also very important parameter for understanding of earthquake mechanism.

The seismicity types of this model is also prepared according to the phenomenological classification in Table 5.10. It is clearly seen from this table that the model mostly shows seismic character (main shocks and some after shocks), episodic dynamic slip strain release. The weak and aseismic areas can also be rarely noticed.

Table 5.10 Seismicity types for functional stress change test according to phenomenological classification of Boatwright and Cocco, 1996

Specimen Name	σ (MPa)	σ (Δσ, %)	B-A (MPa)	Seismicity	Strain release
S2A2	9	78	3.9	B»A, main shocks and after some shocks	episodic dynamic slip
A2B1	5	56	1.25	B»A, main shocks and after some shocks	episodic dynamic slip
A22	5	41	1.41	B»A, main shocks and after some shocks	episodic dynamic slip
SPP1	10	38	2.56	B»A, main shocks and after some shocks	episodic dynamic slip
2A1	5	36	1.74	B»A, main shocks and after some shocks	episodic dynamic slip
SPG1	10	32	1.72	B»A, main shocks and after some shocks	episodic dynamic slip
SPG2A	10	30	1.05	B»A, main shocks and after some shocks	episodic dynamic slip
5SIN1	5	30	-0.1	A-B>0, ≤0.1, some aftershocks	creep and forced intermittent dynamic slip
5SIN6	8.2	30	1.4	B»A, main shocks and after some shocks	episodic dynamic slip
5SIN5	6.8	24	1.7	B»A, main shocks and after some shocks	episodic dynamic slip
2BS3	5	22	1.4	B»A, main shocks and after some shocks	episodic dynamic slip
SG2A2	10	18	0.39	B»A, main shocks and after some shocks	episodic dynamic slip
SG2A3	10	15	1.73	B»A, main shocks and after some shocks	episodic dynamic slip
SG2B1	10	13	0.26	B»A, main shocks and after some shocks	episodic dynamic slip
SG22	8.8	11	0.6	B»A, main shocks and after some shocks	episodic dynamic slip
SS5	5	11	0.05	B-A>0, ≤.05, inter seismic eqn., fore shocks, main shocks and aftershocks	creep and intermittent dynamic slip
SG2B2	9.2	5	0.14	B»A, main shocks and after some shocks	episodic dynamic slip

There is no doubt that decreases in normal stress also promote instability as seen from the functional stress change tests. For example in response to a sudden decrease of the normal stress change under the nominal normal stress, the shear strength drops suddenly by an amount that is controlled by the amplitude ($\Delta\sigma$) and period (T) and increase toward the new steady value but below the initial shear strength. The effect of the stress change amplitude on the friction drop is modelled analytically and is presented in Fig. 5.38.

When the normal stress change is not below the nominal stress value, the shear or coefficient of friction drops promote instability but it is weak seismic characteristics. The transition from a aseismic to a seismic phase assertion in this stage can not be put forward. This assertion should be tested in a further study increasing the number experiments with this type of parametric study.
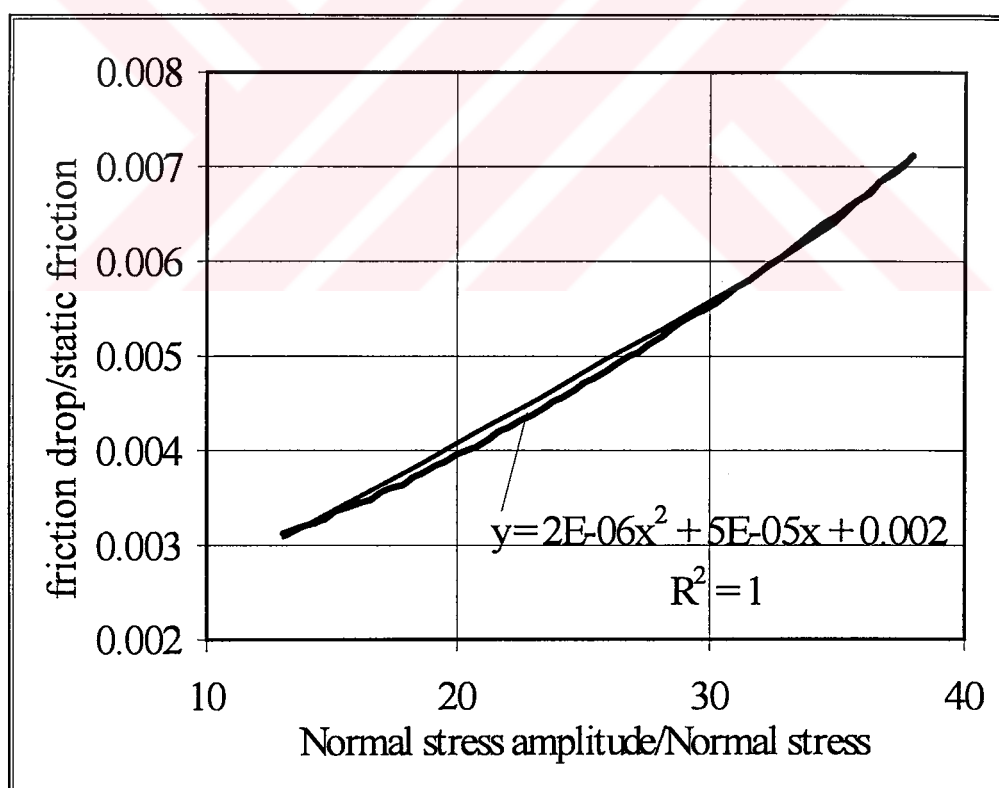
Figure 5.38 The mathematical model of friction drop due to functional normal stress change in amplitude

If the term stress drop refers to the difference between the stresses before and after the rupture of the surface structure of the fault model, the rupture or the intensity of the earthquake can be estimated from the stress drop mathematical modelling. From the literature, it is revealed out that the stress drop occurs in the Earth along the stick or creeping segment of fault surfaces when the stresses exceed the strength of the material leading rapidly to fracture or when the crustal strain exceeds the ultimate strain value. However, the results of this model contradict the above suggestions. Although the amplitude of the stress change influences the stress drop but most of the test results result in overshoot stress drop when the stress variation falls below the nominal stress. This behaviour shows that the stress relief is more dominant than the strength of the fault surface.

Some of the researchers (eg. Dieterich, 1995; Byerlee, 1970) pointed out that the stress drop during slip in laboratory specimen is about an order of magnitude higher than the shallow focus earthquakes. They have also stated that the stress drop during even very large earthquakes is rarely greater than 10 MPa. Tao and Zhang (1990) stated that Tangshan earthquake which took place in July 1976 increased the minor principal stress about 0.3 MPa and decreased the major principal stress 0.4 MPa. As far as the above arguments are considered the shear stress drops observed from this functional stress change model; are in agreement with the field value. In other words, these shear stress drops are in the range of shallow focus earthquakes' value which are less than 10 MPa. The mathematical modelling of the shear stress drop according to functional normal stress change in amplitude is shown in Fig. 5.39.

5.4.6. Simultaneous functional normal and shear stress change

Yin and Rogers (1995) have stated in their article that earthquake rupture, causes the tectonic stress and strain in the crust to release and have remarked that, after seismic rupture, the principal stress directions must be rotated to adapt a change of the state of stress on the fault and surrounding of the fault. They have supported their hypothesis from the field observations. The examples are given from rotation of the stress field due to seismic rupture has been observed in some California earthquake sequences, such as the 1983 Coalinga earthquake, the 1986 Ocenaside earthquake, the 1989 Loma prieta earthquake and the 1992 Joshua Tree and Landers earthquake. They have constrained their studies that the normal stress
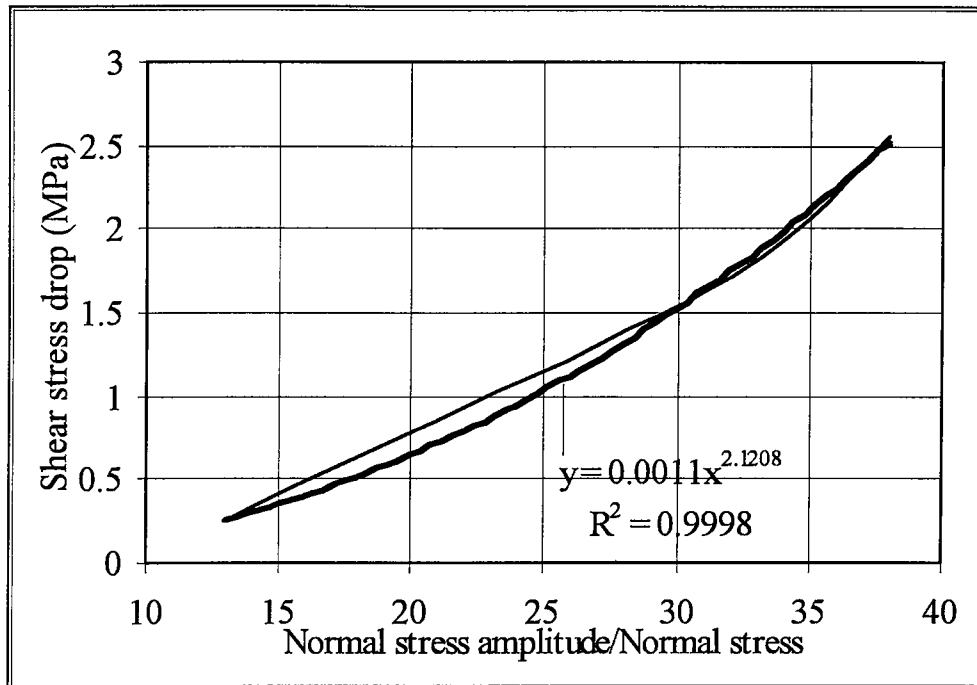
Figure 5.39 The analytical model of shear stress drop due to the functional normal stress change in amplitude

on the fault does not change, this constraints do not resemble the real case as mentioned above. Due to the initial angle between major principal stress (σ_1) and the fault plane, the initial shear stress and normal stress magnitudes acting on the creeping zone of the fault are different. The aftershocks of nearby earthquake, nuclear bomb explosion, mining activities, volcanic eruptions and other agencies causes the stress field to change. Thus the normal and shear stress of the fault plane will be effected at the same time form these change. Scholz (1990) also stated that the orientation of fault planes with respect to the principal stress directions has changed during the main shock. Due to this, some faults which were previously "strengthening" become "weakening".

Within this view, the experimental fault model is investigated under the normal and shear stress change boundary conditions. With these tests, the sliding rate is again held constant at $1 \mu ms^{-1}$ for the duration of the test. The same stress function used for the functional normal stress change experiments is applied. The initial shear stress value was taken as 10 % of the nominal normal stress. This

means that the initial angle between major principle stress (σ) is taken as 80°. This stress ratio is preserved throughout the whole test.

The same methodology used for the functional normal stress change test is followed during the application of these tests. In order to compare the results of this model with the functional normal stress change the same test conditions are tried to be applied to the system.

This model is experienced on three nominal stress level (5, 7, 8 MPa normal stress and corresponding shear stress value according to the shear stress to normal stress ratio of 10% as stated above). As the same characteristics figures are obtained with the functional normal stress change test, rather than giving the detail of the test results the main parameters will be discussed in this section. The shear stress and coefficient of friction variation with the stress change are presented from Fig. 5.40 to 5.45. The shape of the obtained curves is similar to the functional normal stress change output; The only difference is in the magnitude of the studied parameters (e.g. stress drop, coefficient of friction drop). The estimated empirical parameters ($\Delta\sigma$, μ^{SS}, $\Delta\mu$ etc.) directly from the graphical output of this model are given in Table 5.11.
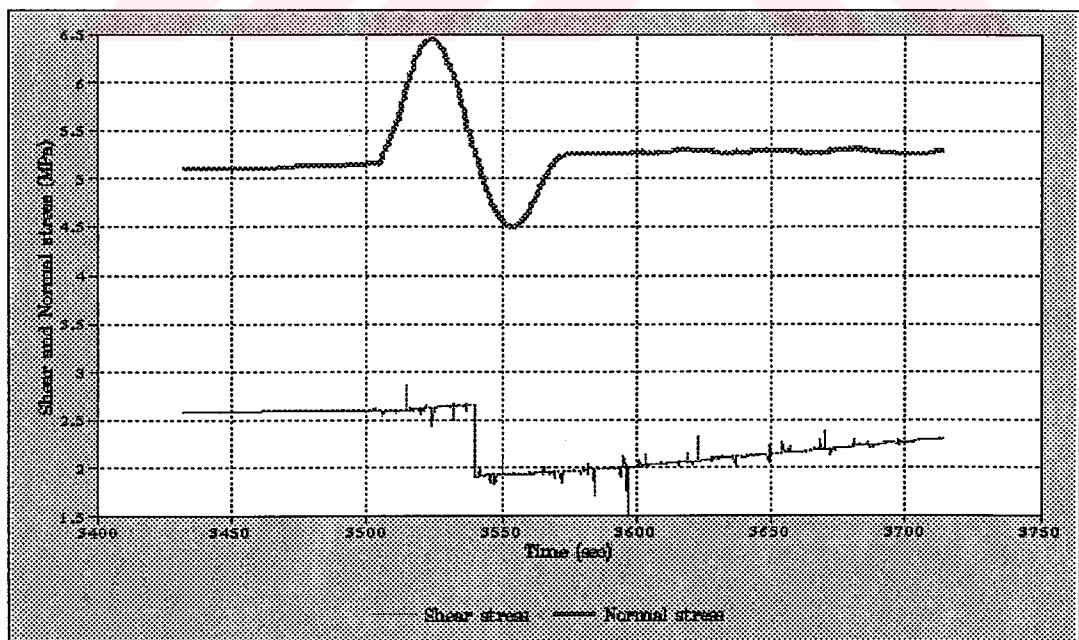
Figure 5.40 The shear and normal stress vs. time for the simultanous functional normal and shear stress change ($\sigma \cong 5$ MPa)

103
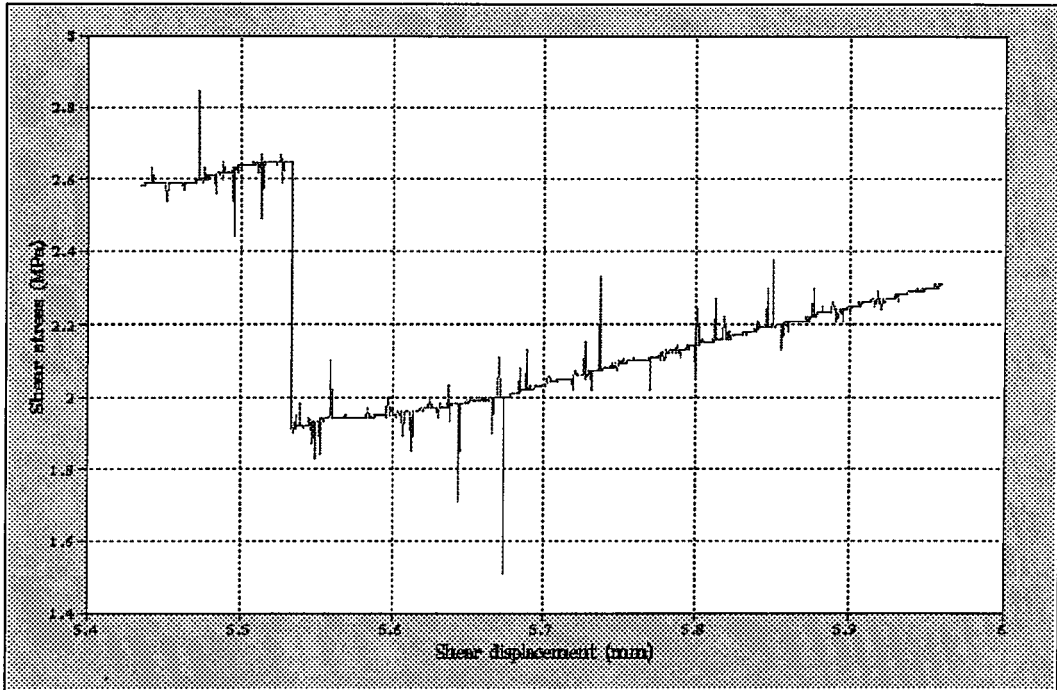
Figure 5.41 The shear stress vs. shear displacement for the functional normal and shear stress change ($\sigma \cong 5$ MPa)
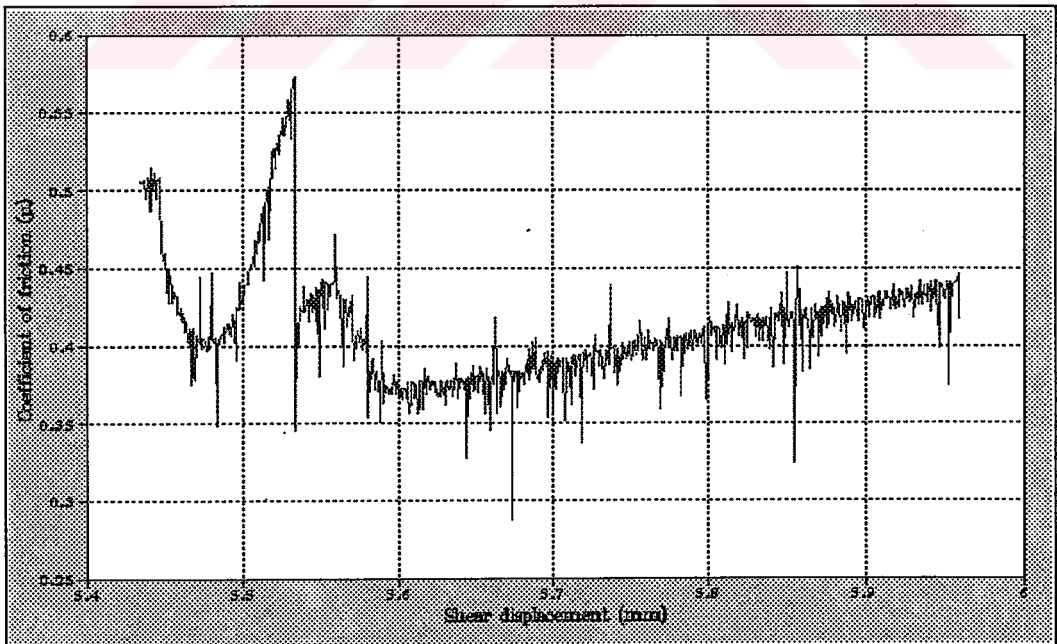
Figure 5.42 The coefficient of friction vs. time for the simultaneous functional normal and shear stress change ($\sigma \cong 5$ MPa)
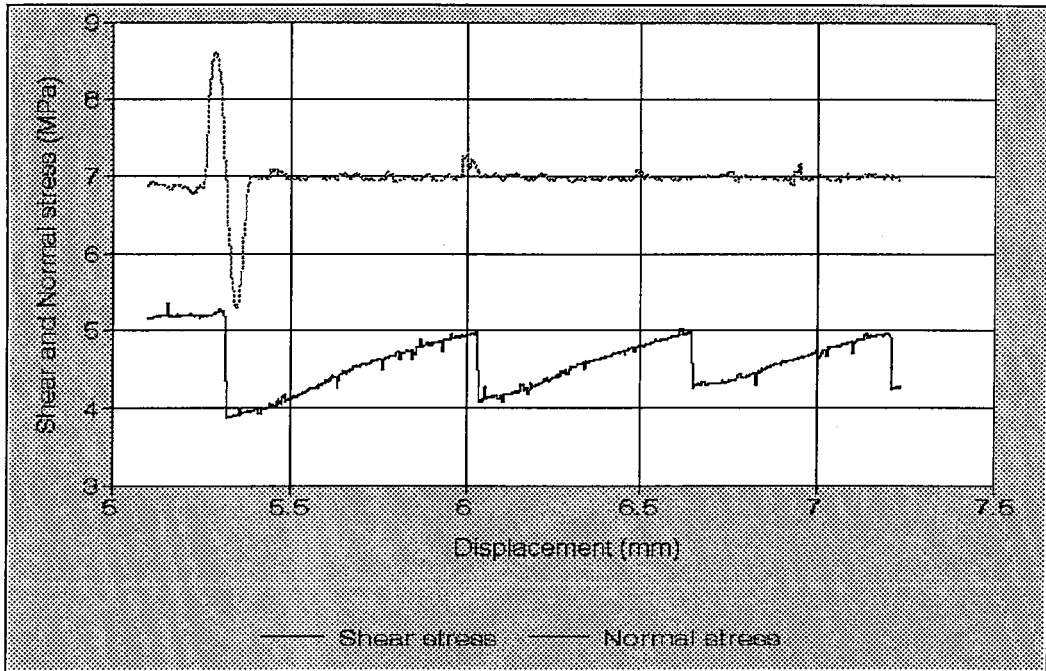
Figure 5.43 The shear and normal stress vs. time for the simultaneous functional normal and shear stress change ($\sigma \cong 7$ MPa)
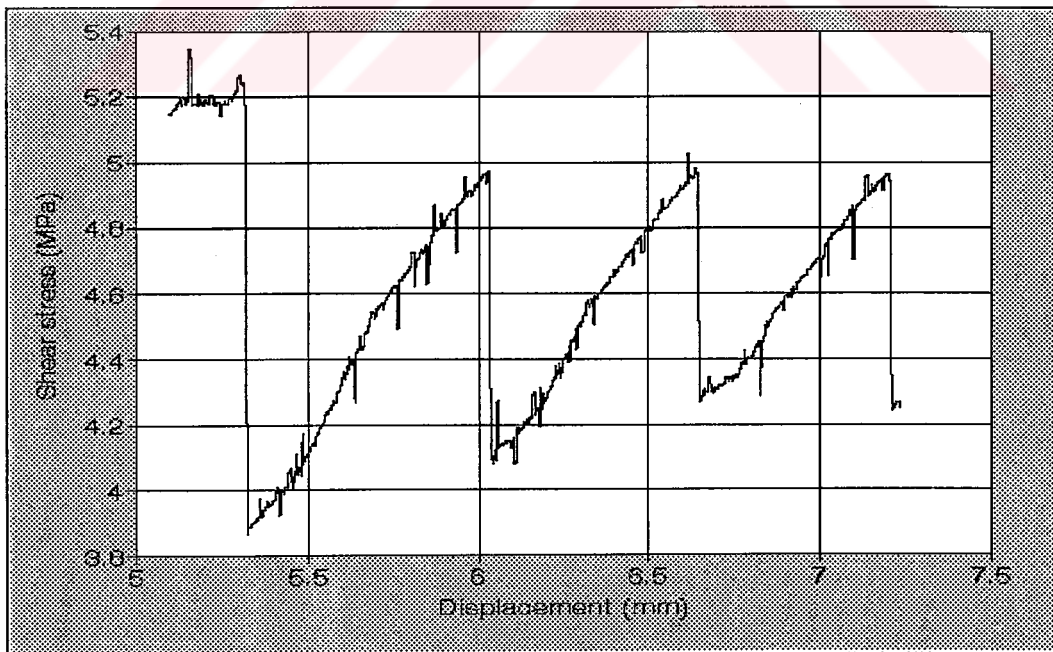
Figure 5.44 The shear stress vs. shear displacement for the simultaneous functional normal and shear stress change ($\sigma \cong 7$ MPa)

105
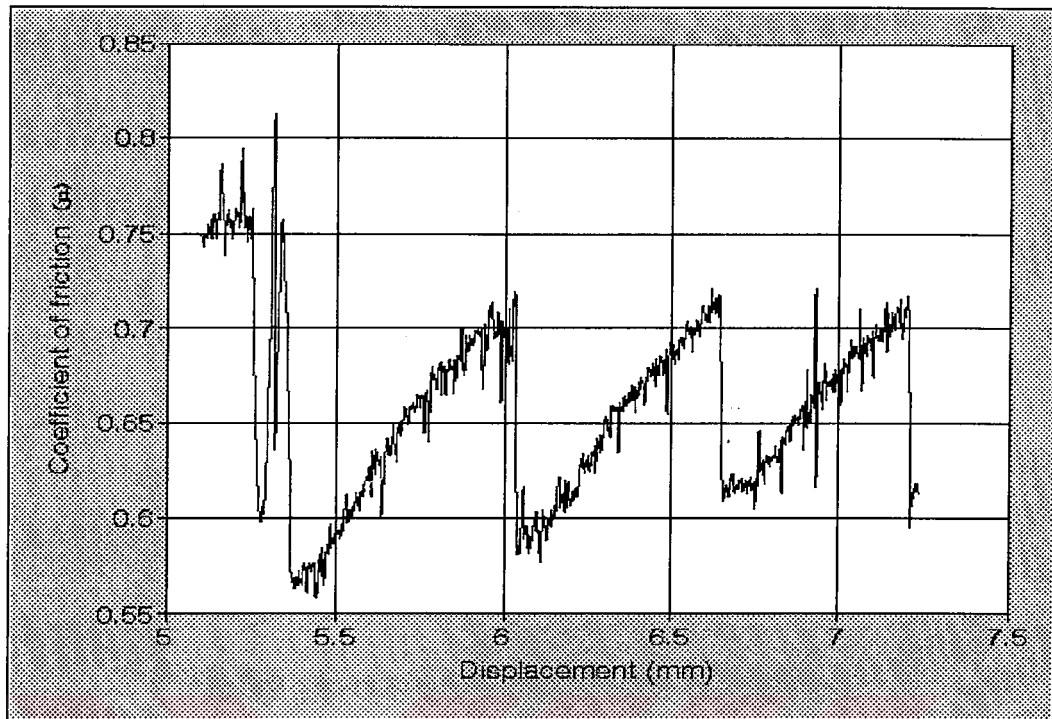
Figure 5.45 The coefficient of friction vs. shear displacement for the simultaneous functional normal and shear stress change ($\sigma \cong 7$ MPa)

Table 5.11 The empirical parameters estimated from the simultaneous functional normal and shear stress change experiment

Specimen Name	Normal stress (MPa)	Stress amplitude ($\Delta\sigma$ %)	Shear stress drop (MPa)	Shear stress drop ($\Delta\tau$,%)	Steady state friction (μ^{SS})	Friction drop ($\Delta\mu$)	Period (T) (sec)	Contact time (sec)
DK1	5	30	0.8	30	0.51	0.14	120	3100
DK2	7	26	1.3	26	0.76	0.20	20	4600
DK3	8	30	1.4	22	0.79	0.18	120	3600

106

5.4.6.1. The simultaneous functional normal and shear stress change model interpretations

The results of this model analysis are consistent with the functional normal stress change model. The different graphs for the same sample show the same characteristic curve's and same kinds of seismicity behaviour. The seismicity types of this model is presented in Table 5.12. According to this classification, the model shows main shocks and after some shocks with episodic dynamic slip strain release.

Table 5.12 Seismicity types for simultaneous functional normal and shear stress change test according to phenomenological classification of Boatwright and Cocco 1996

Specimen Name	σ (MPa)	σ (Δσ, %)	B-A (MPa)	Seismicity	Strain release
DK1	5	30	0.8	B»A, main shocks and after some shocks	episodic dynamic slip
DK2	7	26	1.3	B»A, main shocks and after some shocks	episodic dynamic slip
DK3	8	30	1.4	B»A, main shocks and after some shocks	episodic dynamic slip

The stress change in both direction (normal and shear) is compared with the stress change effect only in normal direction by a parametric study. This parametric study is carried out on the same model under the same loading conditions. The result of this analysis is shown in Fig. 5.46. As it is seen from this figure the coefficient of friction drop obtained from the stress change effect in both direction is lower than the stress change effect application only in the normal direction. These differences prove that, in the crust the direction of the principal compressive stress impose a stress change in both direction according to the direction of the strike of the fault. The direction of the stress change sometimes favours the seismicity when the dynamic load levels are reached. The initial stress acting along the shear direction may cause stress relief and this decreases the shear strength of the fault. Because of this the fault can show creep behaviour (stable sliding) rather than stick-slip (seismogenic).
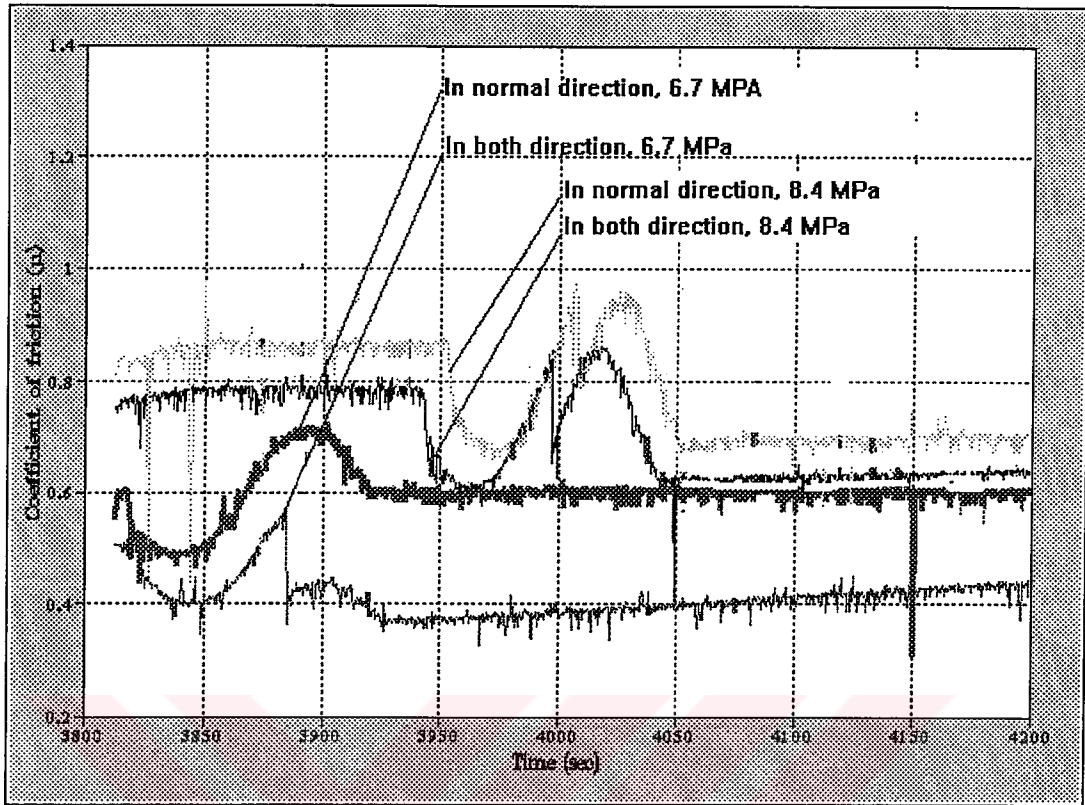
Figure 5.46 The field stress change effects on the model acting in normal, or both of the stress direction (shear and normal) of fault surface

CHAPTER 6

NUMERICAL MODELLING OF THE EXPERIMENTAL STUDIES

6.1. Introduction

In order to meet the requirement of simulations of the experimental studies of the earthquake faults, the numerical method (FLAC) was extensively used in this study. Numerical models provide an excellent tool for the quantitative and qualitative analysis of earthquake engineering problems and rock mechanics studies and are not subject to the same restrictive assumptions required for the closed form analytical solutions especially for the complicated geometry.

In fact, an analytical solution (closed form solution) for the geophysical and rock engineering problem (stress-strain distribution, etc.) still possess great value for conceptual understanding behaviour and for the testing and calibration of numerical models. On the other hand, these models are constrained to very simple geometry and material models. Consequently, the closed form solutions are of limited value in calculating the stresses, displacements of materials associated with faults. A number of computer-based numerical methods have been developed in the past few decades for delineation of these problems.

6.2. Numerical methods of model analysis

In this chapter, rather than giving detail information about the numerical method those are used for the analysis engineering studies and models especially for rock mechanics and geophysics, a brief description of whole methods will be presented. The description of the model and the revealed out solutions are given in the following subtitles.

Numerical methods for the analysis of physical and laboratory models in rock mechanics and geophysics can be divided into three groups:

6.2.1. Boundary element method

The boundary element is the numerical method that derives its name from the fact that only the boundaries of the problem geometry are divided into elements. The boundary element method are grouped into three according to method used as follows:

1. Displacement Discontinuity method, represents the result of an elongated discontinuity in an elastic continuum being pulled apart.
2. Fictitious Stress method, uses the first step in the solution to find a set of fictitious stresses which satisfy prescribed boundary conditions. The calculated stresses are then used in the calculation of actual stresses and displacements in the desired region of interest.
3. Direct Integral method, so named because the displacements are solved directly for the specified boundary conditions.

6.2.2. Finite element and finite difference methods

The finite element method is same with the finite difference method as a whole; thus, they will be treated as the same. The physical meaning of this method is modelled numerically by dividing the entire problem region into elements. The objective is to evaluate the solution to the problem at the nodes or mesh points of the network; the solution between nodes is expressed in a simple, approximate form in terms of the values at the nodes. Relating this approximate solution to the original partial differential equations eventually leads to a system of linear algebraic equations in which the unknown parameters.

6.2.3. Distinct element method

This method embodies an explicit, time-marching solution scheme. This method is based on an explicit time-marching solution scheme (Fig. 6.1) to solve the algebraic equations. The explicit scheme ensures that the numerical solution is stable even when the physical system being modelled is unstable; thus, the model behaves like a laboratory testing system. Due to high degree of non-linearity of the

system being modelled, explicit solution techniques are favoured for distinct element codes. This permits very general constitutive modelling of joint (fault) behaviour with little increase in computational effort and results in computation time being only linearly dependent on the number of elements used. The use of explicit solution method places fewer demands on the skills and experience than the use of codes employing implicit solution techniques (i.e. matrix; finite element methods).
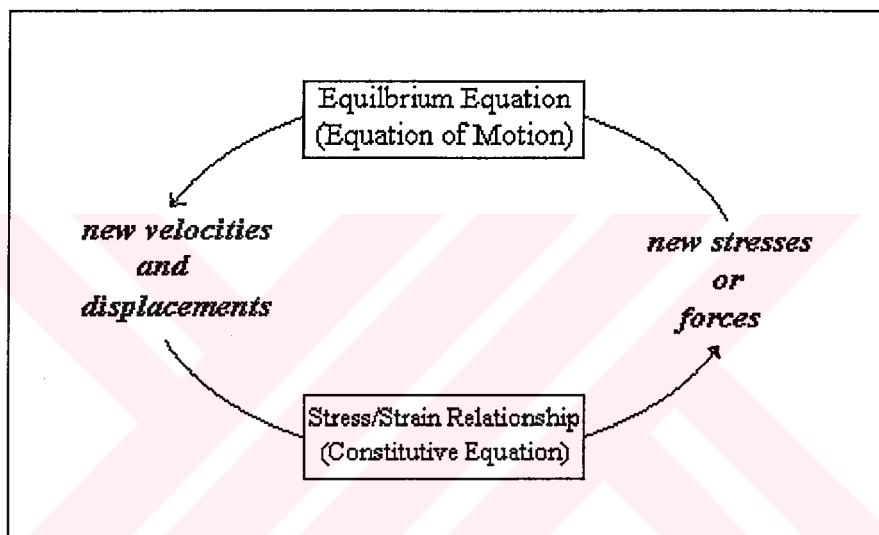
Figure 6.1. Explicit-time marching solution of distinct element method

6.3. Continuum modelling with FLAC

FLAC (Fast Lagrangian Analysis of Continua) is a two dimensional explicit finite difference code which simulates the behaviour of structures of soil, rock or similar materials which may undergo plastic flow when their yield limit is reached. Materials are represented by elements, or zones, which form a grid that is adjusted by the user to fit the shape of the object to be modelled. Each element behaves according to a prescribed linear or non-linear stress/strain law in response to the applied forces or boundary constraints (Cundall and Board , 1988).

111

6.4. Analysed model geometry

The numerical model geometry idealisation provides an adequate approximation to experimental studies. It is taken as simple as possible but resembling the laboratory situations. For this analysis, full geometry condition was used and boundary conditions were applied as shown in Fig. 6.2, while Fig. 6.3 shows the zones and grid of the model. This area was divided into 110 zones, as shown in Fig. 6.3.

Boundary conditions:
  - x- y-displacement fixed at x=0 cm and x=30 cm at lower and x=12 cm and x=18 cm at upper box,

  - y-displacement fixed at the base of the model,

  - mechanical axial stress, σ_n=5 MPa applied to the upper block,

  - initial shear displacement rate υ=1μms^{-1} applied to the lower shear box,
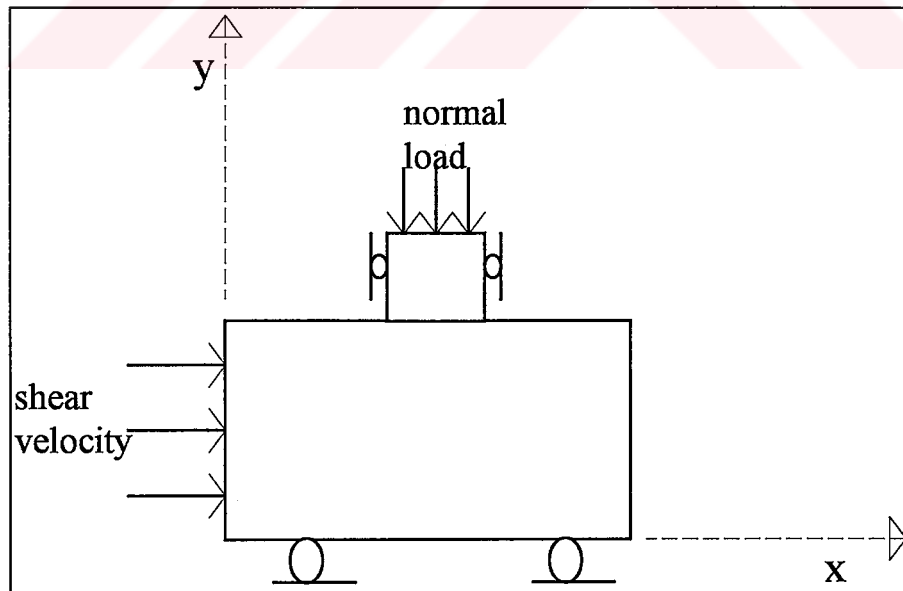
Figure 6.2 Boundary conditions of the model geometry

112
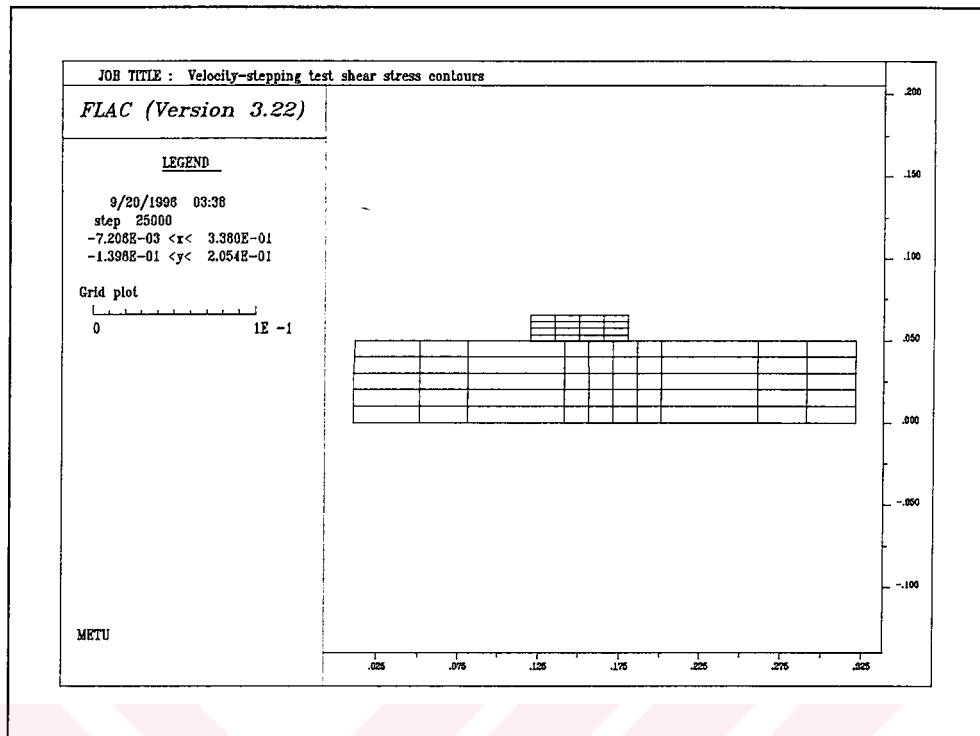
Figure 6.3 FLAC grid of the model geometry

The analyses were performed under plane strain conditions, so the test sample is equivalent to the experimental model (displacement along the z-axis will be equal to zero). It was also assumed that the rock matrix elastic and the fault surface have an elastic-perfectly plastic behaviour, with no strain softening.

6.5. Model material properties

The material properties assigned to the system in a distinct element model represents the real values taken from the laboratory results. The rock matrix has the following material properties:

Density   = 2600 kg/m^3
Shear modulus (G) = 17 GPa
Bulk modulus (K) = 10 GPa

113

The fault (joint) properties:

Normal stiffness (Kn) = 100000 MPa/m
Shear stiffness (Ks)   = 3000 MPa/m
Cohesion (Cj)   = 0-5.02 MPa
Friction angle (ϕj)   = 30-38°
Dilation angle (φj)   = 0 °

6.6. Procedure

The distinct element method modelling with FLAC sequence as follows:
- First, the model geometry is established in a manner mentioned in the previous section and followed by introducing model analysis type (elastic or others).
- Second, the material properties are given according to the data revealed out from the experimental tests (In order to sustain stability of the model some of the properties was taken higher than the real one, e.g. Kn=100000 MPa/m instead 26000 MPa/m).
- Third, the boundary conditions (stress and displacement) and constraints are defined.
- At the last stage, the required output results are plotted to directly to printer or to a file for further processing.
The representative data file for this analysis is given in Appendix D.

The prepared data file automatically is called from the FLAC or can be directly written in the editor's of the package. After several runs the force balance step (time-marching balancing force) is experienced for the stable state of the model; in other words the residual shear strength was reached. The coming stage in this modelling sequence is divided into two phases which are discussed below:

i. Velocity-stepping phase, consists of increasing the initial load point velocity abruptly with ten fold increment (from 0.001 mm/sec to 0.01 mm/sec).

ii. Stress-step phase; in this phase the normal stress is changed explicitly with a predicted percentage of the initial value.

6.7. Results of numerical model

6.7.1. Direct-shear test

The results obtained from the numerical model represent the behaviour observed in the experimental studies results. Confirmation was first done by the standard shear test simulation of the model. Figure 6.4 shows the output of the solely applied normal stress with constant load point velocity $(1\mu ms^{-1})$ boundary condition. As it was seen from this figure the residual shear stress value was reached like as the manner in the laboratory test results (Fig. 6.10). Interestingly, the coefficient of friction was fall into the range obtained from the experimental records (see, Table 6.1 and Fig. 6.9).

In order to simulate the correct form of the experimental studies, first off all the back analysis of the shear strength parameters of the fault surface was carried out. The back analysis results of coefficient of friction, friction angle and normal stress are tabulated in the following Table 6.1, 6.2 and 6.3 respectively. The tabulated variables are modelled analytically by regression analysis and are shown in Fig. 6.5- Fig. 6.8.
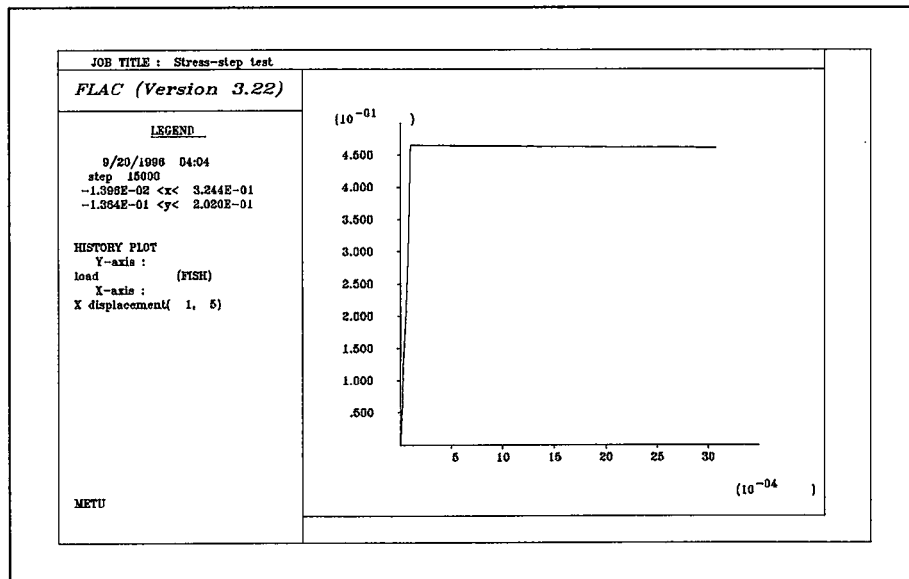
Figure 6.4 Standard direct-shear simulation with FLAC

115

Table 6.1 The variance of static coefficient of friction and shear stress from the back analysis by changing cohesion

Cohesion (MPa)	Static friction	shear stress (MPa)	Internal friction angle (°)	Shear stiffness (MPa/m)	Normal stiffness (MPa/m)	Normal stress (MPa)
0.02	0.44	2.5	38	3000	100000	5
2.02	0.70	3.9	38	3000	100000	5
5.02	1.1	5.9	38	3000	100000	5
10.02	1.6	9	38	3000	100000	5

Table 6.2 The variance of static coefficient of friction and shear stress from the back analysis by changing internal friction angle

Cohesion (MPa)	Static friction	shear stress (MPa)	Internal friction angle (°)	Shear stiffness (MPa/m)	Normal stiffness (MPa/m)	Normal stress (MPa)
2.02	0.56	3.3	30	3000	100000	5
2.02	0.61	3.7	35	3000	100000	5
2.02	0.71	4.1	40	3000	100000	5
2.02	0.80	4.5	45	3000	100000	5

Table 6.3 The variance of static coefficient of friction and shear stress from the back analysis by changing the normal stress

Cohesion (MPa)	Static friction	shear stress (MPa)	Internal friction angle (°)	Shear stiffness (MPa/m)	Normal stiffness (MPa/m)	Normal stress (MPa)
2.02	0.6	5.5	38	3000	100000	8
2.02	0.55	6.5	38	3000	100000	10
2.02	0.52	7	38	3000	100000	12
2.02	0.5	9	38	3000	100000	15
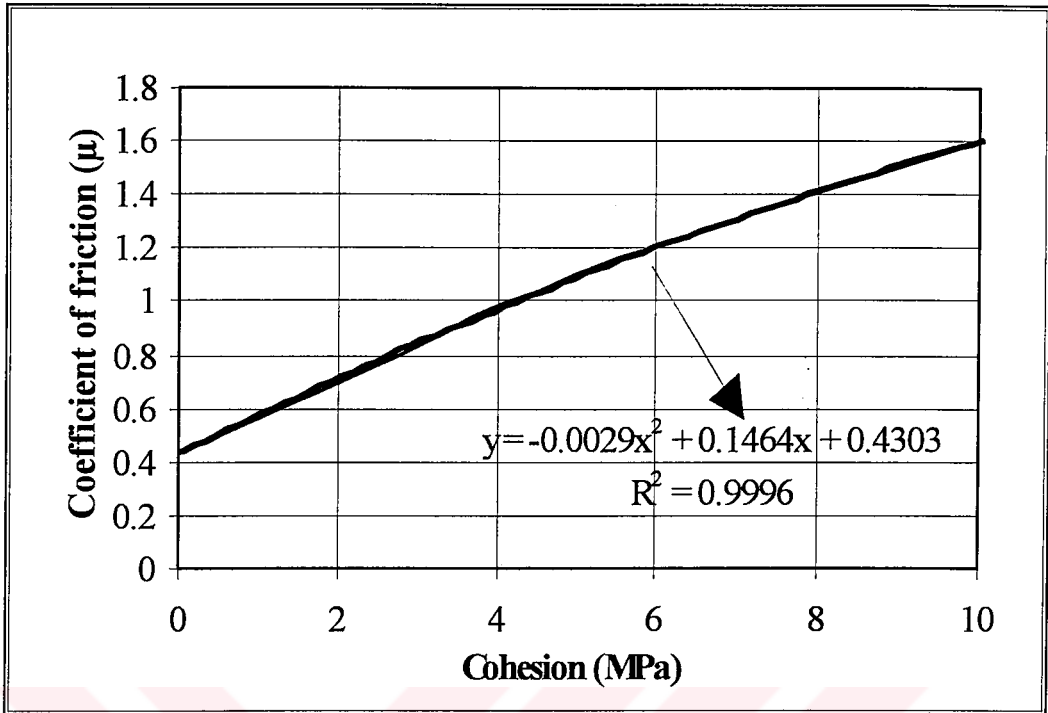
Figure 6.5 The variation of coefficient of friction with respect to cohesion
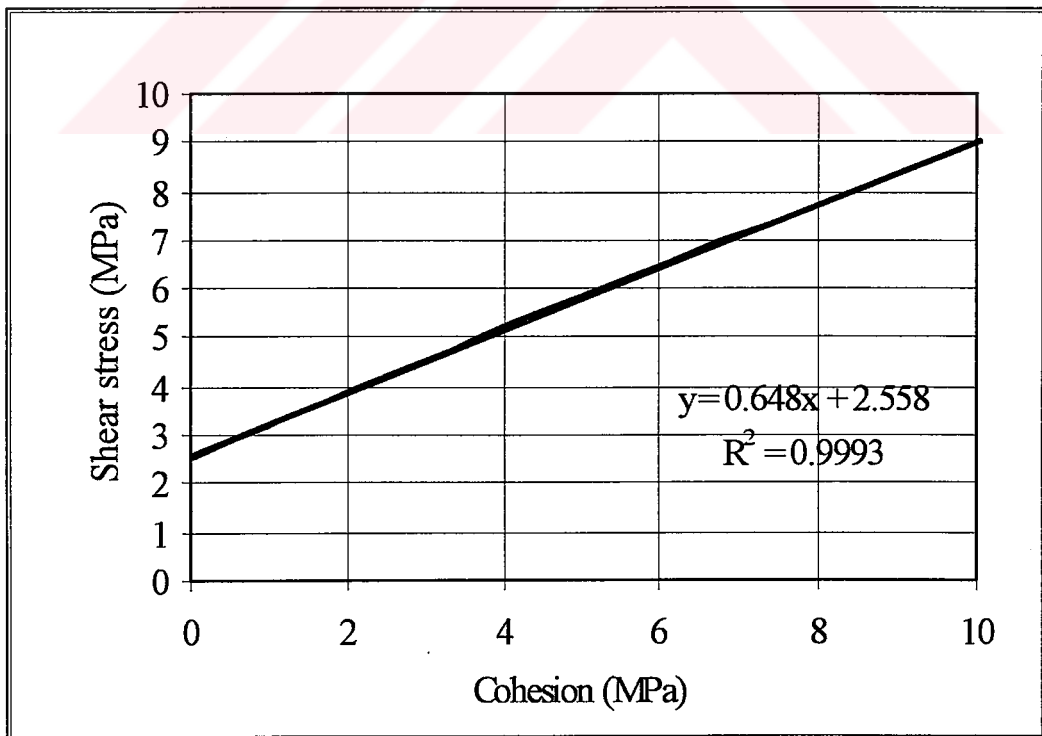
Figure 6.6 The variation of shear stress with respect to cohesion

117
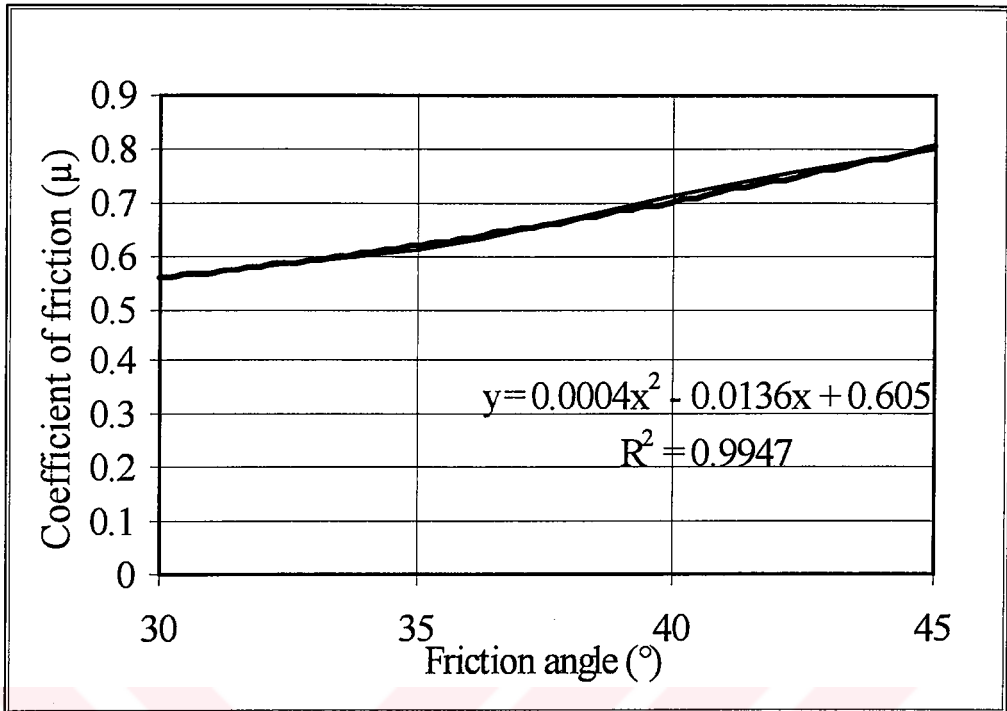
Figure 6.7 The variation of coefficient of friction with respect to friction angle
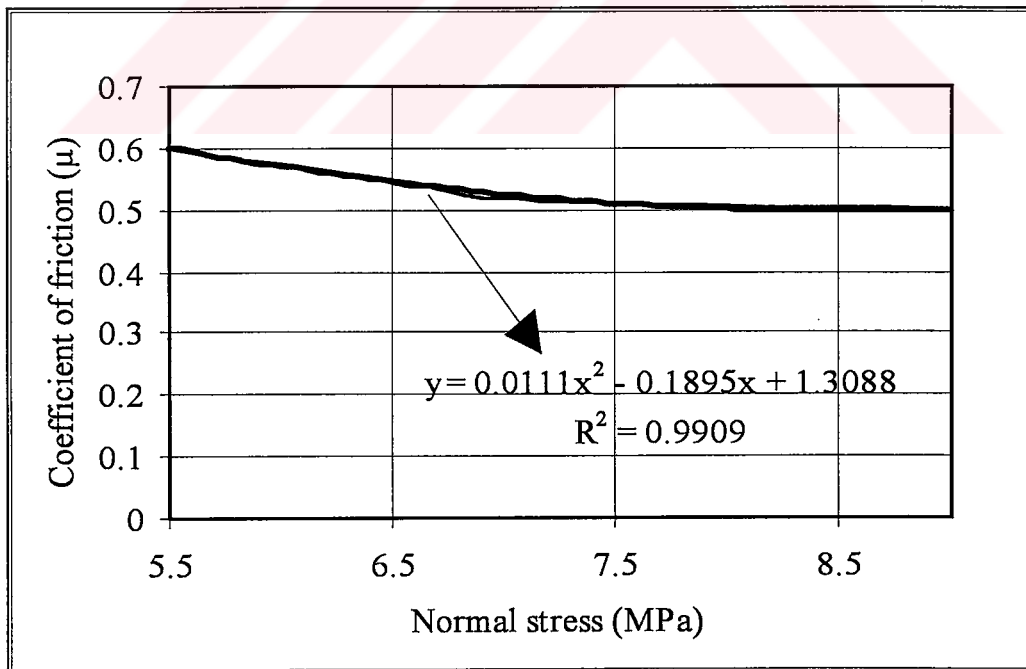
Figure 6.8 The variation of coefficient of friction with respect to normal stress

118

6.7.1.1. Interpretation of the direct-shear test model

The direct shear test of model the numerical model support the experimental results. The obtained curves (Figs. 6.9-6.10) and strength parameters from the analysis are modelled by regression analysis and consistent with the experimental results (e.g. the obtained coefficient of friction is 0.48 and 0.70 for the cohesion of 0.02 MPa and 2.02 MPa, respectively). The models used for the back analysis purposes are obtained as follows:

$$\mu = -0.0029 \,(C)^2 + 0.1464(C) + 0.4303$$
$$\tau = 0.648 \,(C) + 2.558$$
$$\mu = 0.0004 \,(\phi)^2 - 0.0136 \,(\phi) + 0.605$$
$$\mu = 0.0111 \,(\sigma)^2 - 0.189 \,(\sigma) + 1.309$$

$$(6.1)$$

where:
σ is the normal stress in MPa
μ is the coefficient of friction
C is the cohesion in MPa
ϕ is the friction angle in °
τ is the shear stress in MPa

From the parametric analysis, it is revealed out that the variation of the shear strength and coefficient of friction is sensible to cohesion parameters. The variation of the system normal stress and friction angle of the sliding surface influence the shear strength and coefficient of friction less than the cohesion.

6.7.2. The velocity-stepping test model

The results of the velocity-stepping simulation are graphically shown in Fig. 6.11 and Fig. 6.12. From these figures it is seen that the velocity-stepping ($1\mu ms^{-1}$ to $10\mu ms^{-1}$) results in a sudden increase in shear stress and coefficient of friction due to elastic coupling between velocity and shear stress. Then the shear stress or coefficient of friction decays toward a new steady state value as sliding proceeds.

119
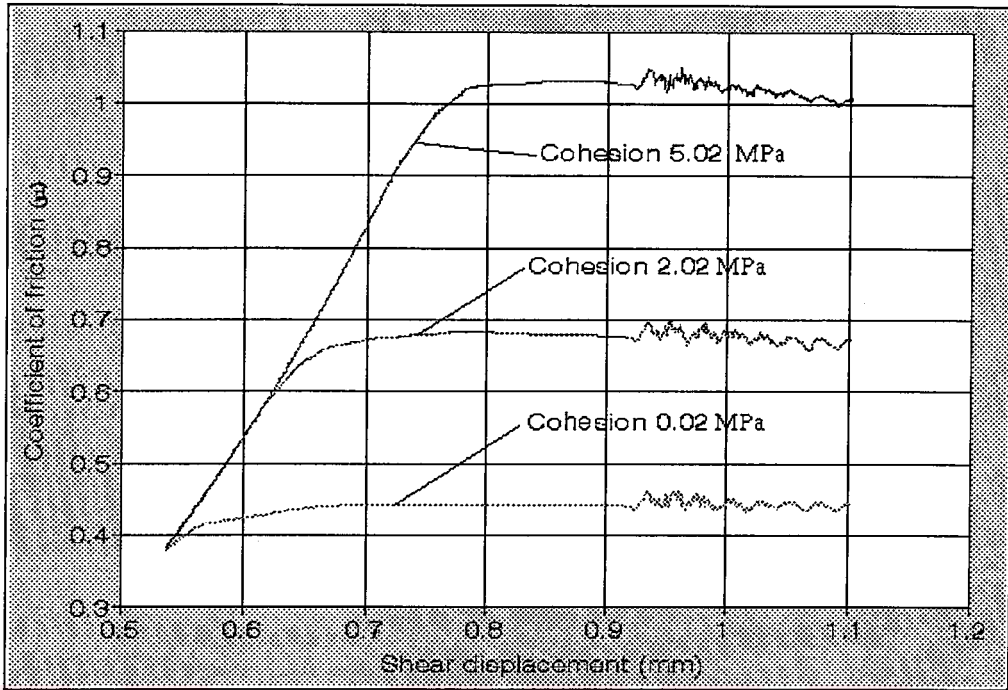
Figure 6.9 The coefficient of friction vs. displacement of velocity-step test
simulation for different cohesion
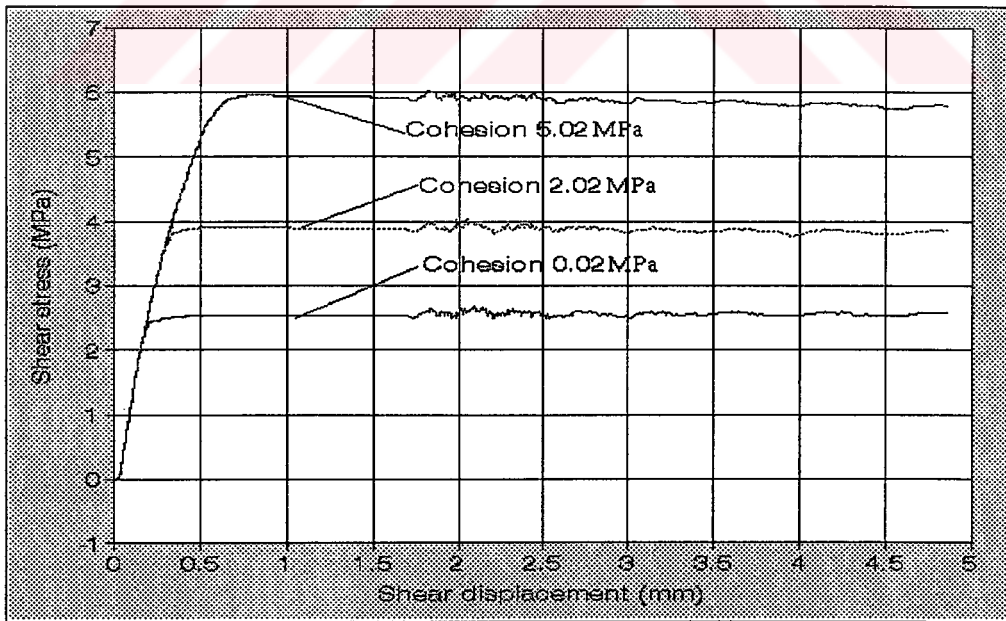
Figure 6.10 The shear stress vs. displacement of velocity-step test simulation for
different cohesion

120
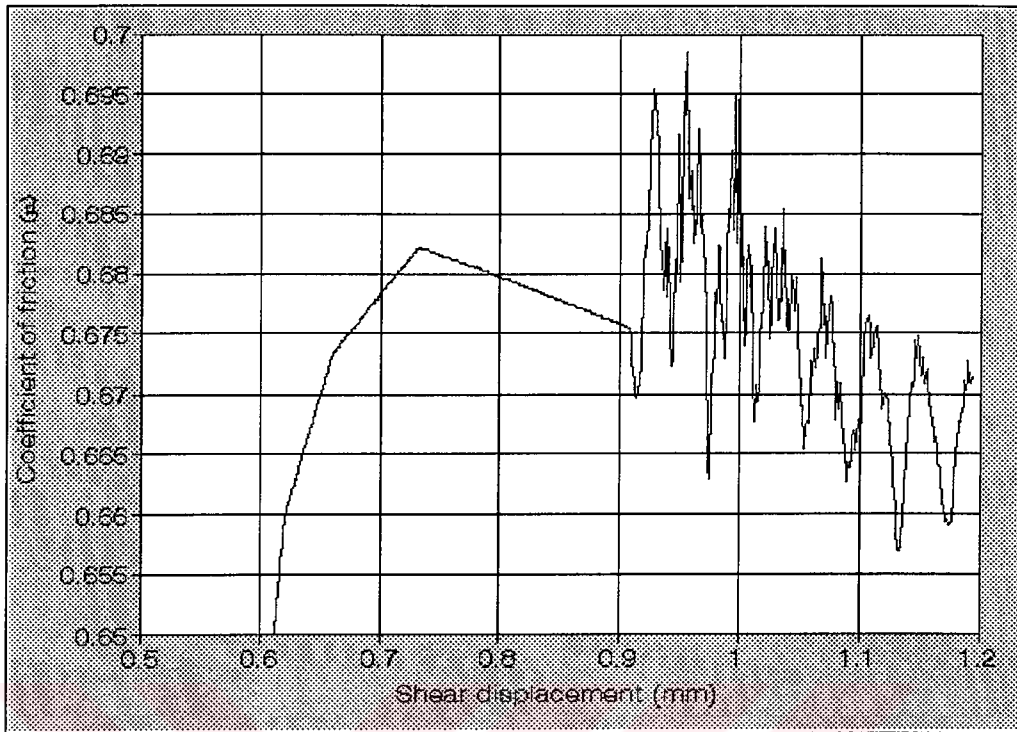
Figure 6.11 The coefficient of friction vs. displacement of velocity-step test simulation
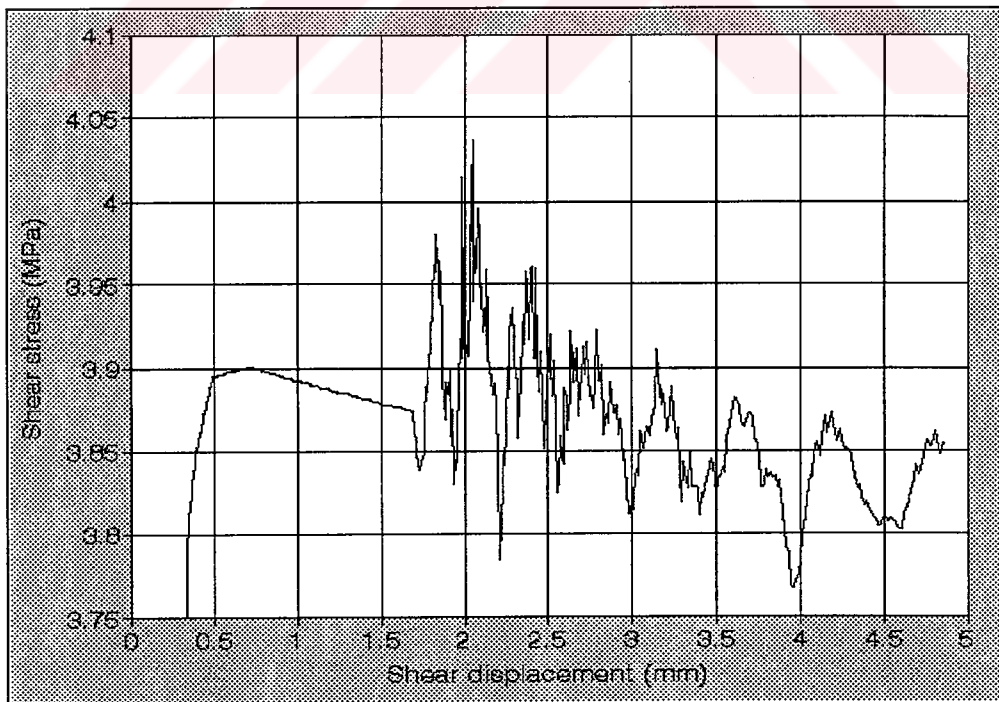
Figure 6.12 The shear stress vs. displacement of velocity-step test simulation

121

The decay roughly follows an exponentially with a displacement Dc. The rate- and State- dependent parameters (a, b, Dc, Kc) and shear stress and coefficient of friction drop are tabulated in Table 6.4.

Table 6.4 The estimated velocity-stepping test parameters from the numerical model

a	b	Dc (mm)	$\Delta\tau$ (MPa)	$\Delta\mu$ (b-a)	Kc (MPa/mm)	σ (MPa)
0.022± 0.005	0.033± 0.006	0.2±0.1	0.04±0.02	0.01± 0.005	0.2±13	5

6.7.2.1. Interpretation of the velocity-stepping test model

The numerical model rate- and state- dependent parameters are found in the range of the previous researchers' estimation. The results of the numerical velocity-stepping model support the experimental results. Even though, the rate- and state-dependent parameters are close to each other, the seismicity and strain release property with the same stability criteria and phenomenological approach differs from each other.

The aseismic character with rarely seismic areas obtained from experimental results show weak seismic mode in the numerical analysis. The seismicity types of the numerical model of the velocity-stepping simulation are given by phenomenological classification in Table 6.5. According to this classification, numerical simulations indicate that the model show a weak seismic and creep, intermittent dynamic slip release. This kind of fault zone is slightly velocity-weakening and contains most of the micro type small earthquakes. These earthquakes can occur during the inter-seismic, pre-seismic or post-seismic parts of the earthquake cycle. As it is noticed from the Table 6.5 The weak seismic areas have positive value of B-A but close to the neutral limit of B≈A.

Table 6.5 Seismicity types of numerical velocity-stepping model according to phenomenological classification of Boatwright and Cocco, 1996

A (MPa)	B (MPa)	B-A (MPa)	σ (MPa)	Seismicity	Strain release
0.16	0.20	0.04	5	B-A>0 and ≤0.05 weak seismic inter seismic eqn. main shocks	creep and intermittent dynamic slip

6.7.3. The normal stress step test model

Simulation results of the normal stress step experiments using the parameters from back analysis and the values listed in Section 6.4. are shown in Fig. 6.13 through Fig. 6.18. Generally, the data in these figures result in a sudden (abrupt) transient peak for the sudden increase in normal stress and subsequent decay to the new steady state value in response to a step decrease in normal stress. This behaviour is seen in opposite manner for the coefficient of friction graphs.

With the same nominal stress ($\sigma = 5$ MPa), the two level of step increments of the normal stress from its initial value was conducted. This step increments are hold a while and then are lowered to the nominal stress value. For the first one, the normal stress increment is 30%, while the second normal stress step is 40% of its initial (nominal) stress value. The resulted shear stress ($\Delta\tau$) and coefficient of friction ($\Delta\mu$) increments are tabulated in Table 6.6 according to the stress step amplitude ($\Delta\sigma\%$).

Table 6.6 The estimated normal stress step parameters from the numerical model

Normal stress (MPa)	Stress amplitude ($\Delta\sigma$ %)	Shear stress increase (MPa)	Shear stress increase ($\Delta\tau$,%)	Steady state coeff. of friction (μ^{SS})	Coeff. of friction increase ($\Delta\mu$)
5	30	0.27	7	0.68	0.05
5	40	0.7	18	0.68	0.07
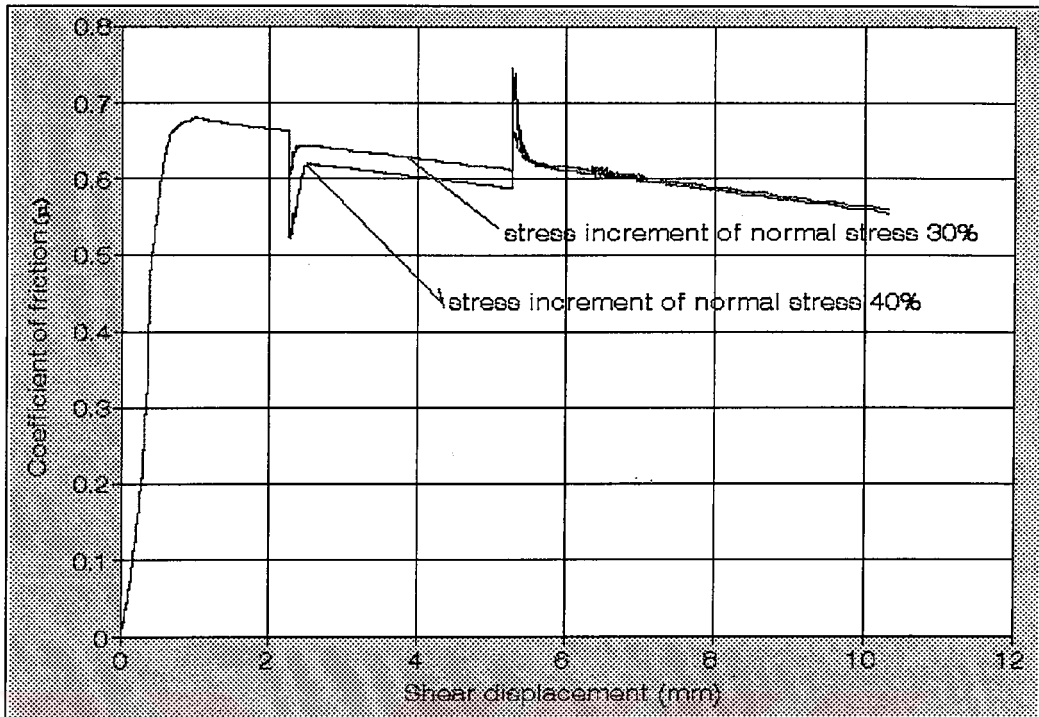
Figure 6.13 The coefficient of friction vs. displacement of the stress step simulation
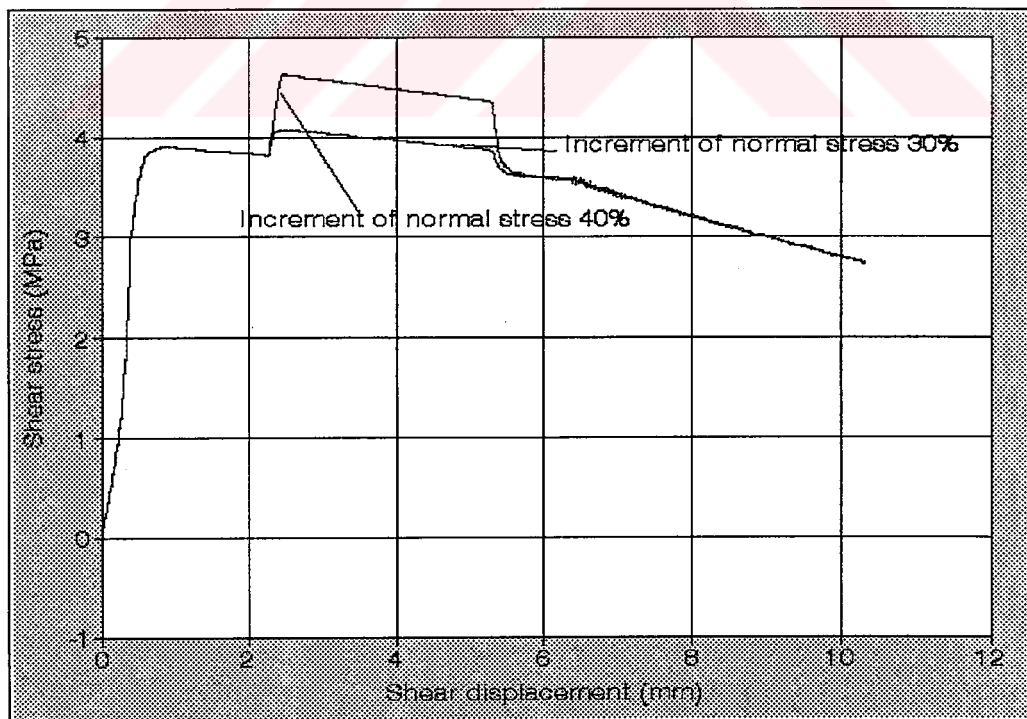
Figure 6.14 The shear stress vs. displacement of the stress step simulation
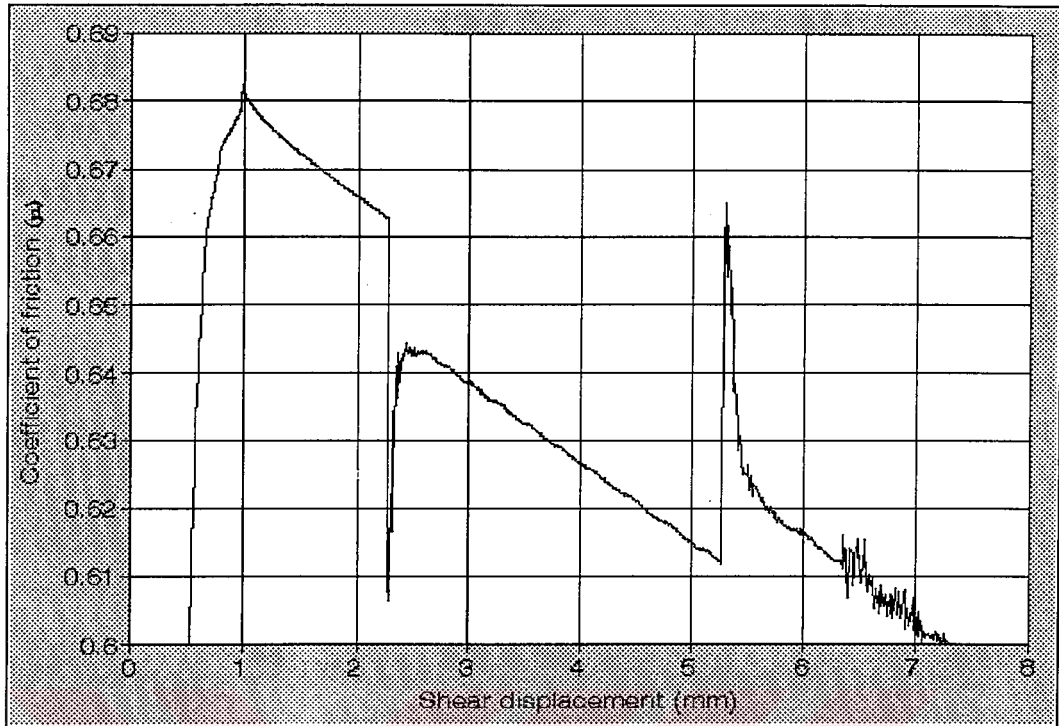
Figure 6.15 The coefficient of friction vs. displacement of the stress step simulation
(30% increment of normal stress)
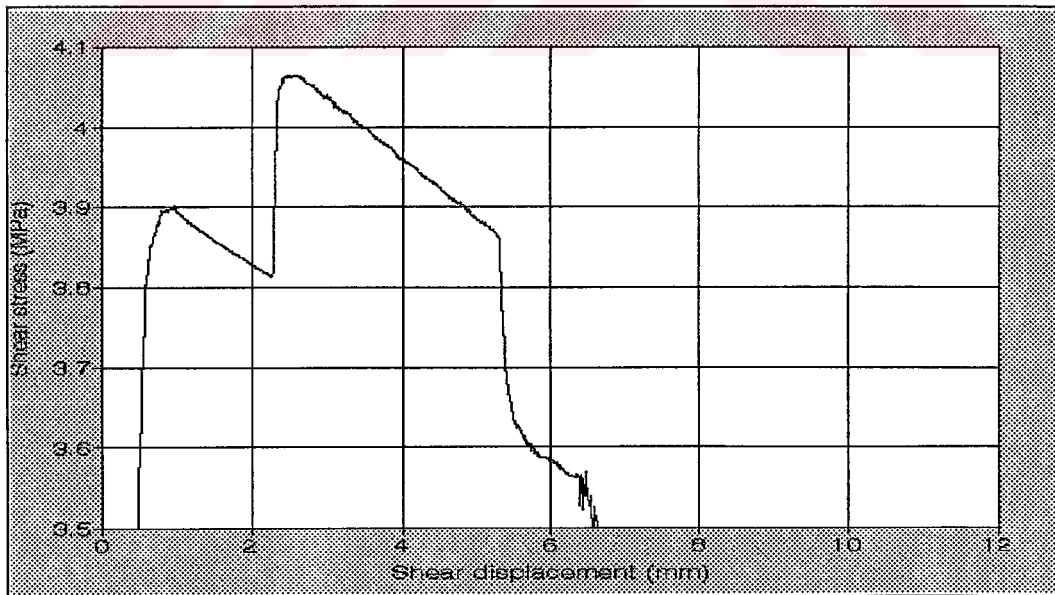
Figure 6.16 The shear stress vs. displacement of the stress step simulation
(30% increment of normal stress)

125
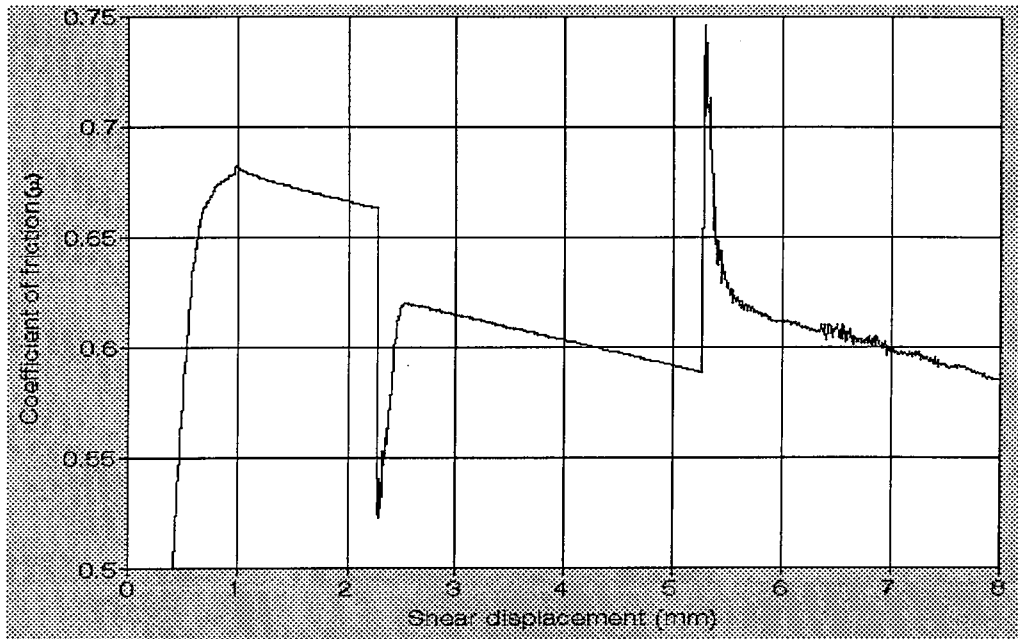
Figure 6.17 The coefficient of friction vs. displacement of the stress step simulation
(40% increment of normal stress)

Figure 6.18 The shear stress vs. displacement of the stress step simulation
(40% increment of normal stress)

126

6.7.3.1. Interpretation of the normal stress step model

The numerical modelling of the normal stress step test shows the same characteristics curve of the experimental results. According to the phenomenological classification, the model shows no seismicity like as experienced in the experimental model also. The seismicity types of the model is shown in Table 6.7 according to the phenomenological classification. This numerical model implies that the increment of the normal stress step causes the system to be more strengthening. In other words, stress increment is not on behalf of the unstable sliding.

Table 6.7 Seismicity types of numerical model for stress step test according to phenomenological classification of Boatwright and Cocco, 1996

σ (MPa)	σ (Δσ, %)	B-A (MPa)	Seismicity	Strain release
5	30	-0.27	A»B none	stable sliding
5	40	-0.7	A»B none	stable sliding

The results of all the numerical simulations show that the numerical model could be needed to investigate the effect of the experimental parameters such as stress perturbations, sliding rates, cohesion of the sliding surfaces.

CHAPTER 7

CONCLUSION AND RECOMMENDATIONS FOR FURTHER RESEARCH

In this thesis, the shallow focus earthquake mechanism is extensively investigated by experimental and numerical approaches. The effects of the sudden regional stress field changes associated with great earthquakes, artificial and geologic disturbances, on a vertical strike-slip faults are simulated. The main conclusions drawn are:

i. Transition from a quasi-static creep (very slow motion of the fault; tectonic movement) to dynamically driven (seismic motion) is simulated by rate-dependent and state-dependent frictional phenomenon under the assumption of constant fault normal stress. This model shows a seismic (stable sliding) with rarely seismic character in the experimental simulation. On the other hand the same model with the numerical approach is characterised with the weak seismic occurrence. Although the obtained rate-dependent and state-dependent parameters (such as a, b, Dc) are very close to each other, the seismicity and strain release characteristics according to phenomenological classification differs from each other. The weak seismic behaviour obtained from the numerical model implies that the aseismic character resulted from the experimental model is close to the weak seismic zone. It can be deduced that the frictional variation during a sudden velocity change does not yield a large dynamic instability (seismicity) marked by a sudden shear stress drop and seismic slip in this type modelling.

ii. The sudden normal stress change of the field stress simulation implies an aseismic and strong seismic behaviour for stepwise and functional normal stress change, respectively. This result indicates that the sudden normal stress increment in stepwise from the nominal regional field stress field along the strike of the earthquake fault is not critical

128

behaviour for seismicity. But the lateral variation of the normal stress in functional form shows a transition from quasi-static (creeping) to a dynamic (seismic) slip. This transmission occurs when the stress change of normal stress falls under the nominal field stress value. This shows that the stress relief phenomena on or near the seismogenic fault surface caused by nearby earthquake after shock or other agencies is a more critical behaviour than the strain release process. In other words, the effect of functional type of stress change on seismicity is more than the velocity change effect. Therefore, the investigations on the mechanism of shallow focus earthquake have to be directed towards the study of lateral variation of frictional phenomena along the strike of active seismogenic faults associated with stress change.

iii. The simultaneous change of both normal and shear stress causes less shear stress drop than the model with the change of normal stress only. This shows that the orientation of the field stress change affects the seismogenic fault as well as the stress change amplitude (magnitude of the stress change). It is stated in the literature (e.g. Dieterich, 1978; Scholz, 1972) that the increase in the normal stress favours the stick-slip phenomenon (unstable sliding). In this state of the simultaneous stress change at shear and normal stress direction reduces the normal stress change effect and this causes less unstable sliding as the stress release occurs with the continued sliding. This assertion can be supported with further systematic study of the field stress change acting on the active faults from the different orientation.

iv. Another conclusion from this study is that the amplitude of the stress change in the regional stress field influences the frictional sliding and shear stress drop more than the other parameters such as period of stress change, repetition of the stress change (cyclic loading). The obtained mathematical model of this stress amplitude effect on coefficient of friction drop ($\Delta\mu\%$) is:

$$\Delta\mu\% = 2E\text{-}06(\Delta\sigma\%)^2 + 5E05(\Delta\sigma\%) + 0.02$$

v. In seismology, methods have been developed for evaluating the drop in shear stress associated with earthquakes from the spectral analysis of the

signals recorded at far-field stations. These results suggest that, for all earthquakes, irrespective of their magnitude, the computed stress drop ranges from 1-10 MPa (Cornet, 1993). This result is apparently contradiction with the results of previous laboratory investigations reported in the literature which are generally an order of magnitude higher than the value specified above. In this research study, obtained the shear stress drop values interestingly fit to the real case. i.e. within the range 1-10 MPa. This indicates that the stress change model proposed in this study simulates the earthquake fault mechanism close to reality. The mathematical model for this assertion is:

$$\Delta\tau = 0.0011(\Delta\sigma\%)^{2.1208}$$

From this model, the maximum shear stress drop obtained by inserting 100% of normal stress increase would be 19 MPa. This is the extreme point but the result is not even an order of magnitude greater than the in situ values. The average shear stress drop is about 5-7 MPa for normal stress increase of 50-60%.

These results suggest that the experimental process leading to instability in the simulated earthquake fault model may also be responsible for the triggering of earthquakes and can highlight the some aspects in the shallow focus earthquake mechanism.

The future studies to supplement this research could be as follows:

i. The experimental studies and numerical modelling should be supported by the field observations and studies. For this purpose, the North Anatolian Fault Zone may be the case to investigate as it is a major tectonic feature with a well-defined fault trace and established history of seismicity

ii. The effect of the field stress change directions should be investigated thoroughly. In order to do this, the apparatus should be modified. The enhancement of the developed direct-shear test apparatus can also be done to conduct the experiment easier than it could be done at its present condition.

REFERENCES

Baleshta, J.R. and Dusseault, M.B., 1988. Triaxial testing of intact salt rocks: pressure control, pressure systems, cell and frame design, Advanced Triaxial Testing of Soil and Rock, ASTM STP 977, pp. 155-168.

Barzagni, M. and Dorman, J., 1969. World seismicity map of ESSA coast and geodetic survey epicenter data for 1961-67, Bulletin of the Seismological Society of America, 59, 369-380.

Barbat, A.H. and Canet, J. M., 1989. Structural response computations in earthquake engineering, Pineridge press, Swansea, U.K.

Beeler, N.M., Tullis, T.E., and Weeks, J.D., 1994. The roles of time and displacement in the evolution effect in rock friction, Geophys. Res. Lett., 21, 1987-1990.

Blanpied, M.L., Tullis, T.E. and Weeks, J.D., 1987. Frictional behaviour of granite at low and high sliding velocities, Geophys. Res. Lett., 14, 554-557.

Blanpied, M.L., David, A.L. and Byerlee , J.D., 1995. Frictional slip of granite at hydrothermal conditions, J. Geophys. Res., 100, 13,045-13,064.

Boatwright, J. and Cocco, M., 1996. Frictional constraints on crustal faulting, J. Geophys. Res., 101, 13,895-13,909.

Bolt, B.A., 1981. Terremotos, Editorial Reverté, S.A.

Brace, W.F. and Byerlee, J.D., 1966. Stick-slip as a mechanism for earthquake, Science, 153, 990-992.

Brace, W.F. and J.D. Byerlee, 1970. Calofornia earthquakes why only shallow focus?, Science, 168, 1573.

Brace, W.F. and Kohlstedt, D.L., 1980. Limits on lithospheric stress imposed by laboratory experiments, J. Geophys. Res.,85, 6348-6252.

Brace, W.F., 1972. Laboratory studies of stick-slip and their application to earthquakes, Tectonophysics, 14, 189-200.

Bridgman, P.W., 1936. Shearing phenomena at high pressure of possible importance for geology, Journal of Geology, 44, 653-669.

Bro, A., 1992. Stick-slip behaviour of smooth joints, Int. J. Rock Mech. Min. Sci. & Geomech. Abstr. , 29, 171-177.

Brown, E.T, 1981. Rock characterization testing and monitoring, ISRM suggested Methods, Pergamon Pres, pp. 211.

Byerlee, J.D., 1967. Frictional characteristics of granite under high confining pressure, J. Geophys. Res., 72, 3639-3648.

Byerlee, J.D. and Brace, W.F., 1968. Stick-slip stable sliding and earthquakes - effect of rock type, pressure, strain rate and stiffness, J. Geophys. Res., 73, 6031-6037.

Byerlee, J.D., 1970. The mechanics of stick-slip, Tectonophysics, Sept.

Byerlee, J.D. and Summers, R., 1976. A note on the effect of fault gouge thickness on fault stability, Int. J. Rock Mech. Min. Sci. Geomech. Abstr., 13,35-36.

Chester, F.M., 1988. The brittle-ductile transition in a deformation-mechanism map for halite, Tectonophysics, 154, 125-136.

Chester, F.M., 1994. Effects of temperature on friction: Constittutive equations and experiments with quartz gouge, j: Geophys. Res., 99, 7247-7261.

Chen, W.P. and Molnar , P., 1983. Focal depths of intracontinental and intraplate earthquakes and their implications for thermal and mechanical properties of the lithosphere, J. Geophys. Res., 88, 4183-4214.

Clough, R.W., and Penzien, J., 1975. Dynamics of structures, McGraw-Hill, Inc., New York.

Cornet, F.H., 1993. Stress in rock and rock masses, Comprehensive Rock Engineering Principle Practice & Projects, 3, 321-323.

Cox, S.J.D., 1990. Velocity-dependent friction in alarge direct shear experiment on gabbro, Deformation Mechanism, Rheology and Tectonics, Geological Society Special Publication, 54, 63-70.

Cruden, D.M., Leung , K. and Masoumzadeh , S., 1987. A tecnnique for estimating the complete creep curve of a sub-bituminous coal under uniaxial compression, Int. J. Rock Mech. Sci. and Geomech. Abst., 24, 265-269.

Cundall, P.A. and Board, M., 1988. A microcomputer program for modelling large-strain plasticity problems, Proc. 6th Int. Conf. on Numerical Methods in Geomechanics, Innsbruck, 2101-2108.

Dieterich, J.H., 1972. Time-dependent friction in rocks, J. Geophys. Res., 77, 3690-3697.

Dieterich, J.H., 1978. Time dependent friction and the mechanics of stick slip, Pure Appl. Geophys., 116, 790-806.

Dieterich, J.D., 1979. Modelling of rock friction I. Experimental results and constitutive equations, J. Geophys. Res., 84, 2161-2168.

Dieterich, J.D., 1981. Constitutive of faults with simulated gouge, in Mechanical Behaviour of Rocks, Geophys. Monogr. Ser., AGU, 24, 103-120.

Dieterich, J.D., 1987. Nucleation and triggering of earthquake slip: Effect of periodic stresses, Tectonophysics, 144, 127-139.

Dieterich, J.H., 1994. A constitutive law for rate of earthquake production and its application to earthquake clustering, J. Geophys. Res, 99, 2601-2618.

Gu, J., Rice, J.R. Ruina, A.L. and Tse, S.T., 1984. Slip motion and stability of a single degree of freedom elastic system with rate and state dependent friciton, J. Mech. Phys. Solids, 32, 167-196.

Hobbs, B.E. and Brady, B.H.G., 1985. Normal stress changes and the constitutive law for rock friction, Eos Trans, AGU, 66, 382.

Ishlinski, A.Y. and Kraghelsky, I.V., 1944. On stick-slip in friction. Zh. Tekhn. Fiz., 14, 276-282.

Jaeger, J.C. and Cook, N.G.W., 1976. Fundamentals of rock mechanics (2nd ed.)., London, Chapman and Hall, John Wiley & Sons, Inc., New York.

Johnson, T.L. and Scholz, C.H., 1976. Dynamic properties of stick-slip friction of rock, 81, 5, 881-888.

Kaila, K.L. and Narain, H., 1970. A new approach for the preparation of quantitative seismicity maps, Bulletin of the seismological society of America, 60, 339-446.

Kato, N., Yamamoto, Yamamoto, K., H., and Hirasawa,T., 1992. Strain-rate effect on frictional strength and the slip nucleation process, Tectonophysics, 211, 269-282.

Kazakidis, V.N., and Diederichs, M.S., 1993. Understanding jointed rock mass behaviour using a ubiquitous joint approach, Int. J. Rock Mech. Min. Sci. & Geomech. Abstr., 30, 163-172.

Kiratzi, A.A, 1993. A study on the active crustal deformation of the North and East Anatolian Fault Zones, Tectonophysics, 225, 191-203.

Kirby, S.H., 1980. Tectonic stresses in the lithosphere: Constraints provided by the experimental deformation of rocks,

Kohlstedt, D.L., Evans, B. and Mackwell, S.J., 1995. Strength of the lithosphere: Constraints imposed by laboratory experiments, J. Geophys. Res., 100, 17,587-617,602.

Linker, M.F. and Dieterich, J.H., 1992. Effects of variable normal stress on rock friction: Observations and constitutive equations, J. Geophys. Res., 97, 4923-4940.

Lockner, D.A., Summers , R. and Byerlee , J.D., 1986. Effects of temperature and sliding rate on frictional strength granite, Pure Appl. Geophys., 124, 445-485.

Logan, J.M., and K.A., Rauenzahn, 1987. Frictional dependence of gouge mixtures of quartz and montmorillonite on velocity, composition and fabric,Tectonophysics, 144, 87-108.

Mavko, G.M., Scholz ,S., and Brown , B. D., 1985. Effects of the 1983 Coalinga, Calofornia earthquake on creep along the San Andreas fault, Bull. Seismol. Soc. Am., 75, 475-489.

McAlester, A.L., 1973. The earth, Prentice Hall, Inc., Englewood Cliffs, New Jersey.

Okubo, P.G. and Dieterich , J.H., , 1986. State variable fault constitutive relations for dynamic slip, Earthquake Source Mechanics, Am. Geophys. Union., 37,   25-35.

Olsson, W.A., 1988. The effect of normal stress history on rock friction, in Key Questions in Rock Mechanics: Proceedings of the 29th U.S. Symposium, 111-117.

Orowan, E., 1960. Mechanism of seismic faulting, in rock deformation. Geol. Soc. Am. Mem., 79, 323-345.

Rice, J.R. and Ruina ,A.L., 1983. Stability of steady frictional slipping, J. Appl. Mech., 50, 343-349.

Rice, J.R. and Tse ,S.T., 1986. Dynamic motion of a single degree of freedom system following a rate and state dependent friction law, J. Geophys. Res., 91,521-530.

Richter, C.F., 1958. Elementary seismology, Freeman, San Fransisco.

Rikitake, T., 1975. Statistics of ultimate strain of earth's crust and probability of earthquake occurence, Tectonophysics, 26, 1-21.

Rothé, J.P., 1968. Earthquakes and dams, New Scientist, 39.

Ruina, A., 1980. Friction laws and instabilities: A quasistatic analysis of some dry friction behaviour, Ph.D. thesis, Brown Univ., Providence, R. I.

Ruina, A., 1983. Slip instability and state variable friction laws, J. Geophys. Res., 88, 10,359-10,370.

Scheidegger, A.E., 1975. Physical aspects of natural catastrophes, Elsevier Scientific Publishing Company, Amsterdam.

Scholz, C.H., 1990. The mechanics of earthquakes and faulting, Cambridge Univ. Press, New York.

Scholz, C. H., Molnar, P. and Johnson ,T., 1972. Detailed studies of frictional sliding of granite and implications for the earthquake mechanism, J. Geophys. Res., 77, 6392.

Spray, J.G., 1989. Friction phenomena in rock: an introduction, J. Structural Geology, 11, 783-795.

Stacey, F.D., 1969. Physics of the earth, John Wiley & Sons, Inc., New York.

Stesky, R.M., Brace , W.F., Riley, D.K. and Robin ,P.Y.F., 1974. Friction in faulted rock at high temperature and pressure, Tectonophysics, 23, 177-203.

Stesky, R. M., 1978. Mechanisms of high-temperature frictional sliding in Westerly granite, Can. J. Earth Sci., 15, 361-375.

Tao, Z., and Zhang, L. , 1990. The study of factors relative to the fault reactivation, Rock Joints, 487-492, Balkema, Rotterdam.

Tse, S.T. and Rice , J.R., 1986. Crustal arthquake instability in relationship to the depth variation of frictional slip properties, J. Geophys. Res., 91, 9452-9472.

Tuefel, L.W. and Loagn, J.M. , 1978. Effect of displacement rate on the real area of contact and temperatures generated during frictional sliding of Tennessee sandstone, Pure Appl. Geophys., 116, 840-872.

Tullis, T.E., 1986. Friction and faulting-Editor's note, Pure Appl. Geophys., 124, 375-381.

Tullis, T.E., 1988. Rock friction constitutive behaviour from laboratory experiments and its implication for an earthquake prediction program, Pure & Appl. Geophys., 126, 555-588.

Weeks, J.D. and Tullis , T.E., 1985. Frictional sliding of dolomite: A variation in constitutive behaviour, J. Geophys. Res., 90, 7821-7826.

Weeks, J.D., 1993. Constitutive laws for high-velocity frictional sliding and their influence on stress drop during unstable slip, J. Geophys. Res., 98, 17,637-17,648.

Yin, Z.-M., and G.C. Rogers, 1995. Rotation of the principal stress directions due to earthquake faulting and its seismological implications, Bull. Seis. Soc. of America, 85, 1513-1517.

APPENDIX A

CHARACTERISTIC OF HYDRAULIC POWER UNIT

A.1. Hydraulic valves

Proportional pressure relief valve:

Types:
> DBE Series 1X

Characteristics:
> Valve for limiting system pressure
> Operation by means of proportional selonoid
> Single source valve and control electronics
> Control electronics for DBE series:
> > electrical amplifier type VT 2013
> Minimal typical control variation of the signal value pressure characteristics
> Independently adjustable up and down ramp.

Functional description:
> Proportionla pressure relief valve type DBE is operated by means of proportional solenoid. These valves are used to limit system presure. Using these valves it is possible to achieve stepless settings of the system dependent on the electrical signal value.

Electrical amplifier:

Type:
> VT2013 1X

Characteristics:
> Differential input
> Reverse polarity protection

Screening

Voltage stabilising

1 potentiometer for pre-setting signal value

Ramp generator

Performance curve generator

Pulse width modulated current output stage

Technical data:

Operating voltage U_B: 24 V DC

- upper limit value U_B : 35 V DC

- lower limit value $U_{B(max)}$: 21 V DC

Inputs

- Pressure signal value 1 U_e: 0 to 10 V

Differential input

- Pressure signal value 2 U_e: 0 to 9 V

Reference potential is Mo

Outputs

- Solenoid current actual value U_a: 1.6 V

APPENDIX B

INSTRUMENTATION

B.1. Calibration curves
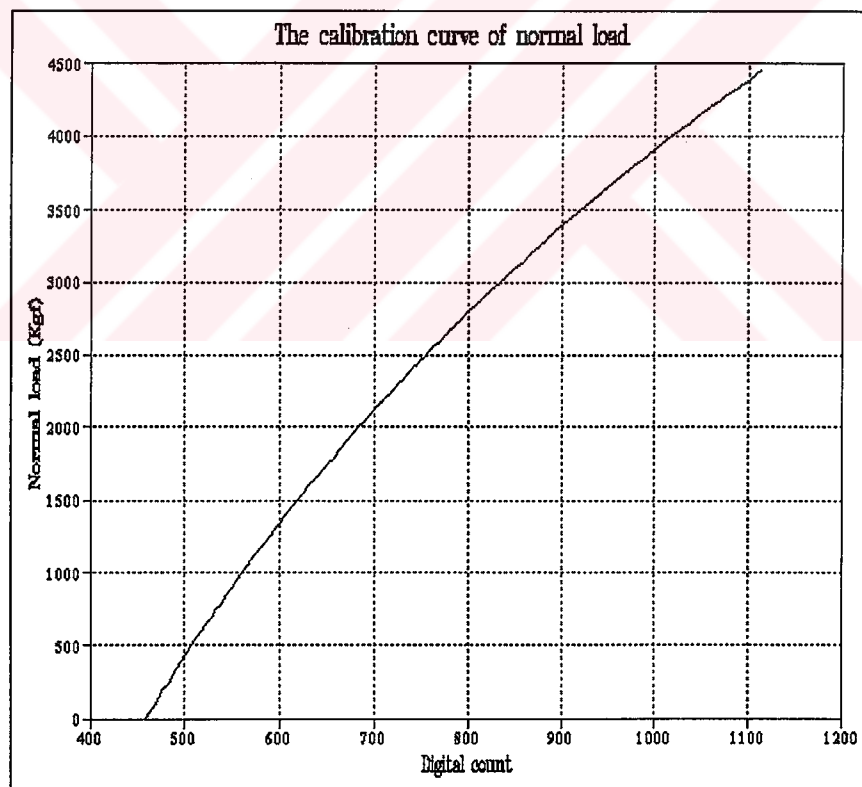
Figure B.1 The calibration curve for normal load measurements

$$\text{Normal Load (kgf)} = e^{\text{Digital count*}}$$

* Digital count = conversion of analog input to digital number
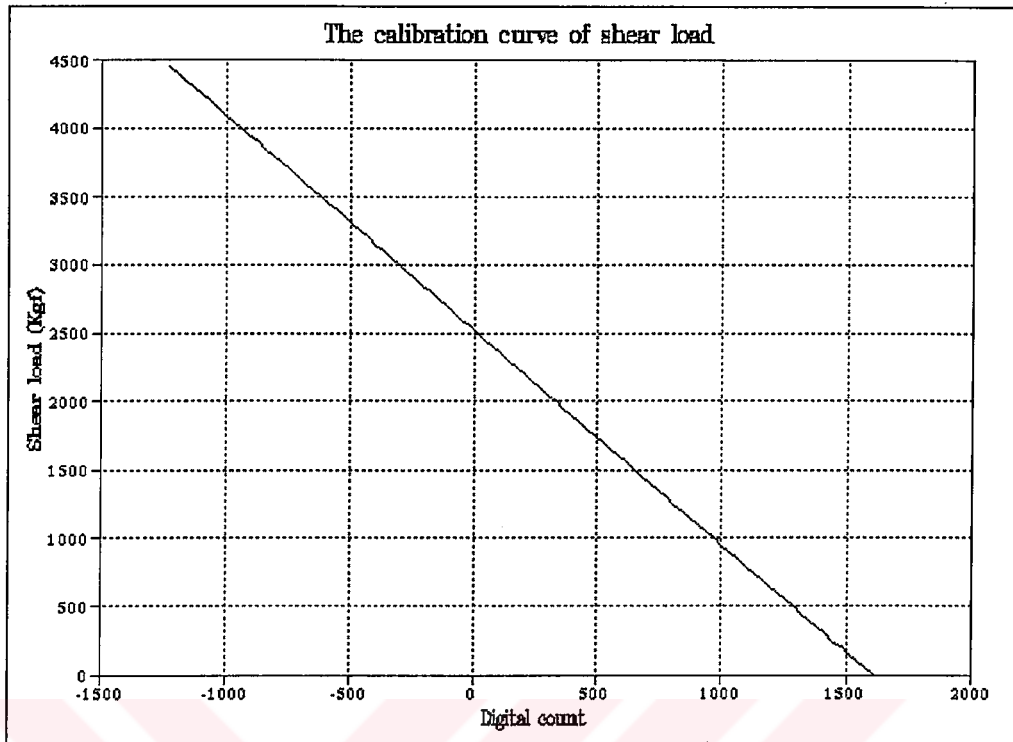
Figure B.2 Calibration curve for shear load measurements
Shear load= -kxDigital count

APPENDIX C

SOFTWARE DRIVERS

C.1 Software for displacement calibration

This is an example software for the calibration pupose. The same logic is carried out for determining the other calibration purposes.

```
'********************************************************************
'
'******** STEP 1: INITIALIZE DRIVER USING FUNC 0 ***************
INPUT "DENEY NO ==>>> ", VT$
VT1$ = "C:\qb\dep" + VT$ + ".DAT"
VT2$ = "C:\qb\dep" + VT$ + ".OUT"
OPEN VT1$ FOR OUTPUT AS #1
OPEN VT2$ FOR OUTPUT AS #2
575 '
DIM DAT%(4), ARY1%(600), ARY2%(600), t(16)
PORT% = &H300        'SET I/O PORT ADDRESS
DAT%(0) = PORT%      'GET I/O PORT ADDRESS
DAT%(1) = 2          'SELECT INTERRUPT LEVEL 2
DAT%(2) = 3          'SELECT D.M.A. IRQ 3
ER% = 0              'ERROR RETURN CODE
FUN% = 0             'FUNCTION 0
CALL PCL718(FUN%, SEG DAT%(0), SEG ARY1%(0), SEG ARY2%(0),
ER%)
IF ER% <> 0 THEN PRINT "DRIVER INITIALIZATION FAILED !": STOP

'******** STEP 3: SET SCAN CHANNEL RANGE USING FUNC 1 ********
CLS
```

```
    START% = 4
    STP% = 4
    BV = 1
    V = VAL(MID$(TIME$, 1, 2)) * 3600 + VAL(MID$(TIME$, 4, 2)) * 60 +
VAL(MID$(TIME$, 7, 2))
    PRINT #1, TIME$


    DAT%(0) = START%      'SET START CHANNEL NUMBER
    DAT%(1) = STP%        'SET STOP CHANNEL NUMBER
    FUN% = 1              'FUNCTION 1
    CALL PCL718(FUN%, SEG DAT%(0), SEG ARY1%(0), SEG ARY2%(0),
ER%)
    IF ER% <> 0 THEN PRINT "SET SCAN CHANNEL FAILED! RE-ENTER":
STOP
    '

    '*** STEP 4: PERFORM SINGLE A/D CONVERSION USING FUNC 3****


570 '

    FUN% = 3             'FUNCTION 3
    CALL PCL718(FUN%, SEG DAT%(0), SEG ARY1%(0), SEG ARY2%(0),
ER%)
    IF ER% <> 0 THEN PRINT "A/D CONVERSION FAILED!": STOP
    t(1) = DAT%(0)
    PRINT t(1)
    PRINT #1, t(1)
    z = 0
    FOR z = 1 TO 1500
    NEXT z
'   PRINT t(j)
    GOTO 575
'   FOR j = 1 TO ABS(START% - STP%) + 1
'   LOCATE 6 + j, 6: PRINT USING "CHANNEL ##   READING ########
VOLTS"; j - 1; t(j)
'   NEXT j
```

C.2. Software for experimental study

This software was developed from the drivers of the PClab 718 software. For the other experimental study, the software like this algorithm has been developed.

```
DECLARE SUB yyuk (r!, s!)
DECLARE SUB press1 (x, y)
DECLARE SUB press2 (x, y)
DECLARE SUB press (r, s)
DECLARE SUB MOTOR (status$)
DECLARE SUB anal (dta)
DECLARE SUB anal1 (dta1)
'*
'**********************************************************
'
INPUT "DENEY NO ==>>> ", VT$
VT1$ = "C:\phd\5nns" + VT$ + ".DAT"
OPEN VT1$ FOR OUTPUT AS #1
'**********************************************************
'******** STEP 1: INITIALIZE DRIVER USING FUNC 0 ****************
'
DIM dat%(4), ary1%(600), ary2%(600), t(16)
PORT% = &H300      'SET I/O PORT ADDRESS
dat%(0) = PORT%    'GET I/O PORT ADDRESS
dat%(1) = 2        'SELECT INTERRUPT LEVEL 2
dat%(2) = 3        'SELECT D.M.A. IRQ 3
ER% = 0            'ERROR RETURN CODE
FUN% = 0           'FUNCTION 0
CALL PCL718(FUN%, SEG dat%(0), SEG ary1%(0), SEG ary2%(0), ER%)
IF ER% <> 0 THEN PRINT "DRIVER INITIALIZATION FAILED !": STOP
CLS
'**********************************************************
*
*
*
'*
```

```
' In this step the time will be started inorder to see the beginnin of the
' record
'
*****************************************************************
    z = 0:
    BV = 1
    v = VAL(MID$(TIME$, 1, 2)) * 3600 + VAL(MID$(TIME$, 4, 2)) * 60 +
VAL(MID$(TIME$, 7, 2))
    PRINT #1, TIME$
'   PRINT #2, TIME$
    PRINT TIME$
'

'

** STEP 3: SET SCAN CHANNEL RANGE USING FUNC 1 *************
'

'   specifying the channel beginning and end number
'   the beginning of channel is 0 and maximum end is 8
'   here is the start of channel 1 to 4 means 5 data will be recorded
'

    START% = 1
    stp% = 5
'

    dat%(0) = START%      'SET START CHANNEL NUMBER
    dat%(1) = stp%        'SET STOP CHANNEL NUMBER
    FUN% = 1              'FUNCTION 1
    CALL PCL718(FUN%, SEG dat%(0), SEG ary1%(0), SEG ary2%(0), ER%)
    IF ER% <> 0 THEN PRINT "SET SCAN CHANNEL FAILED! RE-ENTER":
STOP
'

*****************************************************************

    '* STEP 4: PERFORM SINGLE A/D CONVERSION USING FUNC 3 ******
' In this step   the Analog input converted to Digital input
' t(j) is the stored array
'

'*****************************************************************
'
```

```
    FOR ijj = 1 TO 20000
    NEXT ijj
'

    nkz = 0
'

570 '
'   FOR j = 1 TO ABS(START% - stp%) + 1
    FUN% = 3            'FUNCTION 3
    CALL PCL718(FUN%, SEG dat%(0), SEG ary1%(0), SEG ary2%(0), ER%)
    IF ER% <> 0 THEN PRINT "A/D CONVERSION FAILED!": STOP
    t(j) = dat%(0)
    NEXT j


    v1 = VAL(MID$(TIME$, 1, 2)) * 3600 + VAL(MID$(TIME$, 4, 2)) * 60 +
VAL(MID$(TIME$, 7, 2))
                v4 = v1 - v


    z = z + 1
'   Printing the recorded the digital input
'

'?  FOR j = 1 TO ABS(start% - stp%) + 1
'?  LOCATE 6 + j, 6: PRINT #2, USING "CHANNEL ##   READING
######## VOLTS"; j - 1; t(j)
'?  NEXT j
'

    mint2 = -2034: maxt2 = 1800: lent2 = 11.33
'

    CALL disp(mint2, maxt2, lent2, a2, b2)
    kl = 1000
    IF TTLAK = 1 THEN GOTO 309
    IF kul = 1 THEN GOTO 3099
    kbasinc = 50 * nkz
    IF kbasinc = 0 THEN kbasinc = 5
    IF kbasinc > kl THEN kbasinc = kl
    CALL press1(kbasinc, count)
    CALL press(t(2), normy)
    CALL yyuk(t(3), sheary)
```

146

```
        IF kul = 1 THEN GOTO 30677
'    .............................PRESS= the estimated value
'

'

        disp2 = a2 + b2 * t(4)
        IF normy = 0! THEN normy = .01
        coeff = sheary / normy
        shers = sheary / 275
        norms = normy / 275
'    ---------------------------------------
        PRINT , kbasinc, t(3), t(2), v4, disp2
            PRINT #1, USING "##### "; kbasinc;
                PRINT #1, USING "shy= ##### "; sheary;
                PRINT #1, USING "nry= ##### "; normy;
                PRINT #1, USING "disp= ##.#### "; disp2;
    v1 = VAL(MID$(TIME$, 1, 2)) * 3600 + VAL(MID$(TIME$, 4, 2)) * 60 +
VAL(MID$(TIME$, 7, 2))
                    v4 = v1 - v
                PRINT #1, USING "#### "; v4;

                PRINT #1, USING "coef= ##.### "; coeff;
                PRINT #1, USING "shrs= ##.## "; shers;
                PRINT #1, USING "nors= ##.## "; norms

        IF tlak = 1 THEN GOTO 3099
30677 '
        dta = 0
        CALL anal(dta)
         CALL MOTOR("3")
3099
'

680 CLS
        IF iFLAG = 2 GOTO 309

'

START! = TIMER
'
```

```
' The normal load conditions according to ISRM .5-1.0 MPa/sec
' for the 40 cm2 specimen the loading rate will be 100kgf/sec


'

Finish! = TIMER
ST! = Finish! - START!


      dta = count
          FOR KKK = 1 TO 2000
          NEXT KKK
          tlak = 1
          CALL anal(dta)
        nkz = nkz + 1
       IF (kbasinc < kl) THEN GOTO 570
        iFLAG = 2
309
      dta1 = 100
       CALL anal1(dta1)
       CALL MOTOR("4")
   v1 = VAL(MID$(TIME$, 1, 2)) * 3600 + VAL(MID$(TIME$, 4, 2)) * 60 +
VAL(MID$(TIME$, 7, 2))
               v4 = v1 - v


       IF v4 > 4550 GOTO 5700
     CALL press1(kbasinc, count)
     CALL press(t(2), normy)
     CALL yyuk(t(3), sheary)


     disp2 = a2 + b2 * t(4)
     IF normy = 0! THEN normy = .01
     coeff = sheary / normy
     shers = sheary / 275
     norms = normy / 275
'      --------------------------------------
        PRINT , kbasinc, t(3), t(2), v4, disp2
          PRINT #1, USING "##### "; kbasinc;
              PRINT #1, USING "shy= ##### "; sheary;
                          148
```

```
                    PRINT #1, USING "nry= ##### "; normy;
                    PRINT #1, USING "disp= ##.#### "; disp2;
        v1 = VAL(MID$(TIME$, 1, 2)) * 3600 + VAL(MID$(TIME$, 4, 2)) * 60 +
VAL(MID$(TIME$, 7, 2))
                        v4 = v1 - v


                    PRINT #1, USING "#### "; v4;


                    PRINT #1, USING "coef= ##.### "; coeff;
                    PRINT #1, USING "shrs= ##.## "; shers;
                    PRINT #1, USING "nors= ##.## "; norms


        FOR kjh = 1 TO 20000
        NEXT kjh


        LOCATE 18, 6: PRINT USING "PROGRAM CALISIYO <<<<< ######
>>>>>"; v4
            TTLAK = 1
        v1 = VAL(MID$(TIME$, 1, 2)) * 3600 + VAL(MID$(TIME$, 4, 2)) * 60 +
VAL(MID$(TIME$, 7, 2))
                        v4 = v1 - v


            IF v4 <= 4550 GOTO 570
5700 '
        FOR kjhgf = 1 TO 400
        NEXT kjhgf
        LOCATE 18, 6: PRINT USING "PROGRAM CALISIYO <<<<< ######
>>>>>"; v4


'F v4 >= 4601 THEN kbasinc = kl + (400 * (1 - (COS(3.14 * (v4 - 4601) / 15))))
'F v4 = 4616 THEN kbas = kl + (400 * (1 - (COS(3.14 * (v4 - 4601) / 15))))
'F v4 = 4616 THEN kbasinc = kbas - (400 * (1 - (COS(3.14 * (v4 - 4616) / 15))))
'F v4 > 4616 THEN kbasinc = kbas - (400 * (1 - (COS(3.14 * (v4 - 4616) / 15))))
'F v4 >= 4631 THEN kbasinc = kl - (400 * (1 - (COS(3.14 * (v4 - 4631) / 15))))
'F v4 = 4646 THEN kbas1 = kl - (400 * (1 - (COS(3.14 * (v4 - 4631) / 15))))
'F v4 = 4646 THEN kbasinc = kbas1 + (400 * (1 - (COS(3.14 * (v4 - 4646) /
15))))
```

```
'F v4 > 4646 THEN kbasinc = kbas1 + (400 * (1 - (COS(3.14 * (v4 - 4646) /
15))))
' v4 >= 4662 THEN kbasinc = 2500
'     ==================================
'IF v4 >= 4550 THEN GOTO 54556
'GOTO 54557
'54556 kj = v4 - 4550
'kbasinc = kbasinc + kj * 300 / 50
IF v4 >= 4601 THEN kbasinc = 1000 + 600 * SIN(2 * 3.14 * ((v4 - 4601) / 60))
IF v4 > 4661 THEN kbasinc = 1000

'IF v4 >= 4601 THEN kbasinc = kl + (600 * (1 - (COS(3.14 * (v4 - 4601) / 7))))
'IF v4 = 4605 THEN kbas = kl + (600 * (1 - (COS(3.14 * (v4 - 4601) / 7))))
'IF v4 = 4605 THEN kbasinc = kbas - (600 * (1 - (COS(3.14 * (v4 - 4605) / 7))))
'IF v4 > 4605 THEN kbasinc = kbas - (600 * (1 - (COS(3.14 * (v4 - 4605) / 7))))
'IF v4 >= 4609 THEN kbasinc = kl - (600 * (1 - (COS(3.14 * (v4 - 4609) / 7))))
'IF v4 = 4613 THEN kbas1 = kl - (600 * (1 - (COS(3.14 * (v4 - 4609) / 7))))
'IF v4 = 4613 THEN kbasinc = kbas1 + (600 * (1 - (COS(3.14 * (v4 - 4613) /
7))))
'IF v4 > 4613 THEN kbasinc = kbas1 + (600 * (1 - (COS(3.14 * (v4 - 4613) /
7))))
'IF v4 >= 4617 THEN kbasinc = 1000


    kul = 1
   CALL press1(kbasinc, count)
   CALL press(t(2), normy)
   CALL yyuk(t(3), sheary)
   dta = count
   CALL anal(dta)

   disp2 = a2 + b2 * t(4)
   IF normy = 0! THEN normy = .01

   coeff = sheary / normy
   shers = sheary / 275
   norms = normy / 275
```

```basic
'    ---------------------------------------
     PRINT , kbasinc, t(3), t(2), v4, disp2
        PRINT #1, USING "##### "; kbasinc;
            PRINT #1, USING "shy= ##### "; sheary;
            PRINT #1, USING "nry= ##### "; normy;
            PRINT #1, USING "disp= ##.#### "; disp2;
 v1 = VAL(MID$(TIME$, 1, 2)) * 3600 + VAL(MID$(TIME$, 4, 2)) * 60 +
VAL(MID$(TIME$, 7, 2))
            v4 = v1 - v

        PRINT #1, USING "#### "; v4;

        PRINT #1, USING "coef= ##.### "; coeff;
        PRINT #1, USING "shrs= ##.## "; shers;
        PRINT #1, USING "nors= ##.## "; norms

'

    LOCATE 18, 6: PRINT USING "CHANNEL SCAN COUNT <<<<< #####
>>>>>"; z
    V2 = VAL(MID$(TIME$, 1, 2)) * 3600 + VAL(MID$(TIME$, 4, 2)) * 60 +
VAL(MID$(TIME$, 7, 2))
    v3 = V2 - v
'

    IF z > 15 THEN LOCATE 20, 6: PRINT USING "CHANNEL SCAN RATE
<<<<< ###### >>>>>"; z * (ABS(START% - stp%) + 1) / v3

349 '
        IF normy >= 12500 OR v4 >= 5000 THEN GOTO 755
        IF sheary >= 3500 OR disp2 >= 11 THEN GOTO 755
        GOTO 570

    CLS
    nmk = 0
755 '
FOR lkji = 1 TO 10000
NEXT lkji
    nmk = 1
```

```
7556
FOR lki = 1 TO 3000
NEXT lki

    kbasinc = 1000 / nmk
     CALL press1(kbasinc, count)
    dta = count
    CALL anal(dta)
    dta1 = 0
    CALL anal(dta1)
    CALL MOTOR("3")

            nmk = nmk + 1
            IF kbasinc < 100 THEN GOTO 4592
    GOTO 7556

4592   CLS
    dta = 0
    CALL anal(dta)

    PRINT #1, TIME$
    CLOSE #1
    CLOSE #2
    CALL MOTOR("0")
     END

SUB anal (dta)
'

' This subroutine is used to apply the pressure to the pressure unit
' This subroutine send the analog voltage value
' The analog value is sent to the channel (0)
' dat%(0)=0 (channel 0)
'

    DIM dat%(1), ary1%(600), ary2%(600)
    dat%(1) = dta
'
```

```
'******* STEP 2: SELECT D/A OUTPUT TYPE
***************************
'

'******* STEP 4: OUTPUT DATA TO ONE D/A
***************************
'

    dat%(0) = 0
    FUN% = 15
    CALL PCL718(FUN%, SEG dat%(0), SEG ary1%(0), SEG ary2%(0), ER%)
    IF ER% <> 0 THEN PRINT "PERFORM SINGLE D/A FAILED!"
END SUB


SUB anal1 (dta1)
'

' MOTOR DRIVER VOLTAGE
' This subroutine is used to apply analog voltage to motor drive unit
' The channel is the dat%(1)=1 (1)
'

    DIM dat%(1), ary1%(600), ary2%(600)
    dat%(1) = dta1
'

'******* STEP 2: SELECT D/A OUTPUT TYPE
***************************
'

'******* STEP 4: OUTPUT DATA TO ONE D/A
***************************
'

    dat%(0) = 1
    FUN% = 15
    CALL PCL718(FUN%, SEG dat%(0), SEG ary1%(0), SEG ary2%(0), ER%)
    IF ER% <> 0 THEN PRINT "PERFORM SINGLE D/A FAILED!"


END SUB


SUB disp (minx, maxx, boy2, a, b)

boy1 = 0
```

```
sumx = 0: sumx2 = 0: sumy = 0: sumxy = 0
sumx = minx + maxx
sumy = boy2 + boy1
sumx2 = minx * minx + maxx * maxx
sumxy = maxx * boy2
b = (2 * sumxy - sumx * sumy) / (2 * sumx2 - sumx * sumx)
a = (sumy - b * sumx) / 2
END SUB


SUB MOTOR (status$)


DIM dat%(4), ary1%(600), ary2%(600)
DIM po%(4)


  a$ = status$


  FOR I% = 1 TO 4
  po%(I%) = 0
   NEXT I%



  IF a$ = "0" THEN GOTO mini
  IF a$ = "1" THEN GOTO mt
  IF a$ = "3" THEN GOTO mtgv
  IF a$ = "2" THEN GOTO mtdv
  IF a$ = "4" THEN GOTO stms
  IF a$ = "5" THEN GOTO stp


mini: 'Motors Initialization  (All the channel will be initialized)
   FUN% = 21
   dat%(1) = 0
   FOR I% = 1 TO 4
   po%(I%) = 0
   NEXT I%
   GOTO send


mt: 'Motor calismasi  D/O CHANNEL #2 (Second channel will be activated
```

```
    '

    '

    FUN% = 21
    dat%(1) = 0
    po%(1) = 0
    po%(2) = 1
    po%(3) = 0
    GOTO send
```

mtdv: 'Motor + Dönüş valfi D/O CHANNEL #1 & 2 (1&2 channel will be activated
    '   and the motor will work and directional pressure valfe will be opened
    '   , pressure will be relieved
    '

```
    FUN% = 21
    dat%(1) = 0
    po%(2) = 0
    po%(1) = 1
    po%(3) = 1
    GOTO send
```

mtgv: 'Motor 1 + Gidiş valfi D/O CHANNEL #2 & 3 (2&3 channel will be activated
    '   the motor and directional pressure valf opned and the pressure can be activated
    '

```
    FUN% = 21
    dat%(1) = 0
    po%(1) = 1
    po%(2) = 1
    po%(3) = 0
    GOTO send
```

stms: 'Motor Drive unit   (4 channel will be activated and the motor will be on
    '   the motor will be ready to run
    '

```
    FUN% = 21
```

```basic
      dat%(1) = 0
      po%(3) = 0
      po%(2) = 1
      po%(1) = 1
      po%(4) = 1
      GOTO send


stp: 'Motor  Stop  (All the channel will be off)
'
      FUN% = 21
      dat%(1) = 0
      po%(3) = 0
      po%(2) = 0
      po%(1) = 0
      po%(4) = 0
      GOTO send

send:
      dat%(0) = po%(3) * 2 + po%(2) * 4 + po%(1) + po%(4) * 32
'     PRINT a$, dat%(0)
      CALL PCL718(FUN%, SEG dat%(0), SEG ary1%(0), SEG ary2%(0), ER%)
      IF ER% <> 0 THEN PRINT "PERFORM FUNC 21 FAILED!": STOP
END SUB


SUB press (r, s)
'x is the recorded counted value
'y is the calculated the pressure value
' normal yukun kalibre degerleri

DIM S1(22), S2(22)
S1(1) = 0: S1(2) = 500: S1(3) = 1000: S1(4) = 1500: S1(5) = 2000
S1(6) = 2500: S1(7) = 3000: S1(8) = 3500: S1(9) = 4000: S1(10) = 4500
S1(11) = 5000: S1(12) = 5500: S1(13) = 6000: S1(14) = 6500: S1(15) = 7000
S1(16) = 7500: S1(17) = 8000: S1(18) = 8500: S1(19) = 9000: S1(20) = 9500
S1(21) = 10000: S1(22) = 10500
```

156

```
S2(1) = 402: S2(2) = 514: S2(3) = 542: S2(4) = 625: S2(5) = 728
S2(6) = 803: S2(7) = 855: S2(8) = 910: S2(9) = 961: S2(10) = 1014
S2(11) = 1068: S2(12) = 1120: S2(13) = 1173: S2(14) = 1225: S2(15) = 1285
S2(16) = 1346: S2(17) = 1406: S2(18) = 1460: S2(19) = 1516: S2(20) = 1568
S2(21) = 1669: S2(22) = 1722


FOR I = 1 TO 22
IF r <= S2(I) THEN z = I: GOTO 249
NEXT I
249 :
sumr = 0: sumr2 = 0: sums = 0: sumrs = 0
FOR j = 0 TO 1
sumr = S2(z - j) + sumr
sums = S1(z - j) + sums
sumr2 = S2(z - j) * S2(z - j) + sumr2
sumrs = S2(z - j) * S1(z - j) + sumrs


NEXT j

b = (2 * sumrs - sumr * sums) / (2 * sumr2 - sumr * sumr)
a = (sums - b * sumr) / 2
s = a + b * r


' y is the pressure load


END SUB


SUB press1 (x, y)
'Y is the recorded counted value
'X is the calculated the pressure value


DIM S1(12), S2(12)
S1(1) = 0: S1(2) = 500: S1(3) = 750: S1(4) = 1000: S1(5) = 1250
S1(6) = 1500: S1(7) = 1750: S1(8) = 2000: S1(9) = 2250: S1(10) = 2500
S1(11) = 2750: S1(12) = 3000
```

```
S2(1) = 0: S2(2) = 1994: S2(3) = 3260: S2(4) = 4602: S2(5) = 5982
S2(6) = 7210: S2(7) = 8514: S2(8) = 9971: S2(9) = 11352: S2(10) = 12732
S2(11) = 14190: S2(12) = 15724


FOR I = 1 TO 12
IF x <= S2(I) THEN z = I: GOTO 149
NEXT I
149 :
sumx = 0: sumx2 = 0: sumy = 0: sumxy = 0
FOR j = 0 TO 1
sumx = S2(z - j) + sumx
sumy = S1(z - j) + sumy
sumx2 = S2(z - j) * S2(z - j) + sumx2
sumxy = S2(z - j) * S1(z - j) + sumxy

NEXT j
b = (2 * sumxy - sumx * sumy) / (2 * sumx2 - sumx * sumx)
a = (sumy - b * sumx) / 2
y = a + b * x
' y is the pressure load
END SUB


'

'

SUB press2 (x, y)
'

'x is the recorded counted value
'y is the calculated the pressure value


DIM S2(12), S1(12)
S1(1) = 0: S1(2) = 500: S1(3) = 750: S1(4) = 1000: S1(5) = 1250
S1(6) = 1500: S1(7) = 1750: S1(8) = 2000: S1(9) = 2250: S1(10) = 2500
S1(11) = 2750: S1(12) = 3000


S2(1) = 0: S2(2) = 2310: S2(3) = 3758: S2(4) = 5062: S2(5) = 6366
S2(6) = 7670: S2(7) = 9051: S2(8) = 10278: S2(9) = 11582: S2(10) = 13039
```

S2(11) = 14573: S2(12) = 15877


```
FOR I = 1 TO 12
IF x <= S2(I) THEN z = I: GOTO 1149
NEXT I
1149 :
sumx = 0: sumx2 = 0: sumy = 0: sumxy = 0
FOR j = 0 TO 1
sumx = S2(z - j) + sumx
sumy = S1(z - j) + sumy
sumx2 = S2(z - j) * S2(z - j) + sumx2
sumxy = S2(z - j) * S1(z - j) + sumxy

NEXT j
b = (2 * sumxy - sumx * sumy) / (2 * sumx2 - sumx * sumx)
a = (sumy - b * sumx) / 2
y = a + b * x
' y is the pressure load
END SUB


SUB yyuk (r, s)
'x is the recorded counted value
'y is the calculated the pressure value
' YATAY  yukun kalibre degerleri
DIM S1(22), S2(22)
S1(1) = 0: S1(2) = 750: S1(3) = 1000: S1(4) = 1250: S1(5) = 1500: S1(6) = 1750
S1(7) = 2000: S1(8) = 2250: S1(9) = 2500
S1(10) = 2750: S1(11) = 3000: S1(12) = 3250
S1(13) = 3750: S1(14) = 4000: S1(15) = 4250: S1(16) = 4500: S1(17) = 4750
S1(18) = 5000: S1(19) = 5250: S1(20) = 5500: S1(21) = 5750: S1(22) = 6000


S2(1) = 1983: S2(2) = 1387: S2(3) = 1244: S2(4) = 1135
S2(5) = 957: S2(6) = 767: S2(7) = 539: S2(8) = 344: S2(9) = 155
S2(10) = -60: S2(11) = -190: S2(12) = -434: S2(13) = -564: S2(14) = -670
S2(15) = -892: S2(16) = -1030: S2(17) = -1176: S2(18) = -1323: S2(19) = -1561
```

S2(20) = -1689: S2(21) = -1839: S2(22) = -1972

FOR I = 1 TO 22
IF r >= S2(I) THEN z = I: GOTO 2249
NEXT I
2249 :
sumr = 0: sumr2 = 0: sums = 0: sumrs = 0
FOR j = 0 TO 1
sumr = S2(z - j) + sumr
sums = S1(z - j) + sums
sumr2 = S2(z - j) * S2(z - j) + sumr2
sumrs = S2(z - j) * S1(z - j) + sumrs

NEXT j

b = (2 * sumrs - sumr * sums) / (2 * sumr2 - sumr * sumr)
a = (sums - b * sumr) / 2
s = a + b * r
' y is the pressure load
END SUB

APPENDIX D

DATA FILE FOR THE NUMERICAL STUDY

D.1 An example data file for the analysis of velocity-stepping test

```
;
def load
while_stepping
if step>200 then
sxxy=(sxy(5,5)+sxy(6,5)+sxy(7,5)+sxy(4,5))/4
syyy=(syy(5,10)+syy(6,10)+syy(7,10)+syy(4,10))/4
;coeff=sxxy/syyy
;sxxy=(sxy(5,10)+sxy(6,10)+sxy(7,10)+sxy(4,10))/4
;syyy=(syy(5,7)+syy(6,7)+syy(7,7)+syy(4,7))/4
load=sxxy/syyy

; end_loop
; end_loop
; end_if
  end_if
  end
def ramp
 while_stepping
 if step<12000 then
  ud_app=step*1e-6/15000
  loop j (1,6)
  xvel(1,j)=ud_app
  end_loop
 end_if
      end
 def ramp1
```

```
while_stepping
  if step>12000 then
  ud_app=1e-5*step/15000
  loop j (1,6)
  xvel(1,j)=ud_app
  end_loop
  end_if
  end

  def ramp2
  while_stepping
  if step>12051 then
  ud_app=step*1e-6/15000
  loop j (1,6)
  xvel(1,j)=ud_app
  end_loop
  end_if
  end

g 10 10

;model elas  j=1,5
,model m  j=4,5
,model m  i=4,8 j=7,8
;model elas  i=4,8 j=7,11
m e
;gen 0 0 0 .15 .30 .15 .30 0 i=1,11 j=1,6
;gen .12 0 .12 .15 .18 .15 .18 0 i=4,8 j=1,6
;gen 0 .15 0 .25 .30 .25 .30 .15 i=1,11 j=6,11
;gen .12 .15 .12 .25 .18 .25 .18 .15 i=4,8 j=6,11

gen 0 0 0 .05 .30 .05 .30 0 i=1,11 j=1,6
gen .12 0 .12 .05 .18 .05 .18 0 i=4,8 j=1,6
gen 0 .05 0 .07 .30 .07 .30 .05 i=1,11 j=6,11
gen .12 .05 .12 .07 .18 .07 .18 .05 i=4,8 j=6,11

prop den=0.00265 b=17000 s=10000
```

162

```
;prop den=0.0265 b=70000 s=70000 j=1,5
mark i=1,4 j=6
mark i=4 j=6,11
mark i=8 j=6,11
mark i=8,11 j=6
gen line 1,6 4,6
gen line 4,6 4,11
gen line 8,6 8,11
gen line 8,6 11,6

model null region=1,10
model null region=10,10
model null j=6
apply press 5 i=4,8 j=11
;ini y add -.02 j=7,11
ini y add -.004 j=7,11
int 1 aside from 4 6 to 8 6 bside from 8 7 to 4 7
int 1 kn=10000 ks=10000 coh=.02 fric=38.0 t=0
;apply syy -5 i=4,8 j=11
;
;ini xv 1e-6 i=1  j=1,6
;ini xv 1e-3 i=11 j=1,6
set large
fix x        i=4 j=7,11
fix x        i=8 j=7,11
fix y     i=1  j=1,5
fix y     i=11 j=1,5
fix y     j=5
;fix y x      j=7
fix y     j=1
load
his xdisp j=3 i=1
his sxy   j=7 i=6
his xvel  j=5 i=6
his sxy   j=5 i=6
his syy   i=6 j=7
his load   i=6 j=5
```

```
step 15000
set his disp0.his
his write 4 v 1
set his disp0.out
his write 6 v 1
save disp0.sav
```

VITA

Dursun Sarı was born in Çayeli/Rize, 1964. He received his B.Sc. and M.Sc. degrees from the Mining Engineering Department of Middle East Technical University in 1987 and 1989, respectively. He has been working as a research assistant in the Mining Engineering Department of Middle East Technical University from 1987 until 1996. His main areas of interest rock mechanics, numerical modelling, computer programming, slope stability, tunnelling, earthquake engineering.